UNIVERSITY OF
LIVERPOOL

School of Engineering

Engineering Applications of the Optical Trap

Thesis submitted in accordance with the requirements of the University of Liverpool for the degree of Doctor in Philosophy by

Joseph L. Croft

January 2013

Declaration

I hereby declare that all of the work contained within this dissertation has not been submitted for any other qualification.

Signed: ..... Dated: .....

Abstract

Laser optical trapping is a developing technology. Optical traps have become valuable tools in a number of research fields including physics, optics, fluid mechanics and most significantly – biology. The ability to accurately manipulate micro and nano scale objects, measure forces to piconewton accuracy and integrate alongside other technologies have made optical traps unique devices.

In the research presented in this thesis a complex and versatile optical trapping system is designed, built and developed for investigation of new and innovative engineering based applications for the optical trap. The practical problems associated with optical trapping were assessed and, where possible, solutions are offered.

Various potential engineering applications for optical traps were first identified and then investigated to determine new uses and capabilities for optical traps.

A number of exciting outcomes of the work are presented. These include:

- Accurate placement of silica microspheres into a thermosetting resin, which has potential micro processing applications.
- The manipulation of metallic particles through unconventional trapping techniques.
- Micro scale ablation of glass cover slips with copper particles on the glass surface to assist in the coupling of energy into the glass substrate.

Acknowledgements

Undertaking this research has been thoroughly enjoyable, satisfying, exciting, painful, frustrating, upsetting, fun, frustrating again, absorbing, painful again but ultimately rewarding.

I must first thank my supervisors, Prof. Ken Watkins and Dr. Geoff Dearden for the initial opportunity, their time, support and guidance.

Secondly, a huge thank you to Dr. Stuart Edwardson for all his help and teaching in the early days, his advice and assistance in the middle and perhaps crucially his guidance and calming words towards the end.

A big thank you to the rest of laser group who made the whole PhD experience more worthwhile Paul Fitzsimons, Dan Wellburn, Chris Carey, Kenny Edwards, Taku Sato, Dun Lu, Jian Cheng, Spencer Shang, Jack Mullet. Extra thanks to Craig Williams, Leigh Mellor, Olivier Allegre and Jon Griffiths for helping me directly with my work, often stopping what they were doing to find time to talk through a problem or help me with a programming issue.

A thank you to those kind fellows who have offered relief from the lab over the years and been all round great friends: Brummie, Ed, Andy G, Dom Soanes, Chris Roque, Danny Black, Laura Mac, Tom Ship, Tabsy, Peo, Liam, Pete Armo, Paddy Staunton and all those at Atticus chess club. You lot have kept me sane. Just.

A big thank you to Mrs Pottage, Dave Eland, John Metcalfe and Richard Smith. I have no idea where any of you are now but you were each truly

inspirational teachers (especially about physics or maths) and I am eternally grateful for your enthusiasm.

Finally I would like to thank my family. To my mum and dad: two terrible scientists and wonderful parents. Thank you for always encouraging me to be inquisitive and for rarely having the answers and thus inspiring me to find out myself. Thank you for your encouragement and support throughout my seemingly never ending student career. Big thanks to Dave for the many hours I know he spent proof reading. Also thanks to my brothers, Jack and Al for just being about. Thanks to my grandma for her love, support and supplies of her divine porridge oat cake. Special thanks to my Grandad Stan and Grandpa Geoff: two real scientists and inspirations to me from a very early age. Particular thanks to my Granddad Stan for casting a careful eye over some of my maths from ages 6-26.

An extra special thanks goes to my partner, Sarah, for being ludicrously lovely, generally looking after me and even proof reading this thing and not understanding a word.

The author would like to gratefully acknowledge the EPSRC and NWDA for their funding support for this research.

'All science is either physics or stamp collecting.'

- Ernest Rutherford

'Research is what I'm doing when I don't know what I'm doing.'

- Wernher Von Braun

Nature composes some of her loveliest poems for the microscope and the telescope.

- Theodore Roszak

Contents

List of notation

h = Planck's constant (J s)

ρ = momentum of the photon

λ - wavelength of the photon (m)

k = trap stiffness (pN nm^{-1})

x = displacement of the bead from the traps equilibrium position (μm)

F = the drag force on the sphere (N)

η = viscosity of the fluid (kg m^{-1} s^{-1})

r = radius ofa microsphere (μm)

v = velocity of the sphere in the medium (m s^{-1})

S = Signal from QD (Volts)

ω = frequency of oscillation (Hz)

A = Amplitude (V or μm)

k_B = Boltzmann Constant (J K^{-1})

T = Temperature (K)

σ_x^2 = variance in position of the sphere (μm^2)

γ = drag coefficient

f_c = corner frequency (Hz)

Q = Coefficient of Trap Quality

P = Laser Power (W)

c = speed of light in a vacuum ($m\ s^{-1}$)

n = refractive index

M = magnification

l_O = the focal length of the objective lens (mm)

l_I = focal length of the image lens (mm)

β = annular beam parameter.

α = width of the annular ring.

A_f = amplitude of the fixed sphere's oscillation, (V or μm)

$\hat{s}_{max}$ = mean of the all the 'maximums' from a sine wave (V or μm or pixels)

$\hat{s}_{min}$ = mean of the minimum values of all the 'minimums' from a sine wave (V or μm or pixels)

$A_{m\text{-}fixed}$ = amplitude of oscillation of the fixed sphere (m).

$A_{p\text{-}fixed}$ = amplitude of oscillation of the fixed sphere (pixels).

D - Conversion factor (μm per pixel).

$A_{m\text{-}trapped}$ - the amplitude of oscillation of the trapped sphere (m).

$A_{p\text{-}trapped}$ = the amplitude of oscillation of the trapped sphere (pixels).

L - Conversion factor (V μm^{-1})

δ = the standard deviation in the position data of the trapped sphere (V or pixels)

v = velocity of the sphere in the medium (m s^{-1}).

List of abbreviations

AFM - Atomic Force Microscope

SLM - Spatial Light Modulator

MASER - Microwave Amplification through Stimulated Emission Radiation

QD - Quadrant Detector

NA - Numerical Aperture

YAG - Yttrium Aluminium Garnet

Nd:YVO_4 - Neodymium-doped Yttrium Orthovanadate (Vanadate)

CCD - Charge Coupled Device

LBA - Laser Beam Analyser

AOD - Acousto-Optic Deflector

StAT - St.Andrews Tracker

CGH - Computer Generated Holograms,

Publications

- Croft J., Edwardson S. P., Williams C. J., Allegre O. J., Dearden G. and Watkins K. G. 2010. Embedding arrays of microspheres with optical trapping for micro scale device manufacture. 29th international congress on applications of lasers and electro-optics, ICALEO 2010 - congress proceedings. 1450 p.

- Williams C. J., Edwardson S. P., Croft J., Sharp M., French P., Ansari I. A., Perrie W., Cheng J., Dearden G. and Watkins K. 2008. Production of micro and nano scale features on polymer surfaces with SPM based lithography and ultra short pulsed lasers. ICALEO 2008 - 27th international congress on applications of lasers and electro-optics, congress proceedings. 14 p.

Chapter 1

Introduction

1.1 Background

It is now over forty years since Ashkin's seminal work (1) began the technology of optical traps and over twenty years since he first achieved a genuine single beam optical trap in three dimensions. Since then, the technology has flourished in many research areas including physics, fluid mechanics and of course, biology. In spite of this swift development, there are still many unexplored avenues of interest. In recent times, the optical trap has become a commercially available tool and is fast becoming a standard lab analytical tool to compare with the atomic force microscope (AFM) or the scanning electron microscope (SEM).

The optical trap's natural capabilities lend themselves exceptionally well to biological research offering capabilities not available with any other kind of machine. Thus, biological research has been the main focus of much of the research date. Consequently, it may be timely for other sciences to catch up and for the capabilities of this extremely versatile technology to be realised across a wide range of scientific fields.

1.2 Thesis Aim and Objectives

This work in this thesis aimed to harness an already existing technology, optical trapping, and investigate its potential applications for purely engineering purposes. A significant section of the project involved the building of a new versatile optical trapping system with a variety of functionalities designed specifically for engineering applications. Next, the objective was to find and explore new potential engineering applications for the optical trap. The nature of optical traps meant that the engineering applications being referred to would be of micro or nano scale. Once new applications had been identified, investigations would be undertaken to establish the viability of such a method. Throughout the project the optical trapping system was further developed and configured to meet the needs of these potential applications. This engineering based approach allowed for practical aspects of the optical trap to be investigated in ways not previously seen. As such, this thesis represents a significant increase in the knowledge and understanding of the optical trap an engineering tool.

This work in this thesis uses a practical engineering approach to problems, alongside an understanding of the fundamental physics behind optical trapping. As this work aims to offer an alternative approach to the biosciences work undertaken with optical traps, the biological applications are presented as part of the literature review in terms of how developments in optical trapping technology have enabled new biosciences research.

1.3 Thesis Structure

This thesis is separated into seven chapters which aim to first present the process of developing an optical trapping system and then a series of experiments using of the optical trap as an engineering tool or device are undertaken and the results and outcomes discussed.

It begins with this introductory chapter to outline the background to the topic, the objectives of the research undertaken and the structure of the thesis.

Chapter 2 begins with a brief introduction to the history of the laser and optical traps. It then sets out the current state of the art of the optical trapping field, with particular attention paid to work which has used the optical trap as an engineering tool or device.

Chapter 3 sets out how the system was designed and built. It details why such design decisions were taken, the novel aspects of this particular system, such as the two lasers focussed to the same position, quadrant detector and spatial light modulator, and what added functions these allow, the capabilities and limitations of the system and finally some of the common problems associated with optical traps and the methods used to resolve them.

Chapter 4 details the optical trap as a force measurement tool. It outlines the different methods of calibrating the device and the different methods of obtaining force measurements from the literature. The chapter sets out the various procedures used and corresponding results for trap stiffness, achieved on the system described in Chapter 3, while varying a variety of parameters, such as laser power and microsphere diameter.

Chapter 5 describes a series of new experiments which use the optical trap as a device for placing (and fixing) microspheres in a desired location and formation. It sets out the procedure used and the results obtained, including the newly established capability of placing individual microspheres. The chapter concludes with a discussion of this novel application with thoughts expressed on the capabilities and limitations of such a technique.

Chapter 6 compiles a series of other experiments undertaken each with the purpose of finding new and novel engineering applications for the optical trap. These include:

- Experiment to investigate how the colour of a microspheres effects the optical trapping process.
- Manipulating metallic particles using annular shaped beams formed using a spatial light modulator (SLM)
- An experiment which attempts to fuse of initially silica microspheres and then metallics microscale particles.

Chapter 7 discusses and summarises this body of work as a whole, bringing together the various results and outcomes. It includes recommendations of possible further studies.

Chapter 2

Literature Review and State of the Art

2.1 Optical Trapping

2.1.1 Before Optical Trapping

It is now just over forty years since Arthur Ashkin's initial calculations suggested that a sufficient radiation pressure force could be achieved with a laser in order to cause a microscopic object to move (1). However long before Ashkin, physicists had suggested that photons would 'carry' momentum and thus exert a force, starting with early astronomers (such as Kepler) right through to Maxwell's theory of electromagnetism, which suggested that light may be able to exert force (2).

This early work led two separate groups to attempt to prove the existence of, and quantify, light pressure. Without coherent light sources the radiation pressures were immensely small but both studies nevertheless managed to prove qualitatively the existence of such radiation pressure (3),

(4). One of these groups, Nichols and Hull at Dartmouth University, subsequently went on to quantify their results in 1903 (5,6). The radiation pressures observed were significantly smaller than available today. They measured an average radiation pressure of 1.05×10^{-4} dyne produced by an A.T. Thompson arc lamp, which was neither coherent nor focussed.

2.1.2 How Optical Trapping Began

Optical trapping as we know it began with Ashkin at Bell Telephone Laboratories in 1969. With coherent and highly focusable sources of light then becoming available, Ashkin realised that much greater radiation pressures could be achieved than had been realised by Nichols and Hull. In his seminal paper (1) Ashkin had hoped to quantify the radiation pressure but came across something of possibly greater interest, the gradient force. He demonstrated that the intensity gradient, due to the Gaussian nature of the beam, led objects of high refractive index (relative to that of the surrounding medium) to be drawn towards the axis of the beam. Despite the use of highly transmissive spheres (0.59, 1.31, 2.68μm latex spheres) there was still some reflections which led to a pushing force, down the axis of the laser (a CW argon laser, with wavelength, $\lambda = 514.5$nm). This led Ashkin to his next work: single beam trapping. He achieved trapping using a single beam simply by directing the laser upwards and ensuring the radiation pressure, caused by reflections on the beam's front surface, balanced with the gravitational force on the object (7).

Over the following twenty years Ashkin and his team continued to develop the technology with the first stable optical levitation based trap (8), optical levitation of droplets (9) and finally through to optical tweezers, a single beam gradient force trap achieved through the use of a high numerical

aperture microscope objective in 1986 (10). This was the first system able to trap objects in 3 dimensions without needing to use gravity to counter the pushing force produced by photon reflections.

Since Ashkin's 1986 paper the field has expanded swiftly with many researchers seeing the potential of optical tweezers for all manner of research areas. There have been two excellent extensive reviews of the vast array of research being undertaken with the use of optical tweezers. Moffitt *et al* focusses on the biochemical and biophysical process, including the mechanical properties of biological polymers and molecular machines which drive the internal dynamics of a cell(11). Neuman *et al* focussing on the different optical trapping apparatus employed, such as Spatial Light Modulators(SLMs), Acoustic Optic Deflectors(AODs), piezoelectric stages, calibration methods, and the advances that have been made particularly in biological fields as a result of the technology of optical trapping(12).

As trapping works easiest in water based solutions and with objects in the micron range (of the same order of magnitude as cells) it was only natural that optical tweezers would become a significant tool in the biological field (13). Equally, as it became clear that the forces exerted could be both measured and calibrated such systems appealed to physicists (14,15). However, perhaps surprisingly, there has been much less work in the engineering field. Therefore, the research described in this thesis looks to investigate possible engineering applications for optical traps.

2.1.3 How Optical Traps work

Optical trapping is the term used for the trapping and manipulation of small objects (usually of the micron order of magnitude) through the use of laser light. In reality, there are two distinctly different regimes of optical trapping. Although the phenomenon of optical trapping occurs for both regimes, each results from quite different scientific principles.

The first regime is when the trapped objects are much larger than the wavelength of the trapping laser beam. The second regime is when the trapped objects are much smaller than the wavelength of the light.

The first regime is dependent upon the conservation of momentum of the laser light. This regime can be thought of as a ray optics problem and is thus commonly called the *ray optics regime*(16). In, the second regime, for much smaller objects relative to the laser wavelength, the trapped objects can be thought of as electric dipoles in the electric field of the laser. This regime is commonly referred to as the *Rayleigh regime*(17).

However, in the case of the trapped objects being within one order of magnitude of the laser wavelength, as in this thesis, a combination of the two regimes can be expected(18,19).

The momentum carried by an individual photon, ρ, is defined as:

$$\rho = \frac{h}{\lambda} \qquad \textbf{(Eq.2.1)}$$

Where, h = Planck's constant, λ = wavelength of the photon

Momentum is a vector quantity (i.e. direction dependent), therefore if light is reflected or refracted it will change the momentum of the light.

Newton's Third Law ('every action has an equal and opposite reaction') ensures the conservation of momentum. Therefore, if an object refracts the light passing through it and thus changes the light's momentum vector, the object must experience an equal and opposite momentum change. This leads to a force acting upon the object.

Optical traps usually, though not always, employ a TEM_{00} beam mode. This is essentially a Gaussian beam; that is a beam having a Gaussian intensity profile across its optical axis, in both directions (x and y) orthogonal to its propagation.

The forces produced by this type of beam passing through an object can be split into two components:

- Scattering forces

- Gradient forces

The gradient forces are responsible for trapping the object in the x and y planes whereas the scattering forces are responsible for trapping the object in the z dimension (where the z dimension is the direction of propagation of the laser beam and the x and y dimensions are perpendicular to this).

The gradient forces also arise from the scattering of photons, as in the scattering forces. However, the manifestation of these forces is dependent upon the gradient of the laser intensity profile. This is usually a Gaussian (as shown in **Figure 2.1**). These forces operate in the x-y plane, perpendicular to the direction of propagation by the laser. This force is a restoring force and acts like a Hookean spring. Although the bead may be continually ejected from the centre of the trap by thermal (Brownian) motion, the gradient forces will continually restore the bead back to the centre of the trap (as shown in **Figure 2.2**).

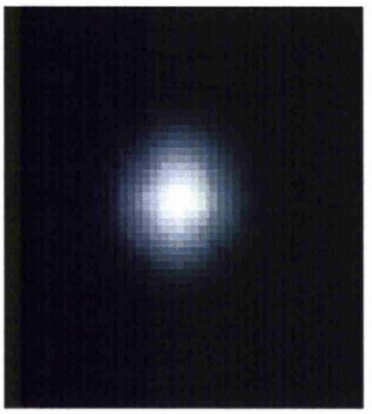

Figure 2.1: A TEM_{00} mode beam. Also known as a Gaussian beam.

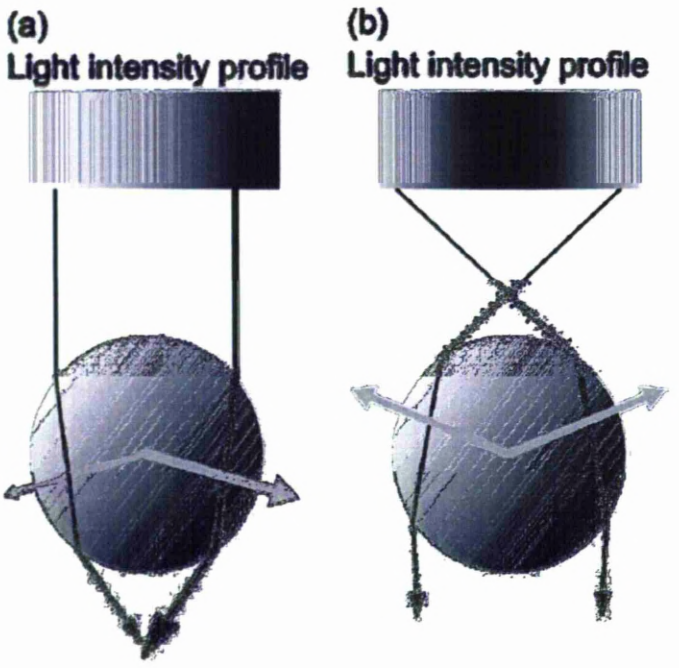

Figure 2.2: Taken from (12). The ray optics regime of optical trapping. The black arrows show the photon propagations. The grey arrows show the resultant force experienced by the bead as a result of the photons.

Figure 2.2 (a) Shows a schematic of a transparent bead within a laser beam with laser intensity increasing from left to right. The light entering each side of the bead is consequently of different intensities leading to greater refraction in one direction (left) than the other (right) and thus a greater reactive force upon the sphere in one direction (right) over the other (left). The black arrows represent the direction of the light. The grey arrows represent the forces exerted upon the bead by the refracted rays. As these forces do not balance the overall force on the bead is to the right, i.e. towards the area of highest laser intensity light and also slightly downwards. Figure 2.2 (b) Shows a schematic of a transparent bead in a stable trap. The lateral (x and y) forces balance due an equal amount of photons being refracted either side the bead's centre. The reactive forces caused by the refracted light, shown by the grey arrows, balance, leading to zero net lateral force upon the bead. The grey arrows indicate a small upwards force which will push the sphere up to the focus of the beam.

The scattering forces are perhaps less easy to understand than the gradient forces. These forces are generated in the same way as gradient forces, from scattering of photons by the sphere.

There are two basic ways in which the photons can be scattered: reflection and refraction. Upon incidence to the bead a percentage of the photons will be reflected entirely at the first surface. For highly transmissive materials (such as silica glass or polystyrene used throughout this study) this percentage is very small. On being reflected, a photon changes direction so, through conservation of momentum, it imparts a large proportion of its momentum to the bead in the direction of laser propagation. The forces produced by reflection alone would cause the bead to be pushed 'down' the laser axis away from the laser source. However, the forces produced by refracted photons being scattered as they leave the bead, now travelling in

a different direction (and thus momentum) to that of when they entered the bead, can produce a force 'upwards' (dependent upon the position of the laser focus) i.e. back towards the laser source. If the resultant scattering force produced by the refracted photons outweighs the force produced by the reflected rays then a stable trap will exist. In the early optical traps the gradient force (7) was quickly established but the reflective forces outweighed the refractive forces leading to beads being trapped in x and y but pushed along the axis of the laser. This led Ashkin to use two counter propagating lasers of equal power to push against one another with the result being an optical trap between the two (20). Although successful this was not satisfactory to Ashkin who would correctly identify that the refractive force element of the scattering forces could be increased if the laser was focussed using a high numerical aperture microscope objective (10). This idea gave birth to true single beam optical traps (or alternatively optical tweezers.)

2.2 Force Measurement with an Optical Trap

2.2.1 Introduction

Optical tweezers offer a unique method of measuring extremely small forces. Forces of the order of pN (10^{-12} N) are typically achieved by many optical tweezer setups (21). The ability to measure forces on this scale accurately is one of the most exciting aspects of the technology. As many of the forces involved in biological materials are of a similar order, this technology has allowed for the precise measurement of forces in a wide variety of biological objects (22).

However, as with any measurement tool, before forces can be measured accurately, the system must first be calibrated.

Firstly it is important to establish which force is being measured. In optical trapping there are basically two main forces which can be measured. The most common, as it is frequently used in many biological applications, is the 'trap stiffness' of the trap. This is essentially a measurement of the spring constant, k, as an optical trap generated from a Gaussian beam operates like a Hookean spring and thus follows Hooke's spring equation (23)(24):

$$F = -kx \qquad \textbf{(Eq.2.2)}$$

Where:

k = trap stiffness, x = displacement of the bead from the trap's equilibrium position, F = force exerted by the trap on the bead.

The second possible force measurement is the 'escape force'. This is the force required to remove the bead entirely from the trap.

The trap can be considered as a potential well; with the trap stiffness being partially dependent on the steepness of the well (in pN nm^{-1}) whereas the escape force is dependent upon the depth of the well. So a trap with high trap stiffness will have a very steep gradient 'well' and a trap with a high escape force will have a deep well though not necessarily with steep 'walls'.

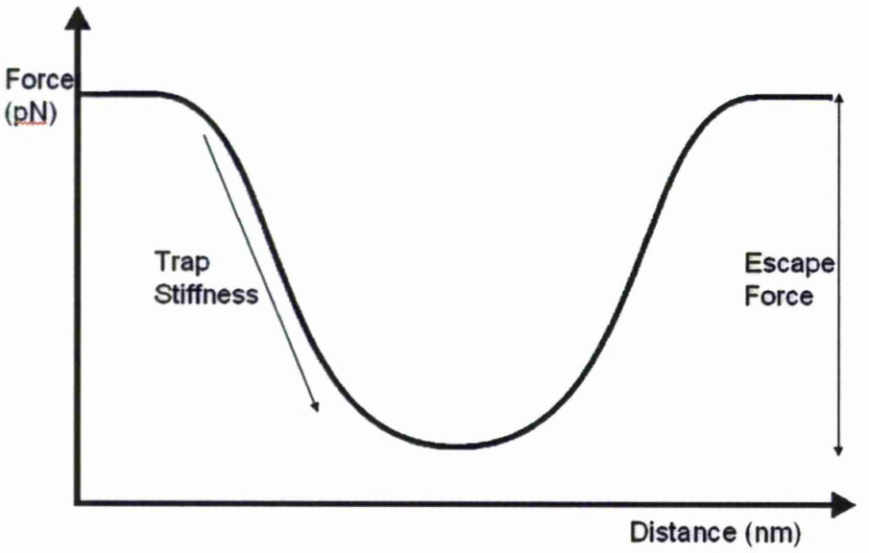

Figure 2.3: A graph to represent the forces of an optical trap. The escape force is the 'depth' in pN of the trap. The trap stiffness is affected by both the gradient and width of the well.

As optical tweezers operate most commonly in a liquid (specifically water for the work in this thesis) there are two main principles of force calibration:

1. Based on Stokes' Law for the drag force – which is made up of two methods based on the same principle.

2. Based on monitoring the dampening of Brownian motion of an object by the laser beam, which again is made up of two methods, as discussed in the next section.

Both methods operate on the principle that an optical trap can be viewed as a spring with a spring constant, k, and will adhere to Hooke's Law

(**Eq.2.2**). These two methods offer alternative ways of establishing the spring constant, k of a trap.

2.2.2 Stokes' Law Method of Force Calibration and Measurement

2.2.2.1 Stokes Method 1 – Simple Drag

Stokes' Law was derived by George Gabriel Stokes in 1851(25). The law is an expression to find the frictional or drag force on a spherical object with a very small Reynolds number (and by definition very small diameter) in a viscous fluid.

Stokes' Law is:

$$F = 6\pi\eta rv \qquad \textbf{(Eq.2.3)}$$

Where:

F = the drag force on the sphere (N), η = viscosity of the fluid (kg m^{-1} s^{-1}), r = radius of the sphere (m), v = velocity of the sphere in the medium (m s^{-1})

As small spheres of the micro scale are available commercially with a known radius and water has a known viscosity, the drag force is only dependent on the velocity of the flow of the water. Hence, the greater the velocity of the water flow past the trapped microsphere - the greater the drag force exerted on the microsphere.

Consequently, as the trapped bead can be moved through the surrounding medium at a known velocity (in practice it is the medium that is moved around the fixed trap position) measuring the displacement of the sphere

from the trap centre allows for the quantifying of the trap stiffness using Hooke's law (**Eq.2.2**).

This can be repeated at a variety of velocities to obtain a characteristic trendline for k, the trap stiffness.

In practice there are some drawbacks to this method. The most obvious of which is that for accurate results, there needs to be a precise knowledge of the viscosity of the water. This is difficult in that viscosity is highly dependent upon temperature and thus any temperature change during an experiment would lead to an inaccurate result. Attempts to measure the temperature during an experiment are also difficult for a variety of reasons. However, even if the temperature of the sample could be monitored during the experiment these results might not be meaningful as it is possible that localised heating would occur in the region of that trap, the overall effect of which would be minimal with regards to the entire sample (26). Secondly, the sample is not entirely water; it usually has a small quantity of surfactant added and also contains the microspheres, these constituents will, albeit only to a small degree, affect the viscosity of the medium. Consequently, this method of force calibration is limited in its accuracy, but does have some major advantages - in that is simple and easy to perform.

2.2.2.2 Stokes Method 2 – Stage Oscillation

This common calibration method involves the same principles as the standard Stokes' law method set out above. However, rather than translate the stage in one direction, the stage is oscillated. The force due to viscous drag is known from Eq.2.3. However, unlike the previous section where a set velocity is inputted, in this method, the variable velocity is inputted.

$$x = x_0 \sin(\omega t) \quad \textbf{(Eq.2.4)}$$

Equation 2.4 represents the position of the stage, x, with time, t, at a frequency, ω, from an initial stage position x_0. As the stage position will mirror its velocity, i.e. at its peak displacement it reaches zero velocity and at its zero displacement it will be at a maximum velocity, its velocity can be expressed thus:

$$v = \omega x_0 \cos(\omega t) \quad \textbf{(Eq.2.5)}$$

Now substituting **(Eq.2.5)** in **(Eq.2.3)** gives:

$$F = 6\pi\eta r \omega x_0 \cos(wt) \quad \textbf{(Eq.2.6)}$$

The signal, S, from the QD, should theoretically follow:

$$S = A\omega \cos(\omega t) \quad \textbf{(Eq.2.7)}$$

This signal from the QD, S, can be measured at a series of frequencies, to establish a series of amplitudes Aω values which produce a series of values for the constant, A, using which an arithmetic mean can be found.

With A now known, **(Eq.2.7)** can be substituted into **(Eq.2.6)** to give:

$$F = \frac{6\pi\eta r x_0}{A} S \quad \textbf{(Eq.2.8)}$$

With all the constants and variables in **(Eq.2.8)** now known, they can be substituted for a calibration factor H:

$$F = HS \qquad \textbf{(Eq.2.9)}$$

Thus, for any signal, S, from the QD an associated force can be found(27).

There are variations to this method, employing a triangular wave instead of a sine wave or by displacing the stage a singular known distance at speed while measuring the response time of the trapped sphere from the QD output.

2.2.3 Brownian Motion Method of Force Calibration

2.2.3.1 Method 1 – Equipartition Method

This method, rather than attempting to ignore or minimise the inevitable thermal/Brownian motion, actually harnesses it to quantify the forces being exerted on a bead by an optical trap. This method is also sometimes referred to as the Equipartition method. In short, it involves accurately monitoring the position of a trapped bead with time. Then, by calculating the variance or standard deviation of the bead's position, the extent to which the thermal motion has been dampened can be quantified. For example, for a loosely trapped sphere, the Brownian motion will be much larger than for that of a tightly trapped sphere.

The formula used to translate the measured thermal fluctuations into a trap stiffness value is called the equipartition theorem and holds true for a particle bound in a harmonic potential (28)(29):

$$k_B T = k\sigma_x^2 \qquad \textbf{(Eq.2.10)}$$

Where k_B = Boltzmann Constant

T = Temperature (K)

σ_x^2 = variance in position of the sphere

k = trap stiffness

As thermal fluctuations are very small (nm scale) this method can only employed if the position of the sphere can be accurately tracked. Indeed, the rate of thermal fluctuations in position mean that the position must not be merely tracked accurately, but also at a very high bandwidth (e.g. 1kHz). Until recently this need for very high bandwidth data capture meant a quadrant detector (QD) (27,30-32). However, the development of high frame rate cameras, alongside increasingly powerful computers has provided another option for the researcher. An interesting comparison between object tracking with a quadrant photo diode (or QD) and a high speed camera was performed (33). This study showed that although the QD remains the more accurate option, the high speed camera can measure object position to an 'accuracy of the order of 10 nm with a bandwidth of a few kilohertz'. The camera also has the advantages of being able to track multiple particles simultaneously and of being able to be calibrated more easily than a QD.

2.2.3.2 Method 2 – Power Spectrum Analysis

As with the previous method of determining trap stiffness, this method involves holding a sphere in a trap while monitoring the sphere position and then analysing the thermal motion of the sphere.

For spheres of known radius, knowledge of Brownian motion in a harmonic potential can be harnessed. The equation of motion of a trapped microsphere can be expressed thus (29):

$$\gamma\frac{dx}{dt} + kx = F(t) \qquad \textbf{(Eq.2.11)}$$

Where k is the trap stiffness, x is the sphere position and γ is the drag coefficient, defined thus:

$$\gamma = 6\pi\mu r \qquad \textbf{(Eq.2.12)}$$

Where μ is the viscosity of water and r is the radius of the sphere.

F(t) is produced by thermal fluctuations, thus it has two significant properties(34):

1. Its fluctuations are random
2. Its mean equals zero

It has been shown that through Fourier analysis, a one sided power spectrum of the thermal fluctuations, which has characteristic features of the trap stiffness, can be produced (12,30,32).

Taking the Fourier transform of both sides of (Eq.2.11) gives:

$$2\pi\gamma(f_c - if)X(f) = F(f) \qquad \textbf{(Eq.2.13)}$$

Where, f_c, the characteristic corner frequency is defined:

$$f_c = \frac{k}{2\pi\gamma} \qquad \textbf{(Eq.2.14)}$$

Therefore, by finding the corner frequency, (sometimes referred to as roll off frequency) f_c, of a power spectrum of the thermal fluctuations of a trapped sphere, the trap stiffness, k can be found.

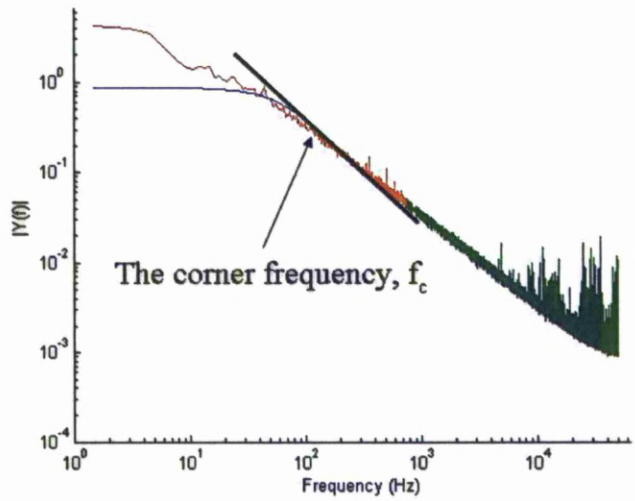

Figure 2.4: A single sided power spectrum of a sphere's position showing the characteristic corner frequency, f_c.

2.2.4 Previously Achieved Force Measurement Results

Much of the work undertaken in this area has been in the biological arena. However, this work will focus on more fundamental variables, such as how the force exerted on the microsphere is affected by the sphere diameter or laser power.

It is also worth noting that some studies use the dimensionless trapping efficiency, Q, as a way of quantifying the quality of the trap as opposed to conventional the more conventional method – trap stiffness (35).

Q is defined as such:

$$F = \frac{nQP}{c} \qquad \textbf{(Eq.2.15)}$$

Where:

F = Force (piconewtons), n = the refractive index of the surrounding medium, P = the laser power (mW), c = speed of light in free space

Simmons *et al* produced one of the early experimental studies on trapping forces for such fundamental variables (32). In their work they investigated the bead diameter and laser power's effect on the trap stiffness. They also investigated how the escape force (the depth of the potential well) varies with laser power:

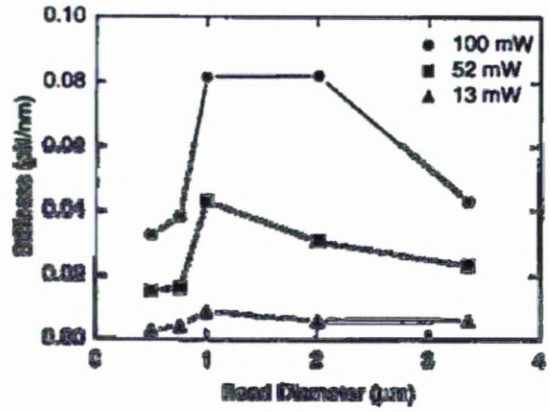

Figure 2.5: Taken from (32). Showing the effects of both the bead diameter and laser power on the trap stiffness.

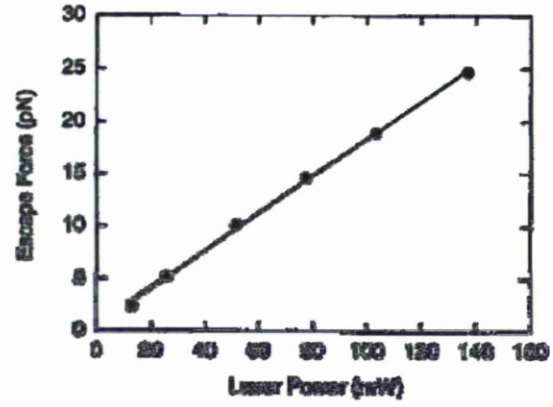

Figure 2.6: Taken from (32). Demonstrating how the escape force increases proportionally with laser power.

Wright *et al* reported a study which aimed to evaluate the accuracy of the ray optics model of optical trapping of polystyrene and silica microspheres

by comparing their model with actual results (15). They found the ray optics model (16) matched very closely with experimental results in the axial direction (z axis/axis of laser propagation) and reasonably closely in transverse forces (x and y axis) for spheres greater than 10μm with a laser wavelength of 1064nm. For spheres of 1μm diameter, the transverse forces were comparable but the axial forces measured were considerably stronger (5x) than the model suggested (15). Wright's study also considered microscope objectives of different numerical apertures (NA) and showed strong evidence that the NA was a significant factor on the axial trapping force generated by the laser.

Alongside the experimental data produced, there have been many mathematical approaches, with various modelling papers produced analysing the forces in optical trapping (15,36-42). Nieminen *et al* have shown mathematically how the forces experienced by a trapped object change with the shape of the object. They considered polystyrene spheroids and cylinders of varying aspect ratio and showed that the shape of the object becomes less significant upon the forces experienced, the smaller the object. Furthermore, they found little difference in the forces experienced by spheroids versus cylinders of equivalent aspect ratio (42).

2.3 Overview of Applications of Optical Traps

2.3.1 Introduction

This section of the literature review will look in detail at the various applications of optical traps. A large proportion of optical trapping applications have involved biological applications, these will be only addressed in section 2.4.5. However, the main purpose of this review, and

indeed this thesis, is to look at possible engineering applications for the optical trap.

2.3.2 Engineering Applications of Optical Traps

Although optical trapping was first fully achieved (i.e. with only one beam and trapping in three dimensions without the assistance of gravity) in 1986 (10), there has since been a surprisingly small amount of work with optical traps in the engineering field. This may well be due in part to optical trapping naturally lending itself to biological applications. The forces involved in optical traps were quickly established to be of a similar order ($\approx$ pN) as those involved in biological material (16,19). This fact, together with the need for optical traps to operate in solution, naturally led researchers to look, for the most part, towards biological applications for new and novel applications. However, there have been a number of interesting studies in which the optical trap has been used as an engineering tool across a wide range of engineering based applications.

Ghadiri *et al* have developed a microfabrication technique through the use of optical trapping (43). They used an infrared laser to trap and hold an array of polystyrene microspheres through the use of a Spatial Light Modulator (SLM). Their sample consisted of 12μm spheres coated in the protein Streptavidin (SA) and 3.5μm spheres coated in the vitamin, Biotin. When put in contact Streptavidin and Biotin form strong bonds (the strongest non-covalent binding known) including hydrogen bonds. The smaller Biotin coated spheres were used as 'binding parts' to connect the larger Streptavidin spheres.

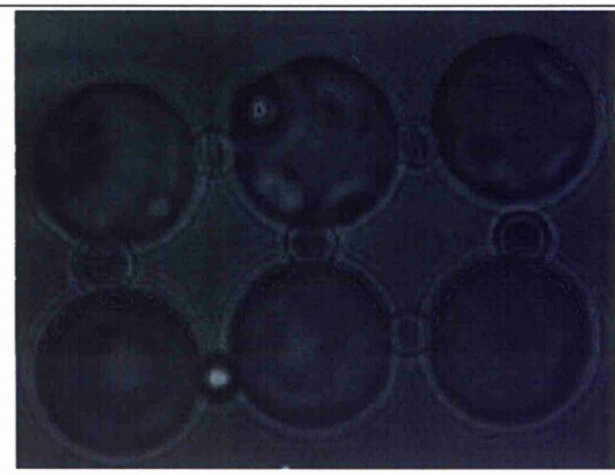

Figure 2.7: Taken from (43). A 2x3 array of the Streptavidin coated 12mm polystyrene spheres. Joined by the Biotin coated 3.5mm polystyrene spheres.

As soon as the Biotin and the Streptavidin come in to contact a bond is immediately formed. Moreover, the bond formed is then strong enough to withstand conventional optical forces in the piconewton range. So once built, these are stable structures which can be added to further but not de-constructed.

Chapurlat et al successfully devised a method of joining microspheres in an optical trapping environment (44). They were able to join the spheres by using a novel material for the spheres. They made the microspheres by 'salting out of hydrophilic resin, ENT-3400'. They then overcame some difficulties with the wide range of diameter spheres produced by this process. Having successfully established a population of microspheres with a similar diameter they were then able to link the microspheres selectively to each other using a UV source, as seen **Figure 2.8**.

Figure 2.8: Showing the produced 'tethered tool'. The darker top left corner of the tool is fixed to the surface. The rest of the tool can be manipulated using several optical traps using SLM. Taken from (44).

The Glasgow optical tweezers group has provided many excellent pieces of work in the wider optical trapping field largely specialising in developing the capabilities of SLMs through their various computer generated hologram programs. Their 'micro hand' work (see Figure 2.9) is perhaps the most relevant to engineering applications. They managed to link directly the movement of the controller's actual hand, or more specifically finger tips, to the movement of silica spheres which could be moved in such ways to manipulate metallic materials through the use of an SLM and ultra-fast hologram regeneration (45).

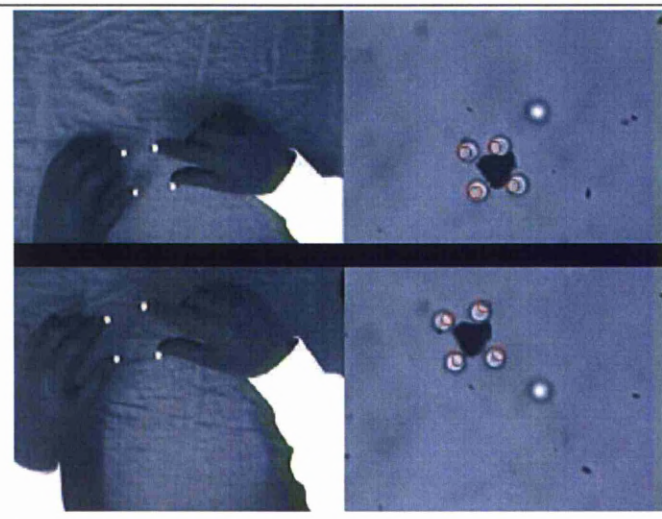

Figure 2.9: Taken from (45). Showing the split screen user interface and trapped beads (5μm diameter). The microhand is used to select and manipulate the position of an irregularly shaped and opaque chrome particle.

Glasgow's LabView based program was able to take the input video from the left hand side of **Figure 2.9**, 'see' the four white spots on the user's thumbs and the index fingers, then produce a hologram for the SLM to use in order to produce trapping sites at the same relative distances apart. Moreover, the program would constantly update and refresh the hologram as any movements in positions of the white dots were detected.

The Glasgow group also achieved some very interesting results in the work to develop and assemble 'micro probes' using optical trapping (46). They first identified a common problem of using microspheres as probes for force measurement that using smaller microspheres means greater Brownian motion of the sphere and thus less position control; and using larger microspheres as probes leads to imprecise knowledge of the interaction area between the side of the sphere and the material being

probed. Having identified this problem, they attempted, with considerable success, to assemble 'nanorods' which included microspheres to act as 'handles' so that they could then be manipulated via holographic optical trapping. They employed the Biotin-Streptavidin bond method suggested previously, coating the silica microspheres in Streptavidin and the nanorods in Biotin:

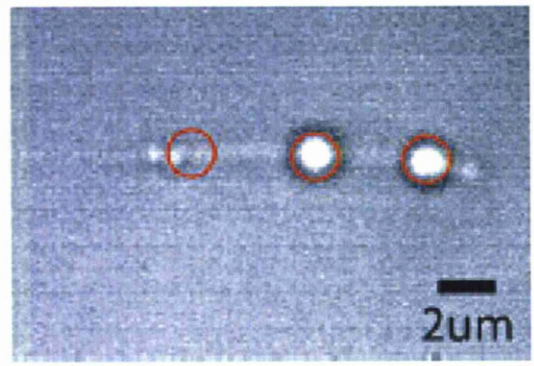

Figure 2.10: 2μm diameter silica spheres joined with a 300nm diameter nano rod which is approximately 12μm in length. The red circles denote the locations of the optical traps. By moving these trap positions the probe can be manipulated. The red circle furthest to left is employed to hold the probe tip in focus. Taken from (46).

Perhaps the work most closely associated with the work presented in this thesis is that of Ito *et al* in 2002 (47). There are some large differences such as the magnitude and material of the spheres used but fundamentally both this work and that of Chapter 5 were about precise placement and fixing of objects to a surface through the use of optical trapping. Ito *et al* used gold nanoparticles, of the order of 80nm, optically trapped them and brought them down to the surface. The regime of trapping was that of Rayleigh scattering due to the size of objects being much smaller than the wavelength of the laser (as opposed to the ray optics regime as with the

work throughout this thesis). A 1064nm beam was used to trap and place the objects, and a 355nm UV beam was used for the fixation of the gold nanoparticles to the glass substrate.

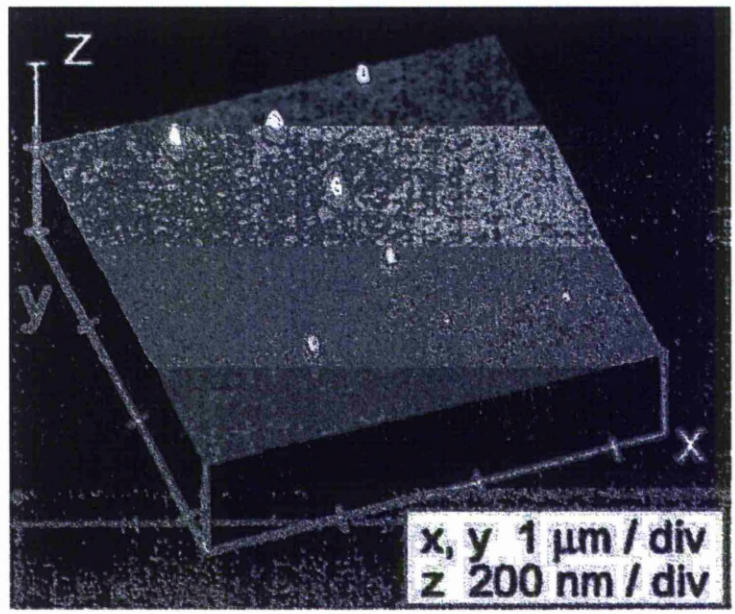

Figure 2.11: Atomic Force Microscope image of fixed gold nanoparticles on a glass substrate. Positioned to form the letter 'I'. Taken from (47).

2.3.3 Other Optical Engineering Processes

It is worth considering the other possible methods of optical engineering specifically for micro and nano scale formations and devices.

Over the past decade alternative optical engineering approaches to optical trapping have developed via the use of novel chemical microfabrication techniques such as two photon polymerisation (48).

In 2001, Klein et al employed a novel method for creating patterned surfaces via direct-write lithography (49). A tightly focused, low power, infrared beam was 'applied to a homogenous precursor solution containing soluble reagents'. When the laser was focused precisely on to the glass-solution interface it induced the 'local precipitation of a solid product that attaches firmly to the substrate'. This allowed for the production of small islands of material by applying the laser for only a small time period or alternatively creating continuous lines of material by the translation of the stage during a prolonged laser exposure. A range of materials have been successfully used such as silver, gold and copper oxide. The use of silver potentially offers further capabilities via the use of further chemical reactions for the functionalization of the silver surface (49).

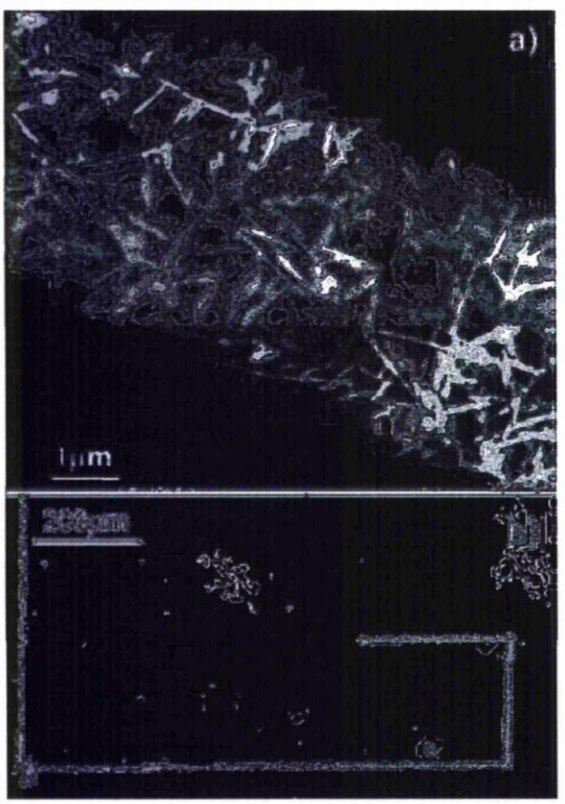

Figure 2.12: Taken from (49).Showing a) high and b) low magnification (SEM) images of a silver line produced by the above explained method. Silver line width ranges from 6-10μm.

Two photon polymerisation has become an increasingly significant tool in terms of optical engineering in recent years. Conventional photopolymerisation was first reported in 1993 (50). A variety of structures, including a coil spring (50μm in diameter and 250μm in length) and a micro valve, were achieved by selectively curing a liquid resin using a UV source. The power of the UV source (Xenon lamp) was selected so that the liquid resin would only be cured at the focus. Then by scanning the focus of the UV source in x, y and z, three dimensional structures could be created. The limit to the resolution of such structures is the smallest possible volume that can be cured at a time. This is largely dependent upon the ability to focus the light down. This study(50) had used conventional one photon absorption of UV light. However, 'two photon absorption', a process developed by Strickler and Webb using infrared light instead of UV light (51), allows for much greater resolution. This greater resolution is due to the probability of two photon absorption occurring being much less than the probability of single photon absorption. The probability of two photon absorption occurring is directly proportional to the light intensity. Once a volume has been cured, all of the uncured resin can be easily washed away using conventional solvents. The first three dimensional structures achieved using the two photon absorption method were achieved in 1997 by Kawata *et al* (52). They successfully demonstrated the technique which allowed for the curing of micro scale volumes of resin in precise and selectable geometries, as seen in **Figure 2.13**:

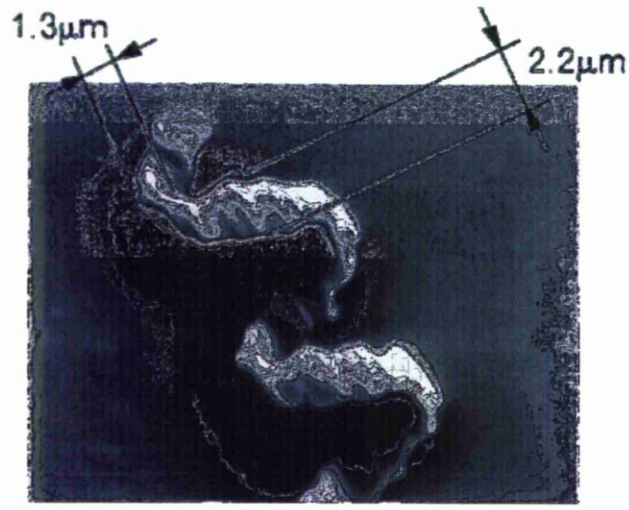

Figure 2.13: Micro fabricated shape. Taken from (52).

Since then there have been various similar works creating a variety of 'micromachines'. The resolution achievable is still being improved upon. In 2001, a micro spring (or more accurately a micro oscillator) was reported with a spiral diameter of just 300nm (48).

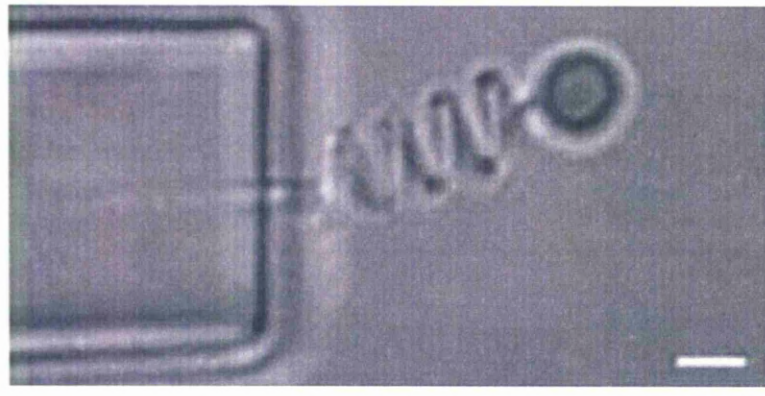

Figure 2.14: Taken from (48). Fully functional micro oscillator which was produced entirely using the two photon absorption mechanism. The bead

on the end of the spring is optically trapped and 'pulled' and then released to set the oscillation in motion. The scale bar represents 2μm.

Galajda and Ormos employed the two photon polymerisation technique alongside conventional optical trapping to construct micro scale devices and then used optical trapping techniques as a way of driving their devices (53). Using two photon absorption, specially designed optical rotators were formed. These rotators were then driven using optical forces:

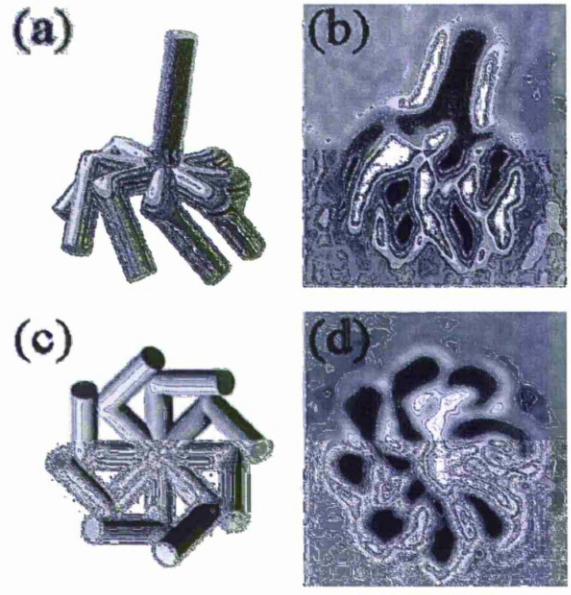

Figure 2.15: (a) and (c) Show the geometry of the designed optical rotator from different angles. (b) Shows the produced device not trapped. (d) Shows the rotator trapped and held in focus so as to achieve reasonable image quality (53).

The above technique is particularly interesting in that it not only using optical trapping to construct the device but it then harnesses the photon momentum forces, provided by the laser, to actually drive the device.

2.3.4 Near-field Processing

Traditional optics operate in the far field and follow traditional laws of optics. However, near-field optics allow light to be focussed to below the diffraction limit. Studies have shown, both mathematically (54) and experimentally (55) the successful use of microspheres as near-field lenses to focus light down below the diffraction limit to a point of high intensity just below the sphere.

In addition to these there have been several interesting studies using optical traps to assist near-field processing, perhaps the most successful being with the use of Bessel beams to force microspheres down to a surface before processing the surface through the trapped sphere. This method allows for direct writing straight on to a surface, producing features of the order of 100nm (56). This direct-write approach certainly enhances the versatility of the near field process.
The motivation for the interest in near-field optics in this work is the possible controlled placement of spheres, through use of the optical trap, into a desired array.

Near-field processing of large areas has been restricted to random arrays of spheres (55) or self-assembling arrays of spheres (for example hexagonally close packed silica spheres (57). This inability to position the spheres in any desired array limits the process to arrays that will naturally assemble. If optical traps could be employed to position the spheres in a surface this could lead to the manufacturing of a reusable device for near-field processing. An example of a possible design for such a device is shown in **Figure 2.16**. The precise nature of such a device, the method for

constructing such a device and the results of the work are discussed in detail in Chapter 5.

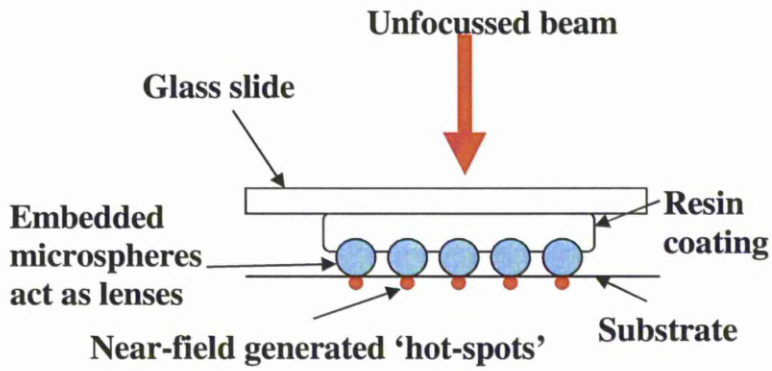

Figure 2.16: An example of what a reusable device for near field processing could consist of.

2.3.5 Biological Applications

As referred to previously, the vast majority of applications in optical trapping to date have been in the biological field. The ability to address individual cells to measure precise forces associated with the cells while causing minimal damage to the cells has made the application unique and invaluable to researchers in the biosciences field. Although biological applications of optical trapping are by no means the focus of this thesis, it is important to discuss them in order to put in to context optical trapping as a current research tool.

Optical traps have become of particular use in single molecule research (58). Forces in standard optical trapping systems are usually of the order of

piconewtons. This is of the same order as forces associated with biological cells. Most cells are highly transmissive to infrared light, and are thus, able to remain undamaged when subjected to such wavelengths. Hence making optical trapping well suited for biological applications (22).

As with much of the work within optical trapping, Ashkin et al led the way. They first trapped tobacco mosaic virus using approximately 120mW of an Argon laser without causing any clear damage to the virus (13), manipulated individual cells (59), and significantly, first measured the force of cell organelle movement inside a living cell (60).

More recently, holographic techniques, such as spatial light modulators (SLMs) have been harnessed to achieve cell sorting capability (61-63)

Guck et al harnessed two counter propagating beams to produce an optical setup capable of stretching cells along the optical laser. Furthermore, through the use of a microfluidic system they were able to give the system high throughput capabilities (64).

A variety of different cells sorts have been probed, using optical trapping, to learn about the mechanical properties of a cell. Such cell types include red blood cells (65), live sperm cells(66-68). Sheetz *et al* produced an important study of the mechanical properties of membranes of migrating neuronal growth cones by using an optical trap to pull out membrane 'tethers'and measured the required force (69).

For more extensive insight in to optical trapping's ever increasing role in biosciences research please refer one of these review papers, although note that they focus on the biological outcomes achieved as oppose to the nature and setup of the optical trapping systems used (12,22,70).

2.4 Summary

Optical trapping has developed from an idea (1) to a widely used technology at an impressive rate (70). This literature review has set out the way in which the optical trapping technology developed and the applications and experiments it has already enabled across many different scientific disciplines. As this thesis aims to develop optical trapping from an engineering perspective, the literature review has included other optical engineering technologies such as two photon polymerisation and near-field processing. This literature review puts begins to put into context the new work reported in the subsequent chapters. Although much optical trapping work has clearly been undertaken, there are still plenty of under explored areas. The work presented in rest of this thesis aims to add new and significant knowledge to the optical trapping field by approaching optical trapping as a whole, considering the development of the trapping system to enable new studies a fundamental part of the work. The understanding gleaned from this literature review on the fundamental physics behind optical trapping will better inform the engineering and experimental decisions taken throughout the subsequent optical trapping system development and experimental phases of this body of work.

Chapter 3

System Development and Initial Results

3.1 Introduction

For the experimental work in this research study to be undertaken, an optical trapping system had first to be designed and built. Over the course of this project a number of different optical trapping setups have been conceived although all contain the same set of fundamental components: a laser, a high numerical aperture objective and a stage in which to mount the sample. In addition to these basic components, there are various additional items that can be employed to give the system greater capability, such as a spatial light modulator or acousto-optic deflector (for more than one trapping site), a piezo electric stage (for greater control over the movement of the sample relative to the laser), a quadrant photo diode (for high precision monitoring of sphere position), or tracking software (for tracking of multiple objects).

The challenge was set to develop a system with versatile and extensive capabilities for the pursuit of new and novel engineering applications. This occurred over an extended period as more hardware became available which could be integrated into the system and more software was written to solve various issues encountered.

As problems and limitations in the system were encountered, solutions were found and new hardware was acquired to enhance the current capabilities of the optical trapping system. Over the course of this research a number of redesigns and rebuilds of the system took place, each time to address a particular problem discovered or to enable a new capability for the system. The final system would incorporate a second laser source, high precision position tracking (though use of a Quadrant Detector), a Spatial Light Modulator, a piezo electric stage, capable of nano scale movements, mounted upon the existing mechanical micro stage and a diode illumination source. This is set out later in this chapter. The system was specifically designed for the purpose of exploring innovative engineering applications for optical traps.

The system's development can be divided into four main stages:

1. The Initial Setup
2. Integration of an SLM
3. Addition of Force Measurement Module and Nano stage Integration
4. Integration of a Second Laser Line

A discussion on the details and progression of these four stages will be the basis for most of this chapter. As new hardware and software are

introduced their details will be given. The problems encountered during this development process will be documented, as will be their corresponding solutions.

The final system produced represents significant work and produced a unique system which fulfilled the criteria of being both versatile and enabling new investigations and new capabilities. Showing the detailed progression of the system, from its initial basic setup through to completion alongside the motivations for each change/development, should enable a greater understanding of the practical use of optical traps, including the common optical trapping pit-falls which are not frequently referred to in the literature.

3.2 The Progression of the Optical Trapping System Development

3.2.1 The Initial Setup

The original system available at the beginning of this research project was a basic inverted optical trapping system which had been constructed to specification by Elliot Scientific (71).

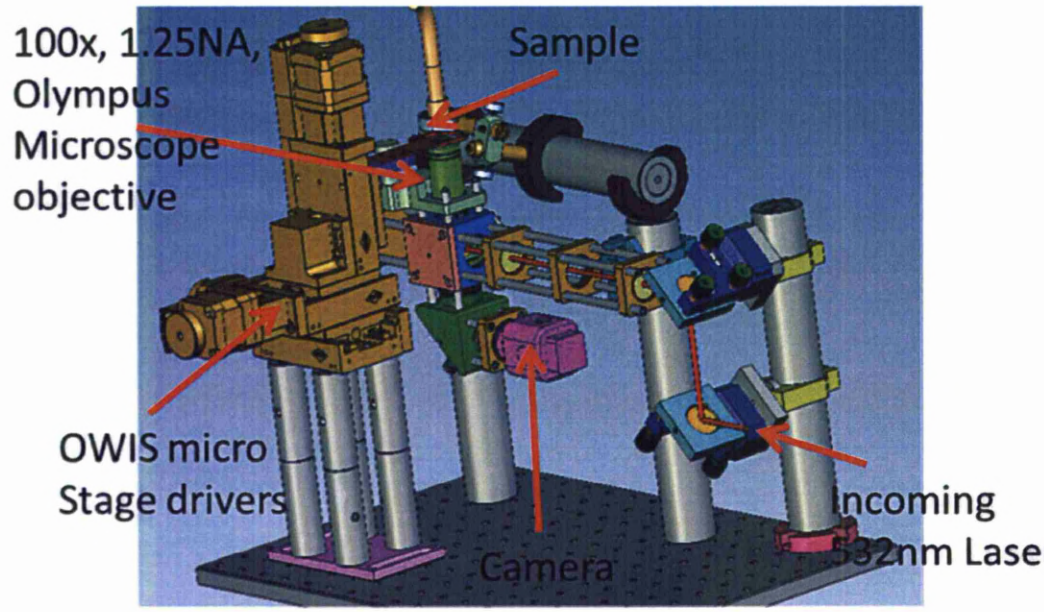

Figure 3.1: Partially taken from (71). The original inverted optical tweezer design.

The system consisted of a single green, 532nm, continuous wave, 2W laser source delivered via standard optics to a high NA (1.25) microscope objective and a mechanical stage capable of micron scale movements of the sample.

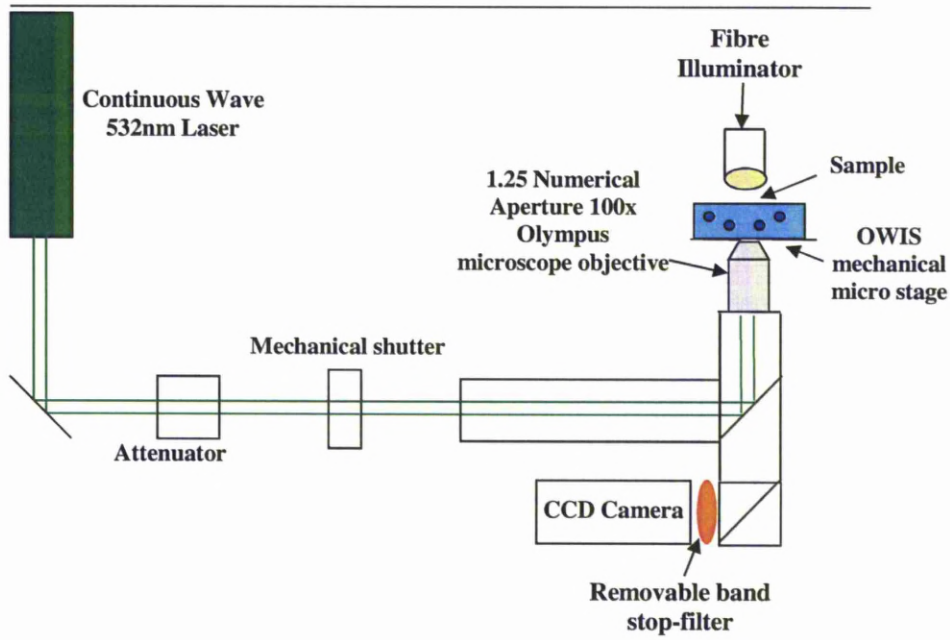

Figure 3.2: Initial Optical Tweezer System Setup

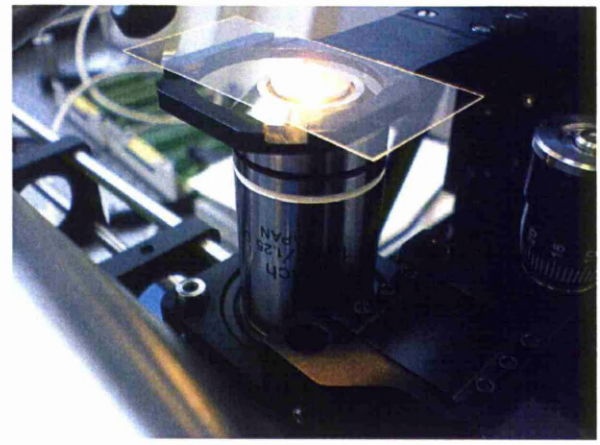

Figure 3.3: Cover slip loaded in original sample holder within the system

3.2.1.1 Hardware

3.2.1.1.1 Coherent Verdi 532nm Laser

The Verdi laser is part of the YAG (yttrium aluminium garnet) family. The various forms of YAG make up most of today's solid state lasers.

Neodymium-doped yttrium orthovanadate or Nd:YVO_4 (Vanadate) is the lasing material used in the Verdi. It is frequency doubled to produce a wavelength of 532nm at up to 2W continuous wave. It is a high quality laser in terms of its M^2 value and bandwidth. It operates with a beam mode of TEM00 and has an M^2 value of less than 1.1. The laser also possesses a bandwidth narrower than most lasers. Although most lasers quote a wavelength to an accuracy of individual nanometres, i.e. a 1064nm or 532nm lasers, in reality lasers usually occupy a broader range of wavelengths than such names imply. The specification of this laser quotes a linewidth of <5MHz which is equivalent to approximately 5 femtometres. Thus, in the case of the 2W Coherent Verdi it can be considered a true single frequency laser.

3.2.1.1.2 OWIS Micro Stage

This is a mechanical motorised stage capable of micro scale movements in x, y and z. The micro stage is controlled through a basic LabView software interface provided in the initial setup. This software allows for the use of a joystick to manoeuvre the stage in x, y or z. The stage and software provide the capabilities of moving the stage at a vast range of speeds. The

minimum and maximum stage velocities are approximately 0.002 mm s^{-1} and 1 mm s^{-1} respectively.

3.2.1.1.3 Microscope Objective

The microscope objective used in the system is an Olympus oil immersion objective. Its magnification is 100X and when used with an oil interface, its numerical aperture, NA, is 1.25. As discussed in chapter 2, having a high numerical aperture (NA) is critical for full three dimensional optical trapping. Without a high NA objective, trapping can be achieved in x and y but not in the z dimension (where z is the direction of propagation of the laser beam) as in (7). A critical factor in the use of a high NA objective, overlooked in the early stages of this work, is that it means a small working distance from the tip of the microscope objective to the focus, 0.150mm for this objective. Numerical aperture is a dimensionless number and is given from:

$$\text{Numerical Aperture (NA)} = n(\sin \mu) \qquad \textbf{(Eq.3.1)}$$

Where, n is the refractive index of the medium between the top of the microscope object and the glass cover slip. This is usually air or oil. μ is half of the angular aperture, see **Figure 3.4**.

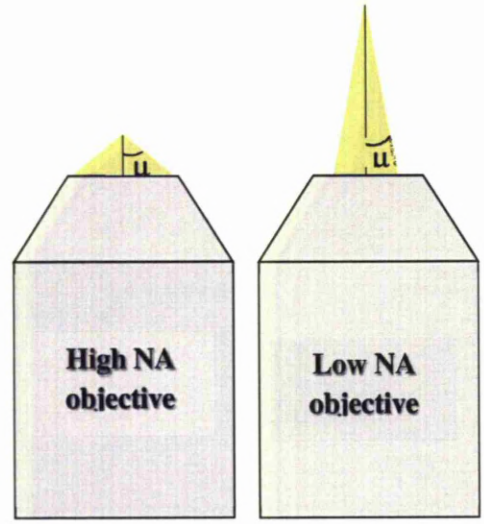

Figure 3.4: The tightly focused nature of a beam from a high NA objective. Showing how the working distance changes with NA.

As can be seen from **Eq. 3.1**, when the imaging medium is air (which has a refractive index = 1), the NA is dependent only on the angle, μ, shown in the above figure. As the sine of any angle has a maximum value of 1, the theoretical limit of NA, for an objective with air as the imaging medium, is 1. Hence, to achieve the high NA required for optical trapping, a different medium with a greater refractive index must be used. Modern microscope objectives are designed for a specific medium, such as water, which has a refractive index = 1.33, to achieve a greater NA.

The microscope objective employed in this system is an oil immersion (which has a refractive index = 1.51) objective. This implies that in theory an NA of 1.51 could be achieved for a sin (μ) value equal to 1 (from μ = 90°). In practice the majority of oil immersion objectives are only able to achieve NA values up to 1.4.

The NA of the objective in the system is quoted by the manufacturer as equal to 1.25. From **Eq.3.1**, this implies a μ value equal to approximately equal to 56°.

3.2.1.1.4 CCD Camera

The charge coupled device (CCD) camera employed in the system is a *Watec LCL-211H*. It is a high resolution (480 TV lines), high sensitivity camera which provides the capability to acquire accurate and detailed real time images at the focal plane of the optical trap within the sample. The camera operates at approximately 30 frames per second.

3.2.1.1.5 Mechanical Shutter

A mechanical shutter sits in the laser line to provide usability and safety to the system. The shutter is addressed electrically and can switch between closed and open modes either through manual operation or at a pre-programmed rate. The shutter is a Thorlabs SC10.

3.2.1.1.6 Computer System

The computer system used throughout this work was an Intel Core2Duo 2 GHz system with 2 GB of RAM. This level of processing power is required in order to run multiple LabView programs, especially the

'memory heavy' Fourier transform programs discussed in the next section such as *Blue Tweezers*. The system included two monitors. One monitor is used to display the live footage obtained from the CCD camera. The other monitor is used to display the various LabView programs in operation during use of the optical trap.

3.2.1.2 Software

LabView is a graphical system design software package. It enables the user to quickly develop and adjust project specific programs that can communicate with and coordinate various pieces of hardware, as well as acquiring data.

The software in the initial setup consisted of two programs:

1. The 'Joystick Axis Control(1)' program:

This program was written in LabView, to allow for the manoeuvring of the mechanical micro stage in x, y and z, via the use of a joystick at a variety of speeds. The program included the use of the 'slide bar' on the joystick to give a spectrum of velocities from which to select.

2. The 'Vision(1)' Program:

This basic program was written in LabView through use of LabView's *Vision* package. This program provided the capability both to access and to view the video footage being acquired by the CCD camera in the system.

3.2.1.3 Initial Results and Discussion

This was a basic optical trapping system consisting of the fundamental elements but nothing further. Moreover, although consisting of all the fundamental components, the optical trap did not work. An influence over microspheres from the laser was observed but true optical trapping, the tight holding of a microsphere in the focus of the laser, all three dimensions, for an indefinite period of time, was not achieved. This led to a period of investigation to solve why trapping was not occurring. Initially, a full realignment process of the laser was undertaken. To an extent, this appeared, through manual observation, to improve the quality of trapping in x and y. However, this was still less than satisfactory optical trapping in these dimensions and there was no trapping achieved in the z dimension. Essentially, when the laser was passed near a microsphere, the sphere would be seen to be 'pulled' toward the centre of the trap and then 'pushed' away along the axis of the laser. Clearly the laser was impacting upon the spheres as desired in x and y, but in z, the sphere was being pushed rather than trapped.

It was postulated there could be numerous explanations for this and each was to be assessed to establish the source of the problem:

First, the laser wavefront was profiled; see **Figure 3.5**, through use of an LBA (Laser Beam Analyser) to check that the beam mode was of the high order specified by the manufacturer. The optical forces responsible for conventional optical trapping are highly dependent on a Gaussian beam for generation of a gradient force.

As can be seen in the subsequent image, the raw beam of the Coherent Verdi was shown to be approximately 3mm in diameter, as was expected from the Verdi laser specification.

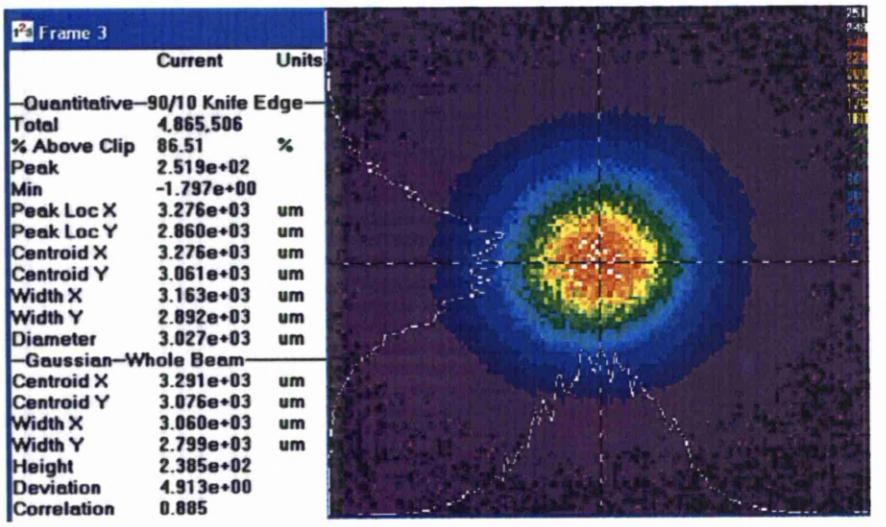

Figure 3.5: LBA image of the raw beam of the 532nm Verdi before the microscope objective, showing a beam diameter of approximately 3mm. and a slight ellipticity in the beam; with the beam wider in the x dimension than in the y.

This image confirmed the high quality of the laser beam mode and thus ruled out the possibility that it was the laser causing the lack of trapping through diminished beam mode quality.

Secondly, through a good understanding of how lasers exert forces in optical traps, as described in Chapter 2, it was hypothesized that the gradient forces were sufficient, causing the trapping in x and y, but the scattering forces, responsible for trapping in the z dimension, were too small. So the scattering forces would need to be increased to achieve true optical trapping in three dimensions. The insufficient scattering forces are

caused by using a microscope objective with an insufficient numerical aperture or by not filling the back surface of the microscope objective aperture. It has been suggested in some studies that overfilling the back aperture of the microscope objective is preferable (72). This work acknowledges that overfilling the aperture will lead to a degree of power loss but in a process which requires very small powers this is not a major problem. Furthermore, the overfilling of the aperture ensures a high flux of photons are delivered from the outer edges of the beam into the outer edge of the aperture. In a high NA objective, the photons in the outer regions of the aperture are refracted the most and thus generate the largest scattering forces due to the high angles with which they are incident upon a sphere. If the back aperture of the microscope objective is only partially filled, as here a 3mm diameter laser beam incidences on a 5mm diameter back aperture, no photons will enter the objective at the edges of the aperture, and thus will not experience the maximum possible refraction from the lens configuration within the objective.

Consequently, it was decided to install a beam expander to increase the beam diameter from the raw beam's 3mm to 6mm, i.e. greater than the 5mm diameter of the microscope objective's back aperture.

This beam expander consisted of two lenses arranged in a standard Galilean beam expander set up, as shown in the subsequent figure.

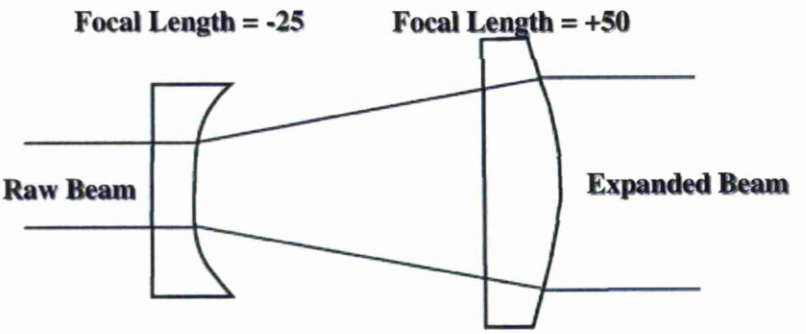

Figure 3.6: Galilean Beam expander setup. Producing a magnification factor of 2. Expanding the raw beam from approximately 3mm to 6mm.

With the above beam expander now in place, the back of the microscope objective was now being overfilled, thus ensuring energy was located in the edges of the beam, which were responsible for generating the bulk of the scattering forces, which provided trapping in the z dimension. However, with the expander in place, trapping in the z dimension remained unsatisfactory so the investigation continued to find the source of the problem.

Minor ablation damage in the plastic cover area surrounding the back aperture of the objective was observed. It was suggested this might be the source of the issue, thus causing the microscope objective not to realise its quoted NA value of 1.25. An investigation was undertaken employing an alternative microscope objective. This alternative microscope objective (Nikon, 0.9NA, x100) had a smaller NA than is usually required for optical trapping (at least 1) but the reasonable quality of the objective and its relatively high NA implied it might be of use at least to establish if the minor damage on the original objective was causing the trapping problems.

Surprisingly, with this lower NA objective in the system, the quality of trapping in the x and y dimensions improved considerably but again z

trapping was less than stable. In half dried out samples and thus shallow conditions, the beads are unable to move in z hence trapping can be achieved. However, this would not be considered true optical trapping. Additionally, while using this lower NA microscope objective an interesting phenomenon was observed:

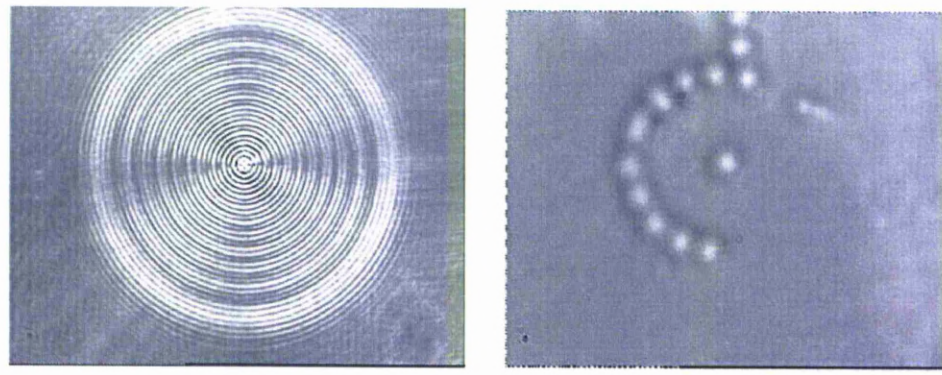

Figure 3.7: Left – The beam profile produced by the lower NA objective. Right – A 2.44μm silica sphere trapped and the centre of the trap within a further semi-circle of trapped spheres, trapped due to the optical landscape on the left.

This profile is seen when the laser is slightly out of focus relative to the focus of the camera. This annular profile is caused by constructive/destructive interference of the laser with itself. Although the use of this second objective gave the interesting result shown in **Figure 3.7**, it was clear that reducing the NA of the microscope objective would not be helpful in attempting to generate the necessary scattering forces to trap in the z dimension, thus the original high NA (Olympus 1.25) objective was returned to the system.

The cause of the z dimension trapping problem was eventually established as the thickness of the cover slips. The thickness of the cover slips used up

to this point in the research was measured, using digital calipers, to be 0.19mm. When these cover slips were replaced with marginally thinner cover slips, measured as 0.17mm, the effect was significant. With the thinner cover slips employed, trapping in the z dimensional was now stable. The cause for this significant change was the position of the laser focus relative to the cover slip. For example, if too thick a cover slip is used, such as the 0.19mm cover slip, the focus of the beam would occur inside the glass cover slip. Thus, within the water medium the laser is already diverging at a rapid rate, meaning that a degree of x and y trapping may still be achieved but that the microspheres appear to be 'pushed' away from the objective towards the top surface and out of the visible region of the sample. Whereas, once the thinner, 0.17mm, cover slip was used, the focus occurs beyond the cover slip, and thus within the sample medium. Note the small difference between the dimensions of the successful and unsuccessful cover slips. A difference of 20μm can make a significant difference. In theory it is also possible to have a cover slip that is too thin leading the laser focus to be beyond the water region of the sample though this is unlikely given the common thicknesses of cover slips and usual working distances of the high N.A. objectives.

3.2.2 SLM Integration

With high quality and efficient trapping now being achieved on the system it was time to enhance the capability of the system. The possibilities of optical trapping are greatly increased if multiple traps are available simultaneously. This can be achieved through use of one of two devices, a spatial light modulator herein referred to as SLM (73,74) or an acousto-optic deflector herein referred to as AOD (75,76). AODs operate via time

sharing the beam amongst multiple spots. Whereas, SLMs operate by taking a single laser beam, and producing multiple spots simultaneously through the use of a hologram.

SLMs also have the capability to modify the intensity and phase of a beam. More recent work allows for the modification of the polarisation of a beam when in conjunction with other optics such as half and quarter wave plates (77).

SLMs are a swiftly growing technology with a wide variety of applications in photonics such as laser parallel processing (78,79), pulse shaping (80) and spatial beam shaping (81),(82),(83). They have also been used in optical trapping applications, to separate a single beam into a desired array of multiple diffracted spots in two or three dimensions (45,73,84-93) .

An SLM surface is made up of an array of liquid crystals each of which can be individually addressed electrically to cause a change in its refractive index.

By selecting the correct liquid crystals to influence, the SLM can be operated as a programmable diffraction grating but allowing for much greater control than a traditional grating (86,91). The programs *Blue Tweezers* and *Holoeye* used in this thesis, both provide the capability to generate holograms to produce desired diffraction patterns. The generation of the holograms (usually referred to as computer generated holograms or CGH) is done through the use of inverse Fourier transforms. The mathematics behind the production of these CGHs is a whole field of research in itself and is not a focus in this work.

3.2.2.1 Beam Expander and Reducer

In order to achieve the full capabilities of the SLM it was necessary to harness the full surface area of the liquid crystal elements. The current beam expander in the system is set out in the previous section and had a magnification factor of 2. This expanded the beam diameter approximately from 3mm to 6mm. The surface area of the SLM was 9.5mm x 14.6mm. Therefore to harness the full SLM surface it was necessary to expand the beam further. Furthermore, for the SLM to be effective, the hologram on the SLM had to be imaged onto the back surface of the objective. Consequently, a Keplerian beam reducer was employed so as not only to reduce the beam but also to image the SLM onto the back of the microscope objective. This made the rebuild complex, as the distance between the back of the microscope object and the SLM was now a set value. The use of a Keplerian beam reducer was also advantageous, over a Galilean equivalent, because, unlike a Galilean, between its two lenses the laser reaches a focus; which allows the removal of zero order if required. The removing of the zero order can be preferable for achieving multiple trapping sites as the zero order can be too dominant over higher order spots in terms of power distribution.

Lenses were selected for the beam expander and beam reducer to ensure the beam was expanded up to close to the size of the SLM surface and reduced down to close to the diameter of the back aperture of the microscope objective. The selected lenses are set out in **Figure 3.8** and **Figure 3.9**.

The lenses employed in the Keplerian beam reducer had focal lengths of +400mm and +150mm as shown in **Figure 3.8**.

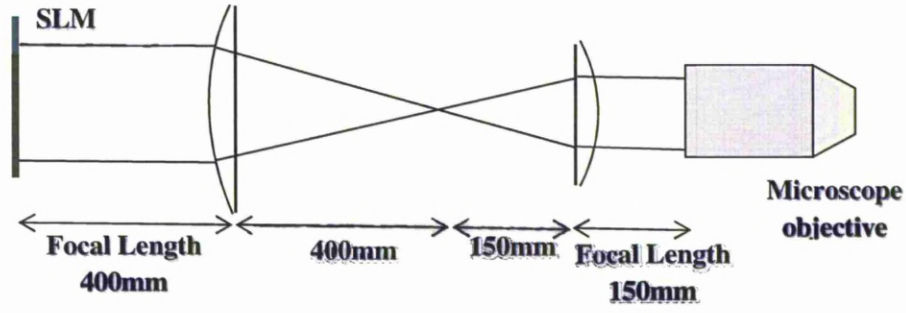

Figure 3.8: Keplerian Beam Reducer Setup introduced in the system

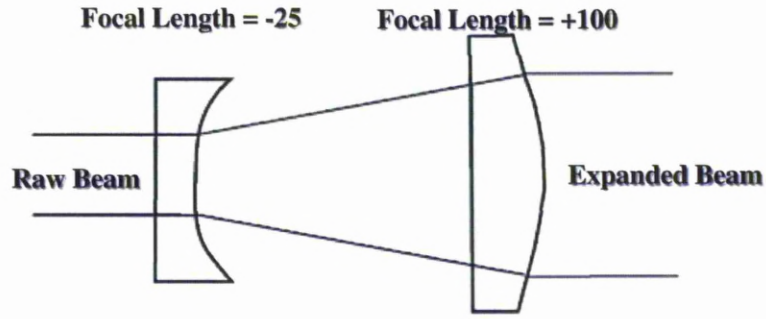

Figure 3.9: Galilean Beam Expander introduced into the system

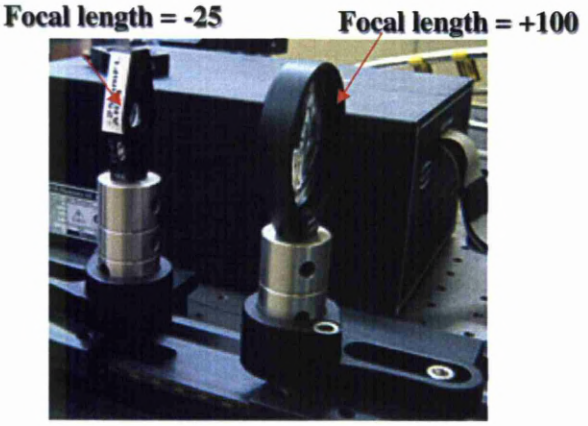

Figure 3.10: The Galilean Beam expander on the optical table

The magnification of the beam expander and reducer can be found thus:

$$M = \frac{l_O}{l_I} \qquad \textbf{Eq.3.2}$$

Where:

M = the magnification, l_O = the focal length of the objective lens and l_I = focal length of the image lens.

So the Galilean beam expander will expand the beam by a factor of 4. The beam reducer will reduce the beam diameter by a factor of 2.67.

Consequently, the beam will be expanded up from its raw beam diameter of 3mm up to approximately 12mm at the SLM surface and reduced to 4.5mm diameter at the back aperture of the microscope objective.

3.2.2.2 Hardware

3.2.2.2.1 Spatial Light Modulator (SLM) - Holoeye LC-R 2500

The spatial light modulator employed was a Holoeye LC-R 2500. The surface of the SLM is a liquid crystal display (1024 x 768 pixels) which can be addressed via computer interface. The SLM device was set up on the system to image the second computer monitor. SLMs are inefficient devices in terms of transmission though this is being improved upon with each generation of SLM. This device transmits 50-60% of the light energy incident upon it. The active area of the device is 9.5 x 14.6mm. The frame rate of the device is 72 Hz.

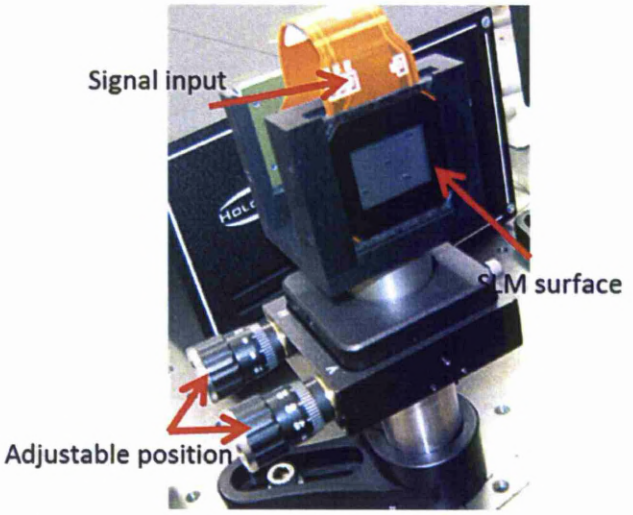

Figure 3.11: Holoeye LC-R 2500 Spatial Light Modulator

3.2.2.3 Software

The additional software requirements for this generation of the system were two programs for operation of the SLM, Holoeye software and Blue Tweezers (86,91) which are set out in the next sections.

A further addition to the software at this stage in the system development was the St.Andrews Tracker (or StAT) which allows for the tracking of the position of objects, such as silica spheres, from video files (94).

3.2.2.3.1 Holoeye Software

The SLM manufacturers, Holoeye, provide software for the production of computer generated holograms, CGH. The software requires input files in .bmp format. The software is then able to convert this into a CGH. This hologram is then displayed on the SLM producing an image which matches the .bmp file.

3.2.2.3.2 Blue Tweezers

The *Blue Tweezers* LabView based program was developed at the University of Glasgow specifically for optical trapping applications. Unlike the Holoeye software, which requires the CGH to be pre-generated, *Blue Tweezers* generates a CGH which can be altered in real time as the desired array of spots is changed manually.

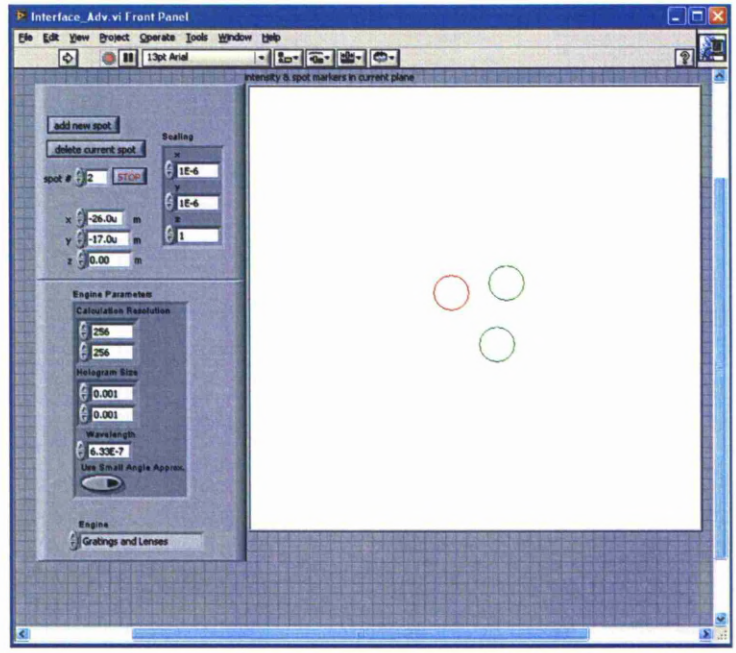

Figure 3.12: Screenshot of original *Blue Tweezers* program

The screenshots shown above are part of the LabView based program - *Blue Tweezers*. The green and red circles on the image designate the desired location of the trapping sites. These circles can be manoeuvred by simple 'click and drag' with a mouse (the selected circle turns from green to red). As a circle is moved, the produced CGH is recalculated and refreshed on the second monitor which feeds directly to the SLM display. The SLM display is setup to mimic the second monitor.

Once integrated into the system it became apparent that the usability of the system could be increased by amalgamating the video capture and the *Blue Tweezers* software. Thus, a video feed was built into the Blue Tweezers software as can be seen in **Figure 3.13**. This meant that the position of each circle could be calibrated with the actual position of the laser spots,

thus allowing for the user simply to click on a silica sphere and then drag it with the mouse. As the circle was translated across the image, the CGH would update, and thus, so would the trap position. Moreover, the software's successful integration into the system provided the ability to trap multiple microspheres simultaneously, as can be seen in the subsequent section.

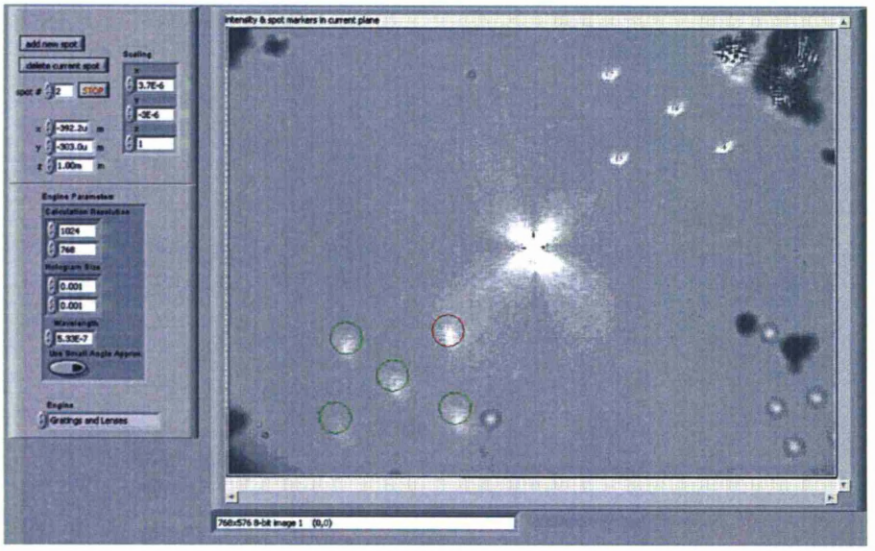

Figure 3.13: Screen shot of the front panel of *Blue Tweezers* with a live video feed from the CCD camera built in. Showing the 5 generated spots in the bottom left quadrant, the central zero order and the ghost 5 spots in the top right quadrant.

There are several different algorithms for hologram generation within the *Blue Tweezers* software. Each one has a trade-off between accuracy and speed. For example, the simpler algorithms such as '*grating and lenses*' (73), are limited in accuracy; but can regenerate at a remarkable rate (for relatively simple holograms). Whereas, iterative algorithms such as the '*Gerchberg-Saxton*' algorithm (95) are computationally intense and can get 'stuck' mid-calculation especially when attempting to compute complex

arrays with many different trapping sites. However, once it has finished computing, this algorithm invariably produces the higher standard of CGH (87). The algorithm selection must therefore be based on a combination of the user's needs and the computational power available. In that for some users, a complex array of trapping sites may be required but once generated no manipulation is required – in such an instance, the slow nature of the Gerchberg-Saxton algorithm is not problematic and it is thus the algorithm of choice.

3.2.2.3.3 The St.Andrews Tracker (StAT)

StAT was developed by Graham Milne during his PhD research at St.Andrews University (94) . The program was developed as a tool for object sorting. It has the capability to track and classify multiple objects. However, it also acts as a useful tool for tracking the position of an individual object. The accuracy of such tracking is limited by the resolution and frame rate of the CCD camera, as discussed briefly in the literature review.

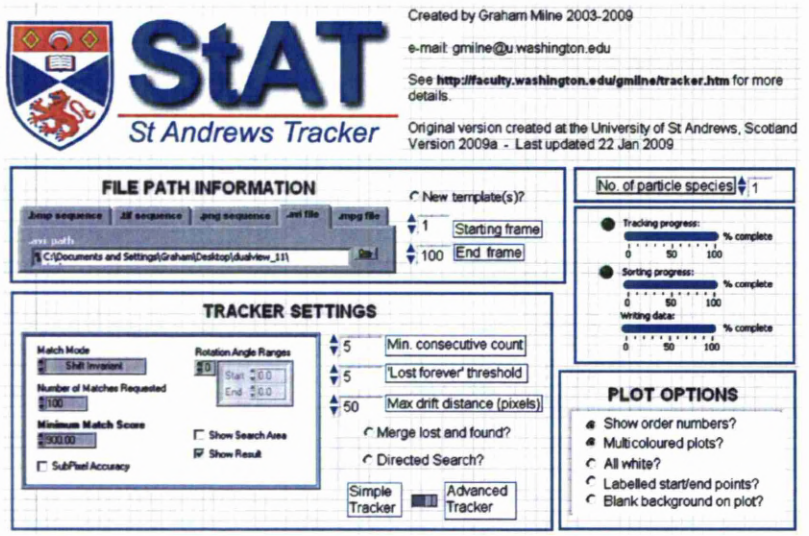

Figure 3.14: Screenshot of the StAT program front screen in LabView.

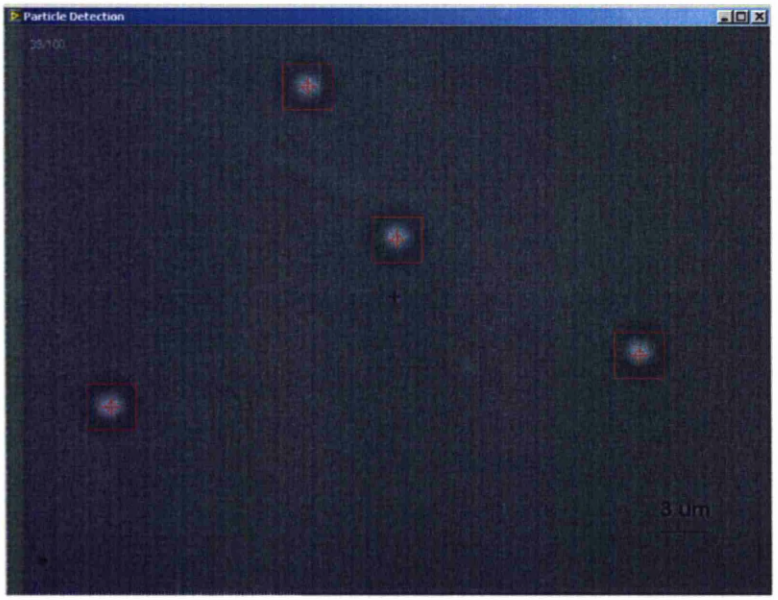

Figure 3.15: Screenshot of StAT program running. The red squares indicate positions where the software is tracking an object that fits the template.

In the front screen of the LabView based StAT program, a variety of parameters can be set. Firstly, it is necessary to select the video file to be processed. Next, the frame number to start and finish processing can be selected. This is a useful aspect of the program if only part of the video file is of interest. Finally, a value described as the 'minimum match score' must be selected. This value informs the program how close a tracked object's image must match the template's image for it to be of interest. So if the match score is too low, the software will start to track in areas where it is clear to the eye there are no objects. Equally, set the match score too high and the program will fail to track any objects or will track objects but will repeatedly 'lose' and 'find' them; each time an object is lost and found again a new position file will be created. The output from the program is a position file, consisting of the tracked objects position in x and y as measured in pixels. Thus, for accurate data, it is important that a tracked object remains tracked throughout the entire selected frame sequence, so that the position data is outputted as one file, as opposed to a series of files each covering a different part of the frame sequence. For the work in this report a 'minimum match score' of 400-600 was found to give the best results when working with uniform silica microspheres. 'Best results', in that the objects would be tracked by the program for entire video sequences, but also that tracking of non-existent objects rarely occurred. When the program was run, the first frame of the video was displayed for the user to select a template of the object to be tracked (by clicking and dragging the mouse to form a square around the sphere to be tracked). The nature of the user manually selecting this template brings an error into the process, as two runs at the same video will produce marginally differing results if two different templates are given.

3.2.2.3.4 Joystick Axis Control(2)

The original 'Joystick Axis Control' program was developed over the course of this work. Initially, it was a program simply for communicating with and driving the mechanical stage. It allowed the driving of each of the x, y and z axes at a series of velocities. Since then a number of new functionalities have been added to the program:

- Shutter control – The program can communicate with the mechanical shutter in the 532nm laser line. Consequently, the shutter can be opened and closed by the simple click of a button on the joystick. As well as enhancing the usability of the system; the ability to close the shutter easily, and at speed, has safety advantages.

- Circle Function - This capability allows the x and y axes to be driven simultaneously causing the micro stage to move in a circular motion at a set radius and speed. This function was critical is enabling the escape speed tests described in chapter 4.

3.2.2.3.5 Vision(2)

Over the course of this research the program was altered and refined to give it greater capabilities. It now includes a measurement palette so that objects on the screen could be measured in real time using pre-calibrated pixel-micron knowledge simply by using the mouse to 'click and drag'. The program also allows for freeze frame image files or video files to be

taken. These video files were then post processed using other programs such as StAT (St. Andrews Tracker) as discussed previously. The program, limited by the camera specification, captures video information at a rate of 30 frames per second.

3.2.2.4 Initial Results and Discussion

Initial work with the SLM and related software showed a significant improvement in the system capability. Where previously only individual objects could be trapped, multiple objects could now be trapped simultaneously, as can be seen in **Figure 3.16**:

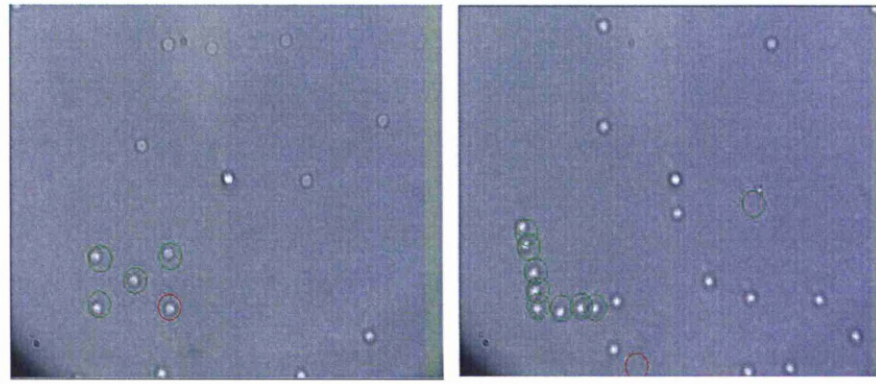

Figure 3.16: Trapping sites denoted by green circles. 'Five point trap array' on the left and assembled 'L', made up 8 individually trapped 2.44μm diameter silica spheres, on the right.

As well as the multiple spots capability shown in the previous figure, beam shaping was attempted using the SLM to create an annular beam profile as

shown in the next figure. This became a useful tool and is discussed in further detail in Chapter 6.

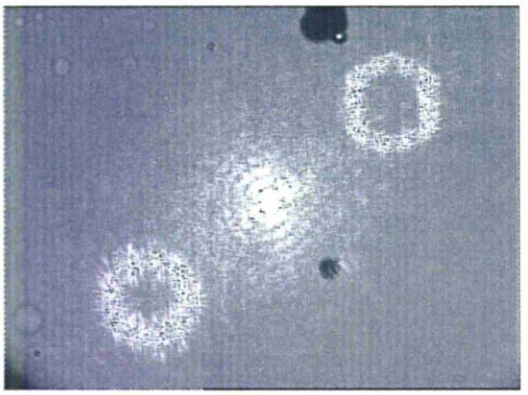

Figure 3.17: Image of SLM produced annular ring. The top right annular ring is the real image. The bottom left ring is the 'ghost' image with considerably less power. In the centre is the zero order which still contains over half of the total power.

Initial work with StAT showed that it could be used as a tool to measure the standard deviation in the position of a trapped sphere. This work is presented in Chapter 4.

3.2.3 Force Measurement and Nanostage Integration

The relatively large minimum steps achievable with the micro stage (0.1μm open loop) meant that the system was limited in the experiments it could carry out. As the work in Chapter 5 of this thesis required the ability to bring a trapped sphere down to a surface at a low velocity and thus required small minimum step size from the stage further development was needed. Additionally, the measurement of forces aspect of optical trapping

is becoming an increasingly important part of the technology. A large proportion of the biological applications harness optical trapping system's ability to measure piconewton forces accurately. Furthermore, a force measurement capability in the system could allow for the measurement of fundamental aspects of optical trapping forces. Consequently, efforts were made to ascertain new hardware to help fulfil the need for greater stage position accuracy and force measurement capability. On their arrival a further redesign was required to retro fit them in to the system. The rest of this section sets out the hardware and software additions at this stage of the setup's progression and the initial results achieved with the new capabilities.

3.2.3.1 Hardware

3.2.3.1.1 Thorlabs Nano stage (NanoMax)

The stage had a total travel capability of 4mm while the piezo actuator drivers allowed for nano scale precision movements over 20 μm of travel in 3 orthogonal axes. The piezo actuators allowed for 5nm step closed loop movements when used in conjunction with strain gauges. The piezo actuators also allowed for the modulation of the position of the stage at high frequency, which is critical in the process of calibrating the force of the optical trap.

The stage was operated through use of the T-cube devices or via the computer using either the LabView based APT software or custom made LabView programs. The nano stage was fitted onto the front of the mechanical micro stage. Removing the micro stage entirely from the

system was considered but the relatively small travel of the nano stage would have made the loading and unloading of samples difficult. By attaching the nano stage to the micro stage, the micro stage's large total travel could still be harnessed in certain applications, such as when loading and unloading samples.

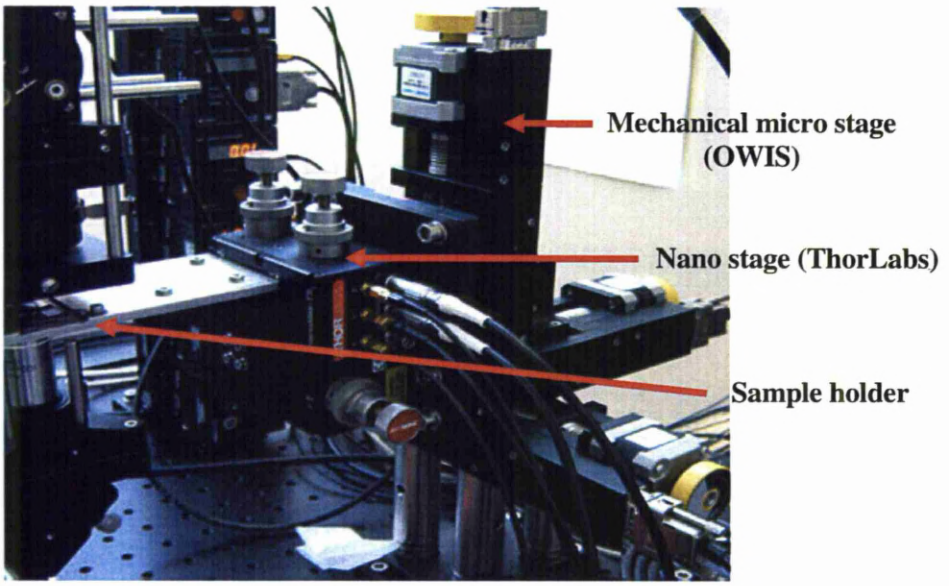

Figure 3.18: The setup showing the custom made sample holder mounted on the Nano stage, which in turn is mounted on the mechanical micro stage.

3.2.3.1.2 T-cube Devices

T-cubes are Thorlabs products which are designed for use with the Thorlabs NanoMax stages (see **Figure 3.18**). The system included:

- Three piezo controllers, one driving each of the three axes on the nano stage

- Two stain gauge readers for tracking the actual position of the nano stage. These are attached to the x and y axes.
- One Quadrant detector to monitor the trapped objects position. More detail on the quadrant detector is offered in the next section.

The T-cubes are all powered via the T-cube 'hub' which has six T-cube 'docks'. This hub can be connected to the computer via a USB cable. This connection allows the computer to communicate with all six of the T-cube devices.

The second way in which the computer can receive information from the T-cubes is via the voltage terminals on the side of each T-cube.

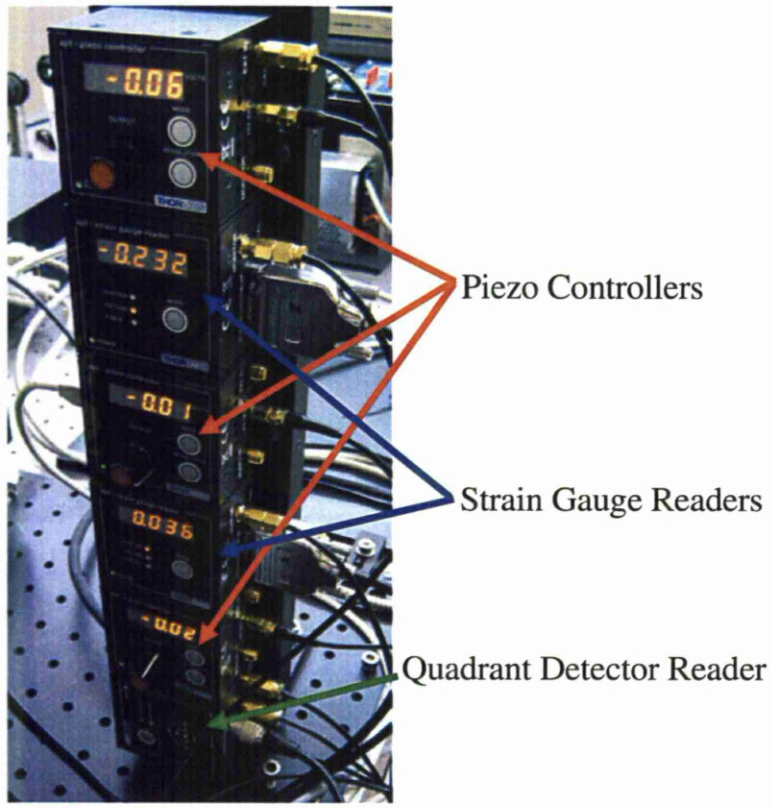

Figure 3.19: The T-cube Hub with the six T-cube devices installed. The T-cube hub provides power to the six devices and allows for communication between all six devices and a PC.

3.2.3.1.3 Quadrant Detector or QD

The quadrant detector was a PDQ80A (Thorlabs). It was a quadrant photodiode array which provided for accurate monitoring of the beam position. In addition a sum value was provided of the overall beam power incident upon all four quadrants. The quadrant detector detected the power arriving at each of its four quadrants and thus, by comparing these relative values, provided information on the precise beam position.

x-axis sensor: x-diff = (Q2+Q3)-(Q1+Q4) Eq.3.2

y-axis sensor: y-diff = (Q1+Q2)-(Q3+Q4) Eq.3.3

Sum: (Q1+Q2+Q3+Q4) Eq. 3.4

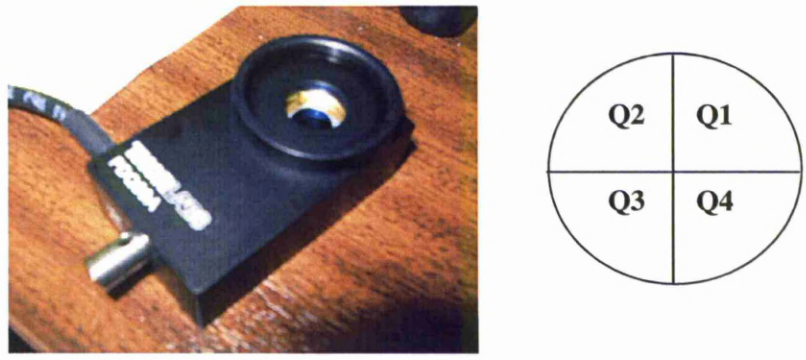

Figure 3.20: Image of the Quadrant detector device (left). Setup of the four quadrants for measuring beam position (right).

These equations make certain assumption. Firstly, that the beam is symmetrical in both axis. From the beam profile generated in Figure 3.6, although not perfectly symmetrical, this is not an unreasonable approximation. This sum value provided by the QD is vital for establishing the actual position of the laser spot on the photo diode. The following example seeks to demonstrate the significance on the sum value. The values represent beam powers incident upon a particular quadrant. Their units can be considered arbitrary as it is their relative sizes that are important:

Consider a situation where the powers incident on each quadrant were:

Q1 =2, Q2=8, Q3=5 and Q4=3. From equations 3.1 and 3.2:

This gives an x diff value of (8+5)-(2+3) = 8

And a y diff value of (2+8)-(5+3) = 2

The sum value is: 2+8+5+3 = 18

If the beam power was then reduced by half giving Q1= 1, Q2= 4, Q3= 2.5 and Q4= 1.5 the x diff and y diff values would halve also; giving x diff = 4 and y diff = 1. Thus implying the spot had moved close to the centre of the diode. However, when the sum is considered alongside x diff and y diff it is clear this is not the case. The sum in the second case has halved also: 18 in the initial case but now equal to 9.

Consequently, all x diff and y diff values must be considered as relative to the simultaneously recorded sum value.

The QDs high bandwidth, up to 150 kHz, allows for tracking of position with sufficient accuracy to monitor the thermal motion (Brownian motion) of a microsphere suspended in water. The responsivity of the QD (shown in **Figure 3.21**) is at its peak at around the 970nm however this QD was chosen for the system as it gives sufficiently high responsivity for the required application at both 532nm and 1064nm.

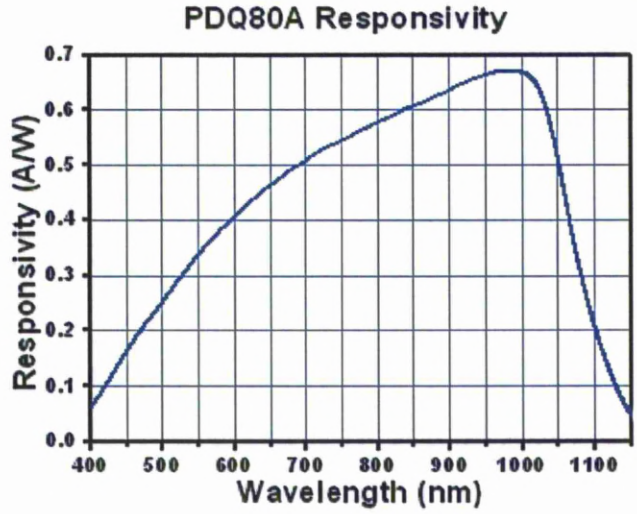

Figure 3.21: Provided by the manufacturer (Thorlabs) showing how the responsivity of the PDQ80A model of Quadrant detector varies with wavelength.

The quadrant detector was installed beyond the sample position. Light that passed through a trapped sphere was refocused on to the QD. This method is referred to as forward scattered position detection as oppose to back scattered position detection. A comparison of the two methods of detection has been carried out (96). Due to the high NA objective, the laser light leaving the sphere is highly divergent. Therefore, it is necessary to introduce a condenser lens after the sample to 'gather' the highly divergent light and refocus it. A second lens is employed to focus the light onto the QD. The setup is shown in **Figure 3.22**.

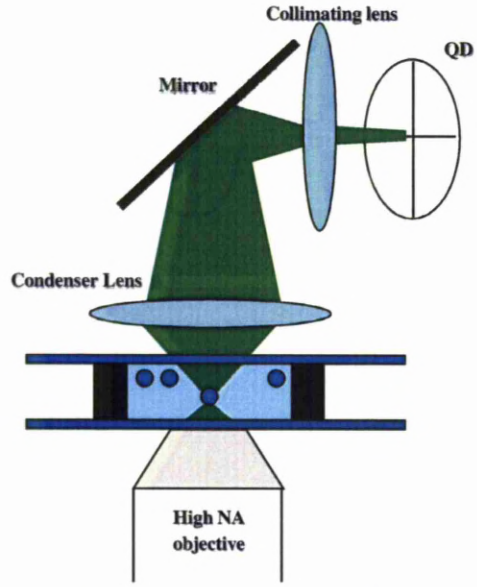

Figure 3.22: The Quadrant Detector Setup

3.2.3.1.4 Custom Sample Holder

The previous sample holder shown in **Figure 3.3** had no system for fixing a sample in position. Furthermore, the newly installed nano stage did not have a method of attaching the sample holder to it. Consequently, a new sample holder was designed with specific dimensions to give greater support and stability to a loaded sample. Additionally, 'clips' were included in the new design of the sample holder to fix down the sample in place, as seen in **Figure 3.23**.The greater stability enabled by the new sampled holder with clips, allowed for increased stability in the height at which the sample sat relative to the microscope objective. This ensured that the sample remained in the image plane over the camera over extended periods of time. Under the previous sample method, over a period of 0-5 minutes the sample could drift out of camera's focus.

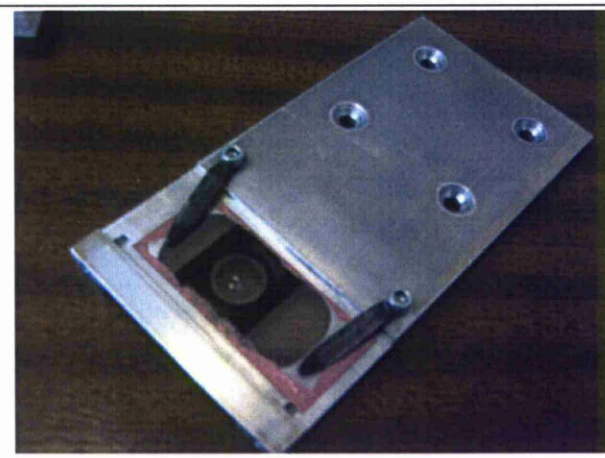

Figure 3.23: Custom Sample Holder

The sample shown above is the spacer method of sample preparation. The 'black spacer with hole' is clearly shown. Within the hole, the sample solution is placed containing microspheres. The pink coating around the edge of the sample is nail polish. This prevents evaporation of the enclosed sample and thus increases the life time of the sample significantly. Without the nail polish seal, samples routinely 'dry out' in 24-48 hours. With the seal, samples last for several weeks before 'drying out'.

3.2.3.2 Software

There was a variety of software needed at this stage in the system development. Firstly, Thorlabs provided with the hardware, a software package called *APT*. This user friendly software allowed for the easy communication between PC and all six of the T-cube devices via the USB connected T-cube hub.

Figure 3.24: Program Display for the Strain Gauge Reader

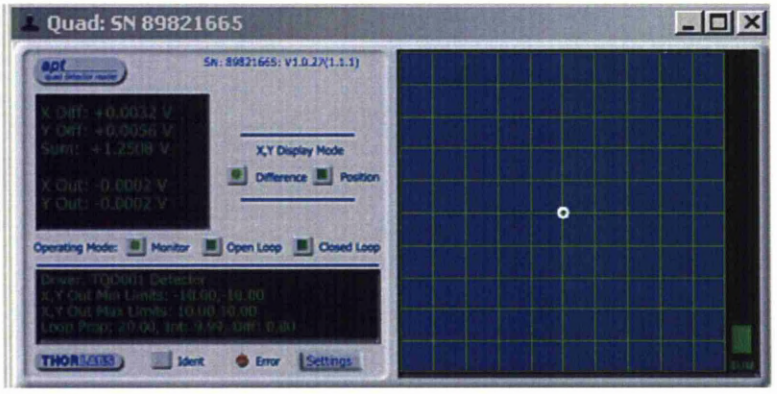

Figure 3.25: Program Display for the QD

Alongside the Thorlabs APT software, new programs were written in LabView for the acquisition and formatting of data. These programs used information taken from the T-cubes via the 'voltage out' ports. As well as operating as data acquisition programs, some of these newly written programs also had a control element, in that they simultaneously drove an oscillation in one of the nano stage axes, while recording data. These programs included:

1. Nanostage2a – Drives one axis (usually y) on the nano stage with a sine function. The amplitude, frequency and an offset could be selected. The output voltages from each of the two strain gauge readers (monitoring the actual position of the stage in each of the x and y axis) and the QD could be simultaneously recorded. The QD outputs were separated into three separate voltages: x axis, y axis and sum (as discussed in section 3.2.3.1.3). Frequency of data acquisition was set at 100 kHz.

2. Nanostage2b – This program had no sine function generation. It simply tracked the QD outputs for x, y and sum. The frequency of data acquisition was set at 100 kHz. This program was written to measure the standard deviation of position of a trapped object.

3. Nanostage2c – Essentially the same program as nanostage2a but with the frequency of data acquisition at 1 kHz.

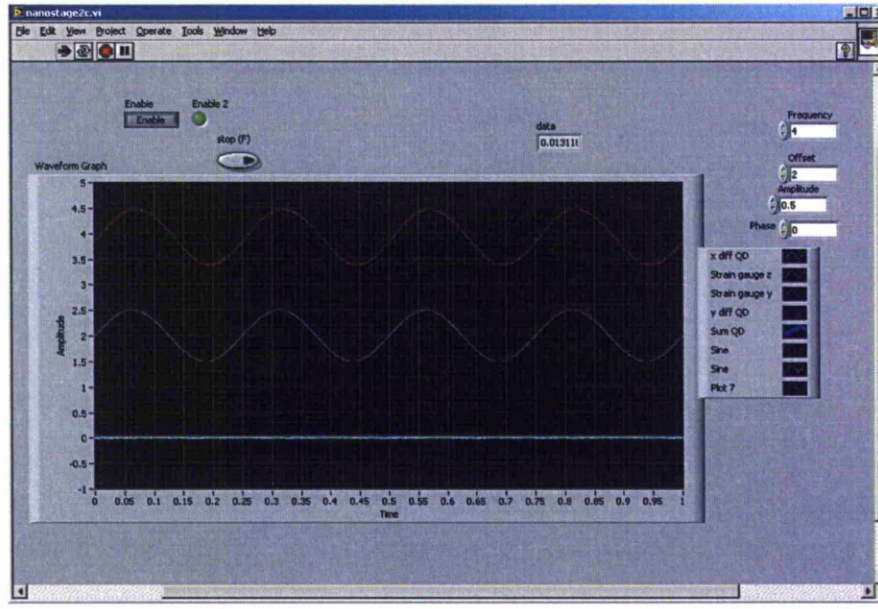

Figure 3.26: Screenshot of the front window of the LabView based program 'Nanostage2c'. The purple sine wave is the generated wave. The red sine wave is the real time position of the stage in one axis.

When taking data at 100 kHz, the program would terminate after just over 0.6 seconds having acquired its maximum amount of data: 65532 data points from each output. This was the case for each of the nano stages 2a and 2b. However, at a lower frequency of data acquisition, the program acquires data sufficiently slowly that the program has time to store it and remove it from its short term memory, thus allowing the program to run indefinitely. Hence the lower frequency program was used during longer experiments or during setups. However, inevitably with lower frequency of data acquisition comes greater inaccuracies so whenever practical, the ultra-high frequency programs were used. This may seem counter intuitive; however, recording data over a longer period is not beneficial if the data is acquired at a lower bandwidth, i.e. acquiring position data at greater intervals. The shorter data runs, at higher bandwidths, enable the data to be acquired with minimum intervals, thus giving a truer data set of the object's movement during the data period.

3.2.3.3 Initial Results and Discussion

As will be seen in the subsequent chapter, the introduction of the piezo electric stage and quadrant detector allowed for the acquisition of large quantities of data. Until now, the experiments undertaken had been largely qualitative in nature; however, with the addition of these devices a more quantitative approach was possible for subsequent investigations.

During the initial work with the quadrant detector, a number of unusual results were found, such as object movement being much larger than was being seen in the camera or object 'jumping' from opposite sides of the QD. It became clear than this was because the QD was a highly sensitive device which must be thoroughly understood in order to know when unusual or unexpected results are genuine or artefacts of the system or sample design.

Firstly, considered was the sample setup. If two cover slips are separated by a self-adhesive sticker then the cavity of the sample (i.e. the area containing the water and microspheres) will have an easily defined geometry as shown in **Figure 3.27** and later referred to as the 'spacer' method.

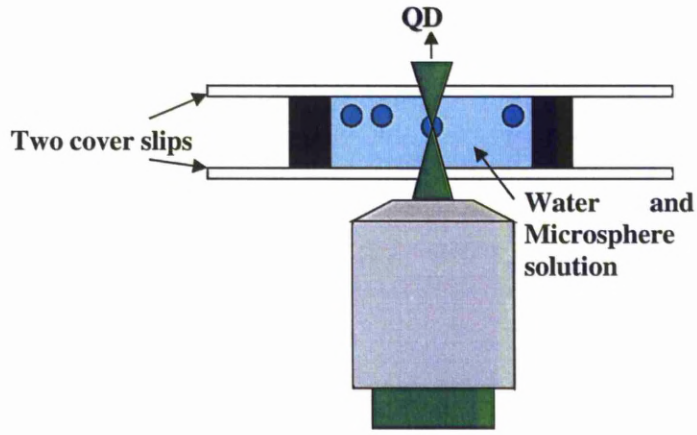

Figure 3.27: Sample Preparation Method 1 - Spacer Method: A cross section of the two cover slip method of sample preparation. The two cover slips are separated by a thin circular black sticker with a 12mm diameter hole in it.

Now consider the second method of sample preparation used in this thesis: a 'microscope slide with a cavity' covered by a cover slip. As with all setups, the cover slip must be the surface which meets the microscope objective due to the finely tuned working distance of the microscope objective. Therefore the far surface, and thus the surface through which the laser must pass to reach the QD, would have to be the 'microscope slide with cavity' as shown in **Figure 3.28**.

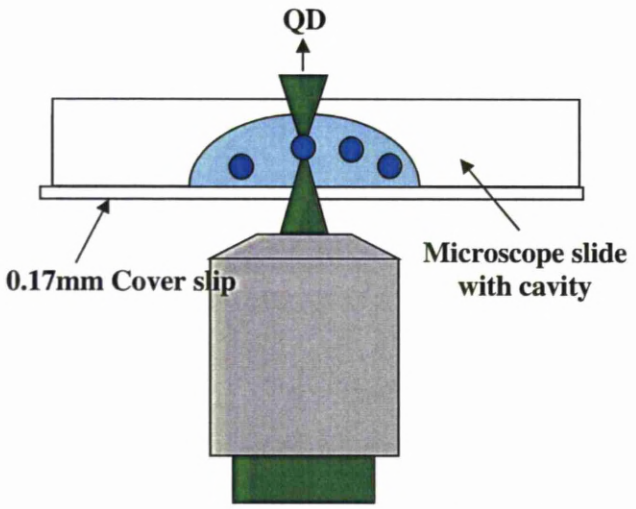

Figure 3.28: Sample Preparation Method 2: A cross section of the cover slip-microscope slide with cavity method of sample preparation. This method allows for a much greater volume of solution. The cavities have a diameter of 12mm and a depth of 3mm.

This method of sample preparation shown in **Figure 3.28** is useful for a variety of tasks but initial results show it cannot be employed where the QD is recording data, since the QD is a highly sensitive device which must be carefully calibrated (as discussed in Chapter 4). The upper wall of the sample chamber is curved and thus has a different gradient relative to the laser at each point across it. As the laser is passed through this curved surface it is refracted differently than when passed through a flat surface as

in sample preparation method 1. The stage moves independently to the laser position, so depending on the sample position above the microscope objective, there could be vastly different angles at which the laser meets the top surface. This in turn will affect the position of the laser on the QD.

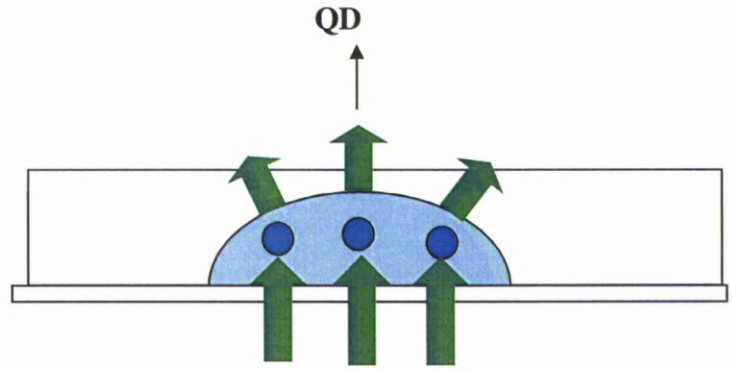

Figure 3.29: How the microscope slide with cavity setup can compromise the quality of QD results. Each of the lower arrows represents a different position of the laser relative to the sample. This shows how a position change could translate in to greatly different QD data.

The next issue with the QD was ensuring a large enough signal reached its surface. During initial tests, it was found that the signal reaching the QD was below the manual quoted preferable range. This was caused by major power loss due to incorrect condenser position. The condenser lens purpose is to 'gather' the highly divergent light from the high NA objective and refocus it. However, if the condenser is positioned too high above the objective, then despite its wide diameter, much of the laser power will have already diverged beyond the width of the condenser by the time it reaches the plane of the condenser. Therefore, the condenser must be positioned very close to the sample in order to minimise losses.

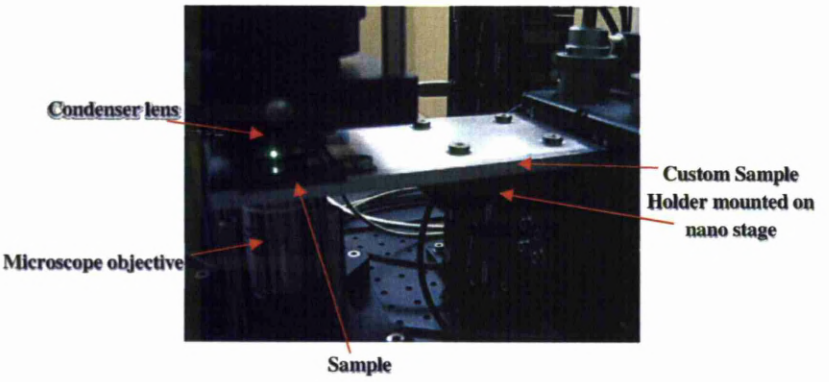

Figure 3.30: Sample Stage. Showing the small distance between the sample and the front surface of the condenser lens.

The next major issue found during initial work with the QD, was that the output signal of position, can vary greatly depending on the distance between the trapped sphere and the near cover slip surface. A trapped microsphere operates as a miniature lens and thus focuses the light. It was observed that in regions where the trapped sphere was very close to a surface(less than 20μm) there was great instability in the QD output. However, at distances greater than 20μm a relatively stable output signal was observed.

Another issue tackled at this stage of the system progression, was the problem of preparing and loading a sample only to find almost all of the microspheres within the sample are fixed to the surface. This is due to a combination of electrostatic and Van der Waals forces. One method of reducing the sphere's natural desire to affiliate to the cover slip surface was by the introduction of a surfactant to the sample i.e. a few drops of Kodak photo solution (Photo Flo 200) was used in this work. This dramatically reduces the extent to which the spheres will fix to the surface or each other.

3.2.4 Second Laser Line Integration

Although, the installed 532nm laser offered excellent trapping capability, its relatively low power meant it is limited in terms of engineering applications. The power available combined with its wavelength, would make ablating or fusing glass like materials impossible in the current system. With aspirations to fuse spheres to each other or to surfaces, it was clear greater powers were required. Furthermore, harnessing two lasers, with different properties, both delivered to the sample through the same high NA microscope objective would undoubtedly add a great deal to the system. As with the SLM, it was reasoned that by having multiple laser spots, one laser could trap objects while another performed an engineering function to enable permanent fixing of objects. The introduction of the second laser line was done with large parts of the work in Chapter 5 being considered. The desire to be able to focus both lasers to the same point, or along the same axis but to varying relative focal positions, made its introduction significantly more difficult but it was decided that if successful this could give the system unique capabilities.

3.2.4.1 Hardware

3.2.4.1.1 SPI Laser

The model is a G3 HS 20W Pulsed Fiber Laser (serial number 318621). This model allows for both continuous wave and pulsed modes of operation. The repetition rate of the laser when in pulsed mode can be

varied between 25 and 500 kHz when operated at full power. Or, 1-25 kHz at a reduced power range. Although commonly referred to as 1064nm in wavelength, the specification of the laser is 1062+/-3 nm. The laser's actual wavelength was measured in the test report at 1061.44nm with an emission bandwidth of 4.5 nm. The M^2 specification of the laser is 1.6-2 with the test report recording a value of 1.93. The beam diameter was measured at 3.2 mm. The maximum energy per pulse was measured as 0.84mJ.

The laser has a built in fan to assist with its cooling. This can be deactivated to minimise vibration on the table but this is inadvisable when running the laser at higher powers. The laser was delivered via a 2 metre length of optical fibre. The laser was software controlled with a wide selection of parameters available: operation mode (CW or pulsed), power (0-20W), pulse rate (1-20kHz), waveform (25 pre-set waveforms). The pre-set waveforms allowed for a high degree of control over the output waveform of the beam when in pulse mode.

3.2.4.1.2 White Light Diode

The original fibre illuminator source employed a fan for cooling purposes. However, this fan produced a small 50Hz vibration which was damaging much of the data collection undertaken in Chapter 4. Therefore, a new illumination source was ascertained to replace the fibre illuminator source. The diode fitted into the system in the same position as the fibre illuminator had previously occupied. The diode introduced was a Thorlabs LIU001 white light diode. As well as removing the oscillation produced by the previous light source, the fibre illuminator, the diode source also produced significantly less heat than its predecessor. This is preferable because temperature changes in the sample will distort many of the

experiments undertaken throughout this research. For example many of the force measurement results taken in Chapter 4 of this thesis are highly temperature dependent in a number of ways. Therefore, any aspect of the design process that can limit temperature changes in the system is encouraged.

Mechanical Shutter 3.2.4.1.3

A second mechanical shutter, again a Thorlabs SC10 has been installed into the system to act on the second laser line.

3.2.4.2 Software

3.2.4.2.1 Joystick Control Additions

The 'Joystick Control' program was again added to. The additions to the program were:

- The SPI laser enable function – The SPI laser is entirely PC controlled. This function communicates directly with the SPI laser and thus provides an easy method of enabling, and importantly in terms of safety, disabling the laser.
- Mechanical Shutter Control – A second mechanical shutter has been installed into the system, for the second laser line. This addition to the program allows the program to communicate with

the new mechanical shutter. As with the previous shutter program, for the shutter on the other laser line, this function provides for greater usability and safety.

- Z line function - This function was developed during the work described in Chapter 5. It provides the capability for the scanning of the mechanical micro stage in z, down and up a specifiable distance and speed. During efforts to cure through the entire thickness of a resin, as explained in Chapter 5, this function ensured the ability to provide energy right through the thickness of the material.

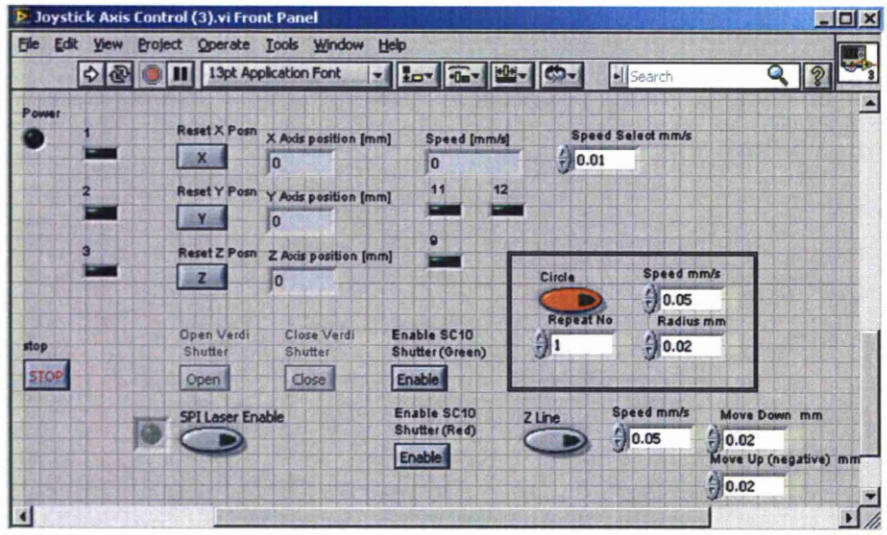

Figure 3.31: Screenshot of the front screen of the final version of the 'Joystick Axis Control' program.

3.2.4.3 Initial Results and Discussion

The addition of the 1064 laser line was a complex process. Attempting to focus place both lasers along the same axis is not trivial. The setup

employed for introducing the second laser line is shown in the next figure. It shows that the two lasers are both reflected off the last mirror before the microscope objective. Therefore, to achieve both lasers running along the same axis, it is not only necessary to have them both arrive at the point of the mirror, but also they must arrive at the same angle. Furthermore, the 532nm line's penultimate mirror is passed through by the 1064 nm line, as shown in **Figure 3.32.** As a result, any alterations to the position or angle of this mirror will affect the trajectory of both lasers.

3.3 Final System Setup

This final system design represents a long process of work to reach a setup with a variety of capabilities and versatility. The system has been specifically designed for the execution of a series of experiments to extend the knowledge of optical trapping as an engineering tool.

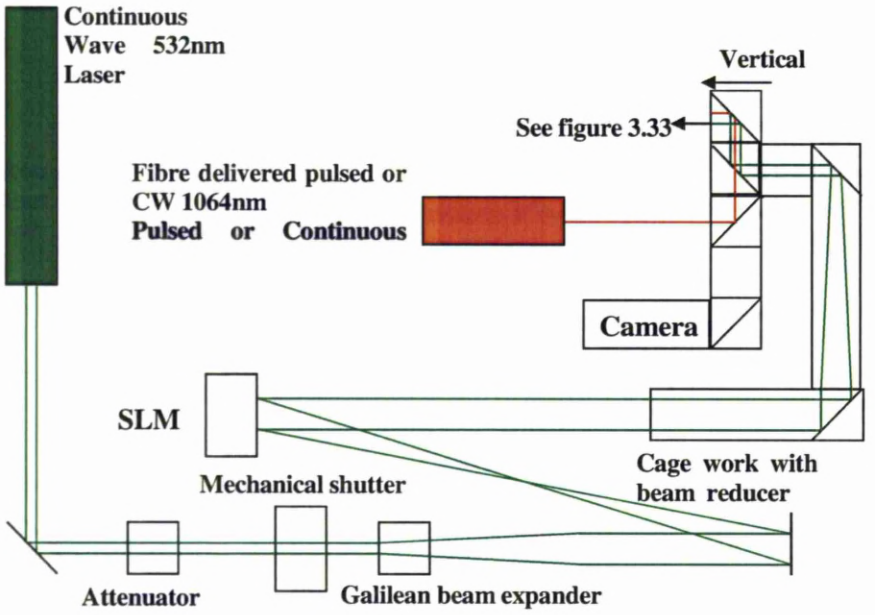

Figure 3.32: The Final Optical Trapping System

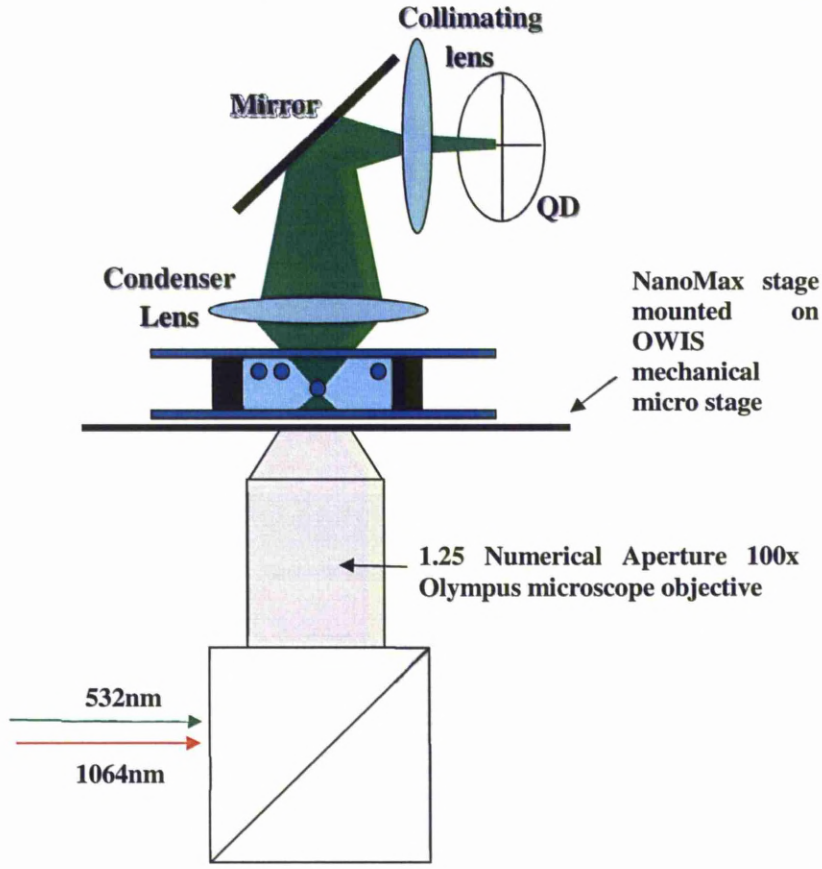

Figure 3.33: The sample setup consisting of the sample itself, which has a variety of different set ups, the nano movement stage (NanoMax) mounted on a micro movement stage (OWIS).

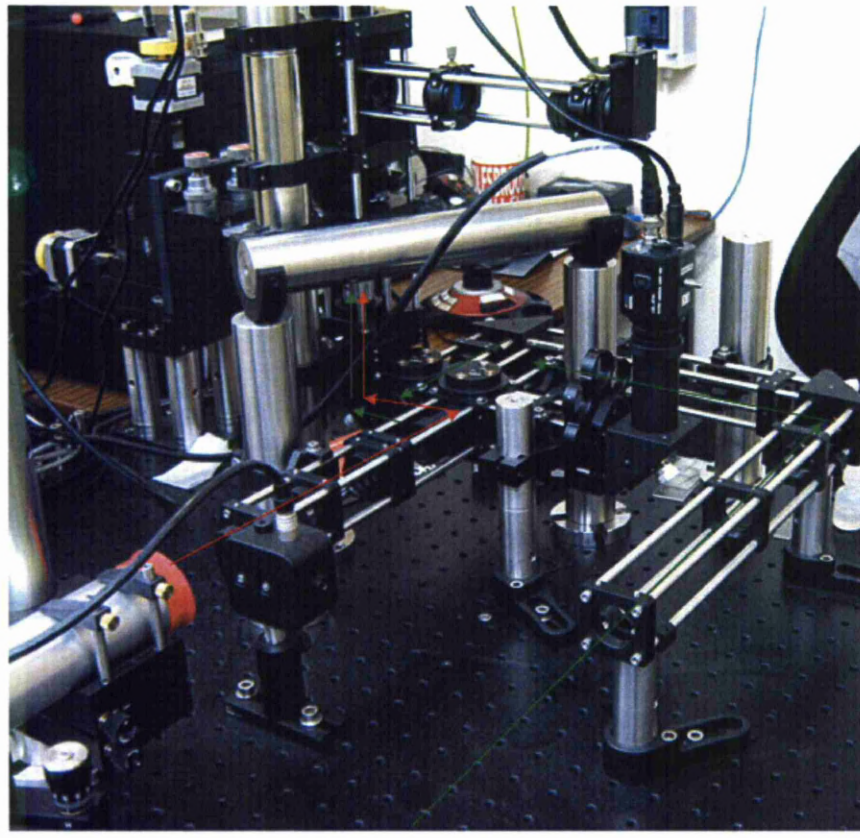

Figure 3.34: Final Optical Trapping Setup showing both laser lines

3.4 General Discussion

As optical traps have developed, the technology has expanded to include other techniques alongside the trapping function. This has allowed researchers to build trapping systems specific to their needs. In the case of biological research this has often meant the inclusion of quadrant detectors to act as a force measurement tool (97-101). Different imaging techniques, such as dark field imaging (102,103), have also been added into existing trapping systems.

The system set out in this chapter was designed, built and developed specifically to facilitate engineering applications. The two laser sources alongside the SLM capability provide for a highly versatile system which can be easily adjusted for a specific task. The idea to have two lasers aligned and with the ability to vary the laser focuses relative to each other gave the system perhaps its unique capability. Admittedly, adding this element in to the system made the alignment of the system immensely difficult. At one stage it looked as if it would not be possible to achieve the level of alignment required for the focuses to be sufficiently close that they would be able to work successfully in tandem. The Keplerian beam reducer, mounted within cage work, allowed for adjustment of the beam focus. By translating the objective lens along the cage work, the position of the 532nm laser focus can be moved in the z dimension. Moving this lens does sabotage the Keplerian beam reducer so the reduction achieved will change but in certain applications this not problematic. The ability to manipulate the focus of the 532nm laser line was useful during the work undertaken in Chapter 5 of this thesis.

Alongside the hardware development it is worth noting that the software development added greatly to the system capabilities. LabView allowed for programs to be updated and enhanced easily as the needs and applications became more specialised.

Consequently, the final system produced was beyond anything available commercially in terms of both abilities and versatility. Furthermore, by going through the process of designing, building and developing this system, a far greater understanding of optical trapping and the inherent complexities of the system, which will affect any subsequent experiments, was achieved.

The various investigations undertaken with the system are set out in the subsequent three chapters.

Chapter 4

Calibration and Measurement of Forces produced by the Optical Trap

4.1 Introduction

One of the most appealing aspects of optical traps is their ability to measure forces accurately at the piconewton level. This has been of particular use within various biosciences based research areas - as discussed in Chapter 2. However, as with any measurement system, before this potential capability could be used by biologists, physicists were required to calibrate the system. The different methods of calibration were discussed in Chapter 2 and in this chapter; various methods are investigated and compared. Once the system was calibrated, a variety of fundamental tests were performed to learn more about the trapping process.

Some of these tests varied parameters that had previously been tested, whereas others were previously untested parameters. For tests similar to those previously undertaken, discussion is included as to how these results fit into the current understanding, including how the results concur or conflict with previously published work. Where new tests are undertaken, efforts are made to understand the results and to discuss how these fit into current optically trapping theory.

4.2 Calibration Procedure

There are three aspects of the system that required calibration:

1. The Strain Gauge Readers
2. Quadrant Detector – As the position of a trapped sphere is measured by the device in Volts, it is necessary to establish the conversion of metres (or rather nano metres) to Volts.
3. The trap stiffness of the trap at a specific power.

4.2.1 Calibration of the Strain Gauge Readers

The stage positions were monitored at high bandwidth (500Hz) using strain gauge readers. One strain gauge reader was required for each axis to be monitored. These readers provided the position data of the stage by outputting a voltage. This voltage had a linear relationship with actual position of the stage in metres. The strain gauge readers were calibrated by

the manufacturers (ThorLabs). However, as the output signal (via the SMA cables used to communicate with the PC) was only available as a voltage, it was necessary to convert this to metres.

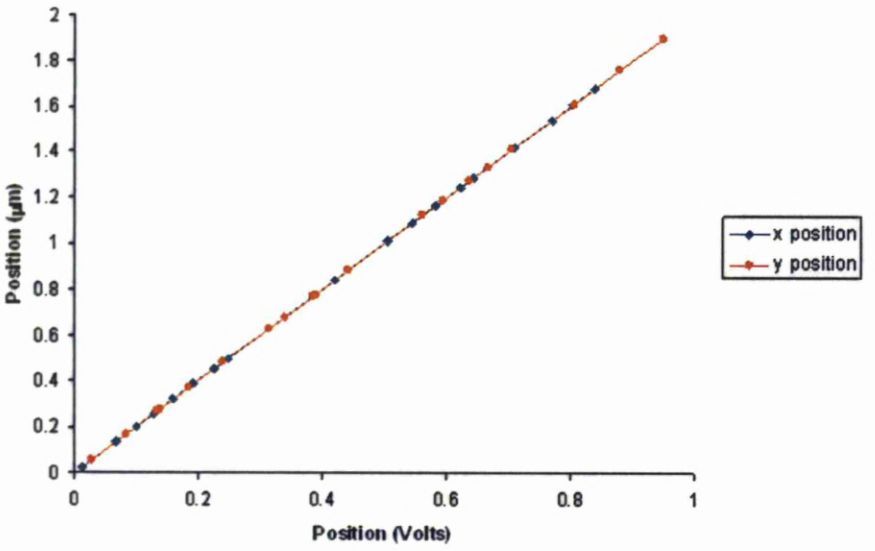

Figure 4.1: Shows the position of the stage in both Volts and micrometres for a given position for both the x and y axis.

The above figure shows the linear relationship between the voltage output from the strain gauge readers and their relative position in µm. Thus the conversion factor was found to be B = 2, according to the relation:

$$Bp_V = p_m \qquad \textbf{(Eq.4.1)}$$

Where p_V is the position in Volts from the strain gauge reader and p_m is the position in µm as measured by the strain gauge reader.

4.2.2 Calibration of the Quadrant Detector (QD)

This calibration was necessary to convert accurately the position, given as a voltage output from the QD, into position data in microns.

A sample of 5.44 μm diameter silica spheres was made up in the 'spacer' method of sample preparation (see **figure 3.27**). In this case, by not using any soap solution the vast majority of spheres were fixed to the surface due to electrostatic forces. A non-fixed sphere was found, trapped and oscillated (at a known frequency and amplitude) in close proximity to a fixed sphere. The sphere that was fixed to the cover slip surface oscillated at the actual frequency and amplitude of the stage, whereas the trapped sphere oscillated at the same frequency but at a smaller amplitude due to the forces exerted by the trap. A video was taken of this process using the Vision software, developed and discussed in Chapter 3. This video was then processed using the tracking program, StAT. StAT gives outputs for the position in pixels with frame number, for both the trapped and the non-trapped spheres. As the non-trapped sphere was fixed to the oscillating cover slip, its oscillation in pixels was equivalent to the oscillation of the stage which is known. Therefore, a conversion factor for pixels to metres could be found. This value could then be used to convert the movement of the trapped sphere from pixels to metres. Finally, as the QD produced data for the sphere position in Volts, this was equivalent to the sphere's position in metres, hence a conversion factor for Volts to metres could be established.

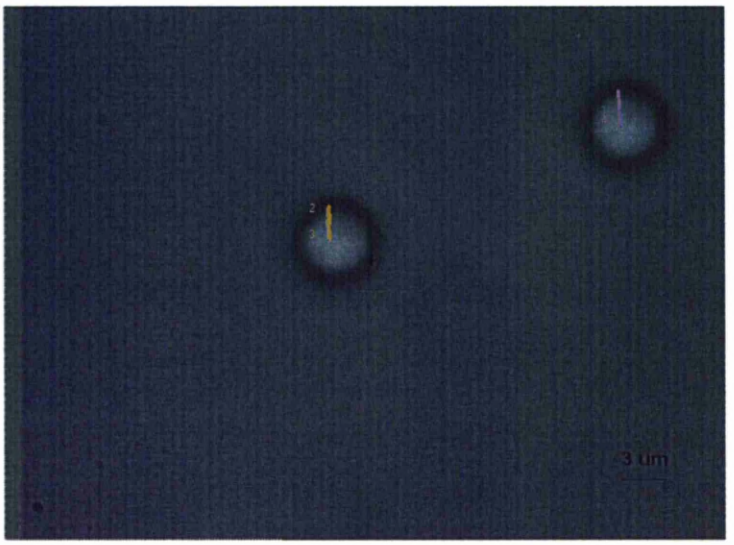

Figure 4.2: Plot produced from StAT. The centre sphere is optically trapped. The sphere to the right is fixed to the surface the, and hence its movement is equivalent to that of the stage. The pink and yellow lines show the movement of the spheres as tracked by the StAT program.

The stage was driven at a frequency of 2Hz, an amplitude of 0.5V and an offset of 2V. From the calibration undertaken in section 4.2.1 and the amplitude conversion to microns, the stage was effectively driven at an amplitude of 1μm. The offset is to move the centre of the sine wave above 0V, as the stages cannot be driven with a negative Voltage, so the offset must be greater than the amplitude.

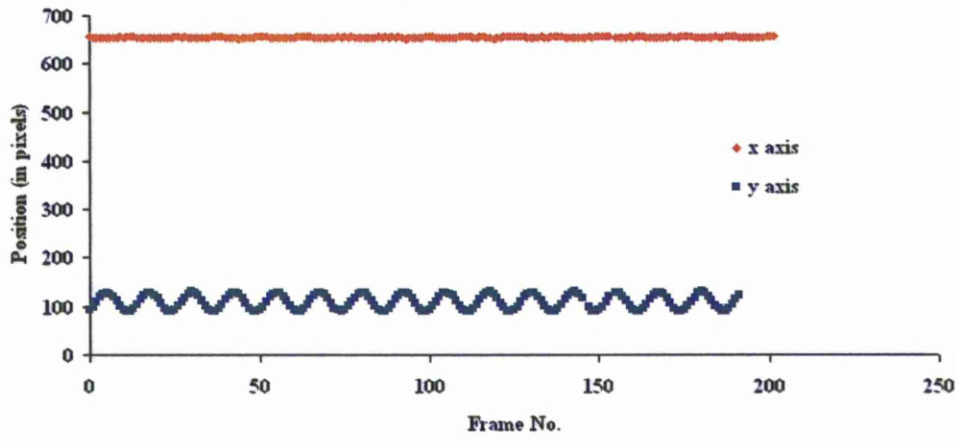

Figure 4.3: Showing (in pixels) the position of a sphere (in pixels) which is fixed to the cover slip, as produced by the tracking program StAT.

From the above data, the amplitude of the y axis oscillation of the fixed sphere was calculated to be 20.2 pixels. The amplitude was calculated from:

$$A_f = \frac{\hat{s}_{\max} - \hat{s}_{\min}}{2} \qquad \textbf{(Eq.4.2)}$$

Where A_f is the amplitude of the fixed sphere's oscillation, $\hat{s}_{max}$ is the mean of the maximum values, and $\hat{s}_{min}$ is the mean of the minimum values.

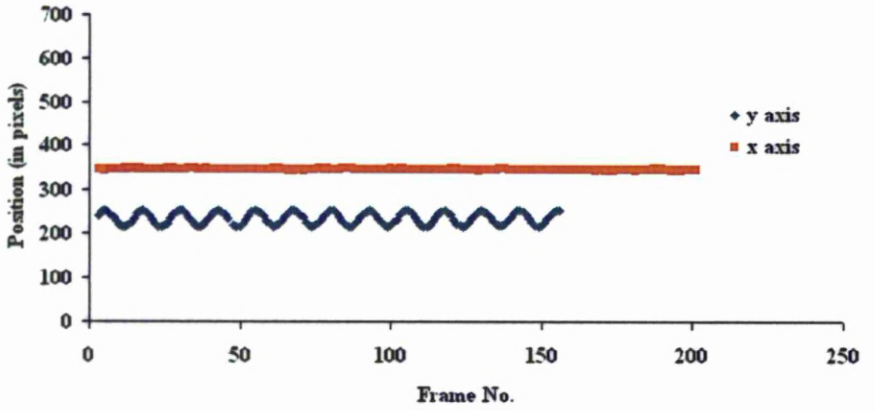

Figure 4.4: The position of a trapped sphere, as produced by the tracking program StAT

From the above data, the amplitude of the y axis oscillation of the trapped sphere was calculated to be 20.0 pixels using equation 4.2.

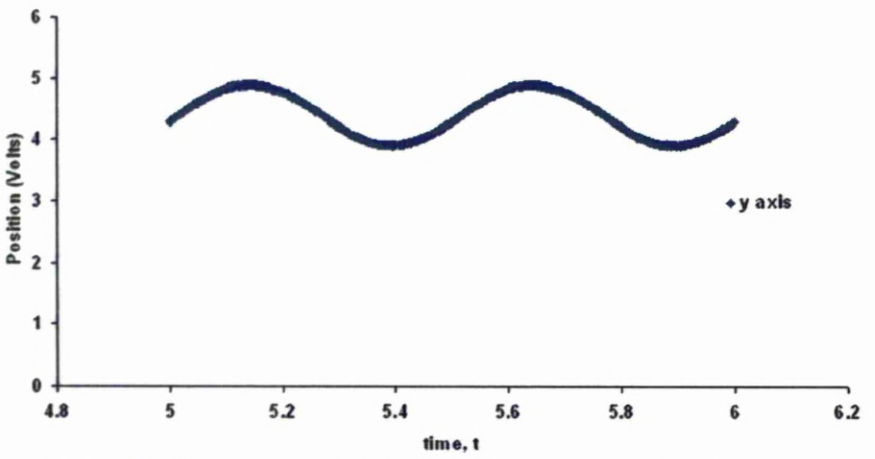

Figure 4.5: Showing portion of the data from the z strain gauge reader which is equivalent to the y axis of the camera. Taken simultaneously to the video used by StAT in the previous two figures. This data is taken at high very bandwidth. The above line is made up of 65536 individual data points.

Figure 4.5 shows that the stage was successfully driven at the desired amplitude of 0.5V or 1μm. Therefore, a second conversion factor could be found from the known movement of the stage, in Volts and the known movement of the fixed sphere in pixels using:

$$A_{m\text{-}fixed} = D\, A_{p\text{-}fixed} \qquad \textbf{(Eq.4.3)}$$

Where $A_{m\text{-}fixed}$ is the amplitude of oscillation in metres of the fixed sphere, $A_{p\text{-}fixed}$ is the amplitude of oscillation of the fixed sphere in pixels and D is the conversion factor. From the above data:

D = 0.098 μm per pixel

This value was used together with the position data of the trapped sphere, taken with the QD. Equation **4.4** was then used to find the amplitude of oscillation of the trapped sphere in metres:

$$A_{m\text{-}trapped} = D\, A_{p\text{-}trapped} \qquad \textbf{(Eq.4.4)}$$

Where $A_{m\text{-}trapped}$ is the amplitude of oscillation of the trapped sphere in metres and $A_{p\text{-}trapped}$ is the amplitude of oscillation of the trapped sphere in pixels. Therefore, $A_{m\text{-}trapped}$ = 1.97 μm

This value was then compared with the QD position data for the same trapped sphere:

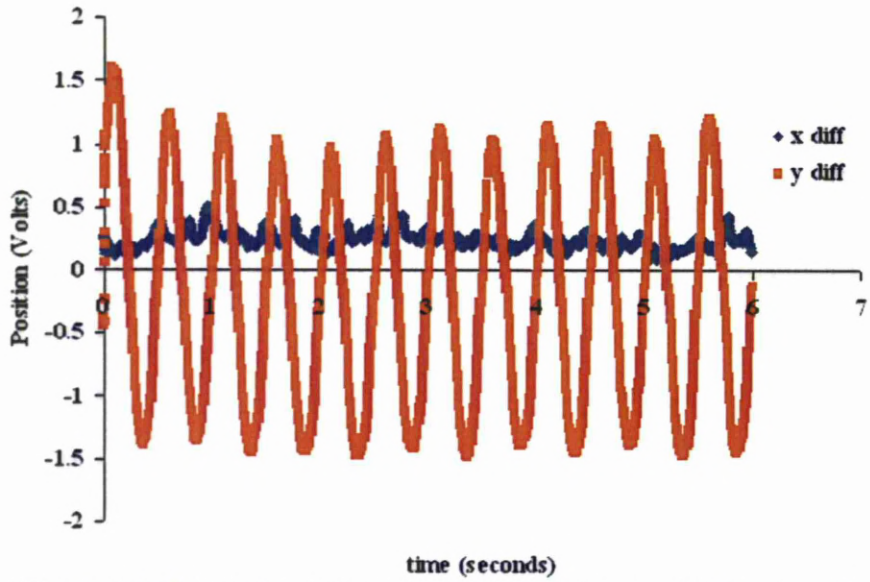

Figure 4.6: Output signals from the QD for x-diff and y-diff showing the position of a laser trapped 5.44 μm sphere during a stage oscillation of 2Hz.

The amplitude of this oscillation was found using **Eq.4.2**:

Amplitude in Volts, $A_V = 1.82$ V

From the above value, a final conversion factor to convert the position in Volts on the QD to a position in μm was derived from:

$$L\, A_{m\text{-}trapped} = A_V \qquad \textbf{(Eq.4.5)}$$

Where L is the final conversion factor.

From this, the value of L was found to be:

$0.925\ V\ \mu m^{-1}$

With the QD conversion complete, measurements of trap stiffness could then be obtained. All measurements were subject to experimental errors. The use of the CCD camera to track the position (only able to achieve a frame rate of 30) was considered to be the main potential source of error. However, the frequency of oscillation was selected specifically to minimise this error. By selecting a low frequency (2 Hz) with which to drive the nano stage, the camera was able to detect a large portion of the sine wave based movement of the sphere. Any drift over the course of the experiment should therefore have been insignificant, given that it was not the absolute position of the sphere that was of interest, rather the amplitude. The amplitude value should not be affected by drift. As can be seen from **Figure 4.6**, a good quality amplitude signal was achieved.

A second source of error is the use of the tracking program StAT to obtain position information of the trapped and fixed microspheres. The manual selection of the template for StAT to use in locating particles is subjective. Attempts were made to quantify this error by using StAT to process the same video image, of a single loosely trapped sphere, 100 times using 100 different manually selected templates. A mean position of the sphere was found for each data set. The standard deviation of the 100 mean position values was found to be less than 2% of the mean value.

This process of calibrating the Volts-micron ration on the QD was regularly undertaken for both the x and y axis.

4.3 Effect of heating in traps on trap stiffness

4.3.1 Introduction

While undertaking measurements of the characteristics of the optical trap, knowledge of the trap temperature was required, since a change in temperature could affect results in two ways.

Firstly, the viscosity of the medium (in the case of this work, water) is highly dependent on temperature. The viscosity of water is inversely proportional to the temperature(34). Consequently, any calculations made with data which involves viscosity could only hold true if either:

a) The temperature remained constant throughout the experiment.

Or

b) Any change is temperature could be measured and corrected for.

The second way in which a change in temperature could affect the validity of the results is that it could not only change the mechanical properties of the medium, but could also affect the Brownian motion of the spheres. The degree of Brownian motion of an object is proportional to its temperature. Consequently, measuring the laser's ability to trap a sphere with a set power, by measuring the extent to which the Brownian motion of the object was damped could be affected if the laser radiation were to heat up the sphere and thus caused the Brownian motion of the object to increase.

4.3.2 Experimental Method

A number of experiments were undertaken to try to detect any heating within the sample.

The crudest method was the simple use of an infrared camera, employed while a sphere was in the trap. The object was held in the 532nm line optical trap at a power of 70mW for over thirty minutes in an attempt to detect any temperature changes within the sample.

The second method employed was to track the position of a microsphere over an extended period of time at a constant laser power. With the laser power constant, the trap stiffness should remain constant, and the standard deviation of the position of the microsphere should remain relatively constant. However, a temperature increase caused by the laser in the localised area of trap would lead to an increase in the standard deviation of the sphere position due to an increase in the sphere's Brownian (or thermal) motion.

Each 'packet' of position data was acquired using the QD at a frequency of 100 kHz for 0.6 seconds (65536 data points in x and y position). Packets of data were taken every 6 seconds for over 5 minutes. Each packet of data produced a standard deviation over that sample period for the object's position in both x and y. These were then plotted against the time at which that packet of data was taken.

4.3.3 Results and Discussion

Firstly, the attempts to detect any localised temperature rise within the sample were inconclusive as shown in the subsequent figure.

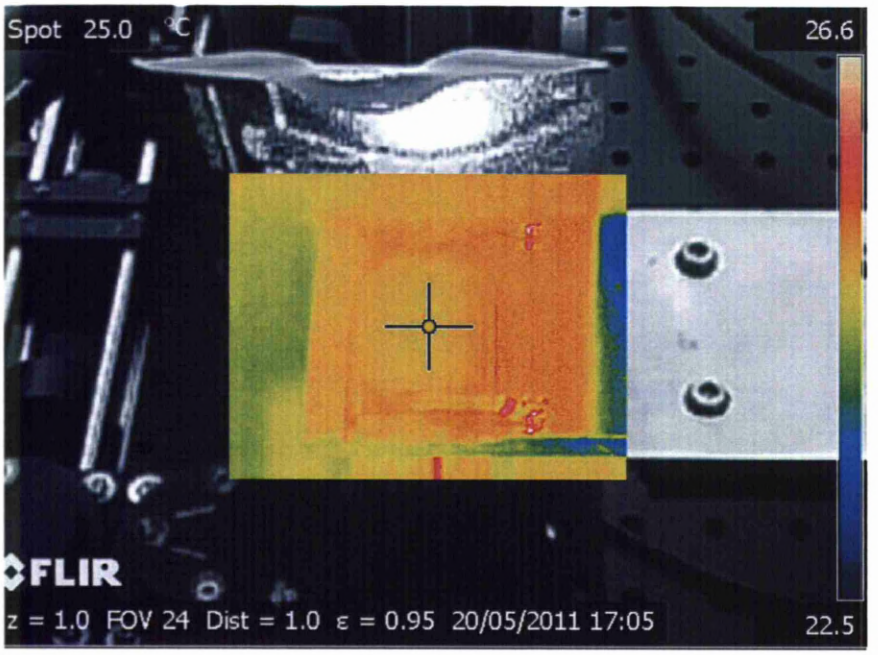

Figure 4.7: Infrared camera image of the sample within a conventional photo image.

Many images were taken showing similar results to that shown above. This image suggests a relatively uniform temperature distribution across the sample. Despite the focussed laser spot being within the water sample for more than thirty minutes, the infrared camera was unable to resolve any localised heating above that of the rest of the sample. This is perhaps expected, given that the focussed spot has an approximate diameter of 300nm. This value is found from **Eq.4.6**.

$$NA \approx \frac{\lambda_0}{\pi w_0} \qquad \textbf{(Eq.4.6)}$$

Where, λ_0 is the wavelength of the laser, w_0 is half the diameter of the beam at its narrowest point.

The second method discussed, regarding the monitoring of microsphere position to detect a change in the Brownian motion of the spheres, has the potential to resolve much smaller areas of temperature increase. This is because the temperature of the microsphere would only need to rise by a few degrees for a noticeable Brownian motion change to be detected (104). The infrared camera method, however, would require a much larger area of the sample to increase in temperature for the said temperature rise to be detected. Two tests were therefore undertaken, the first with the laser power at 20mW and the second with the laser power at 70mW.

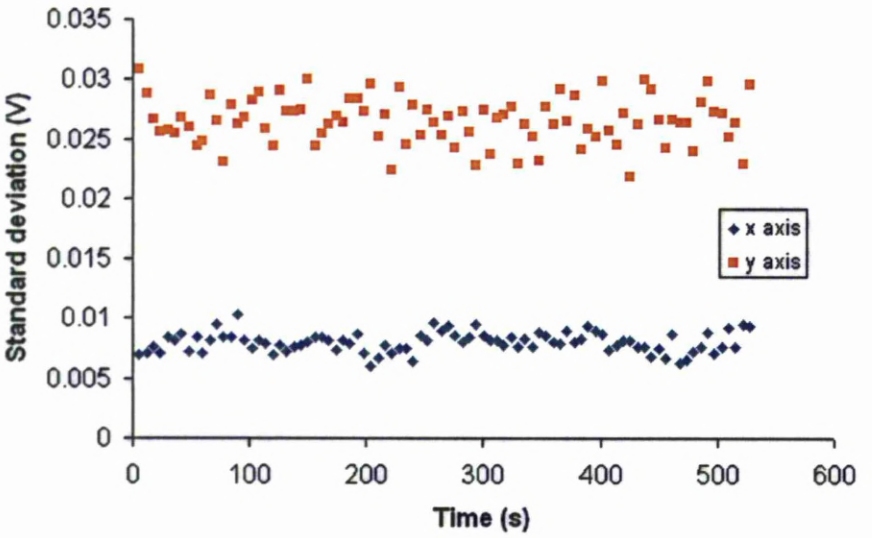

Figure 4.8: The standard deviation of the position of sphere held in a 20mW trap.

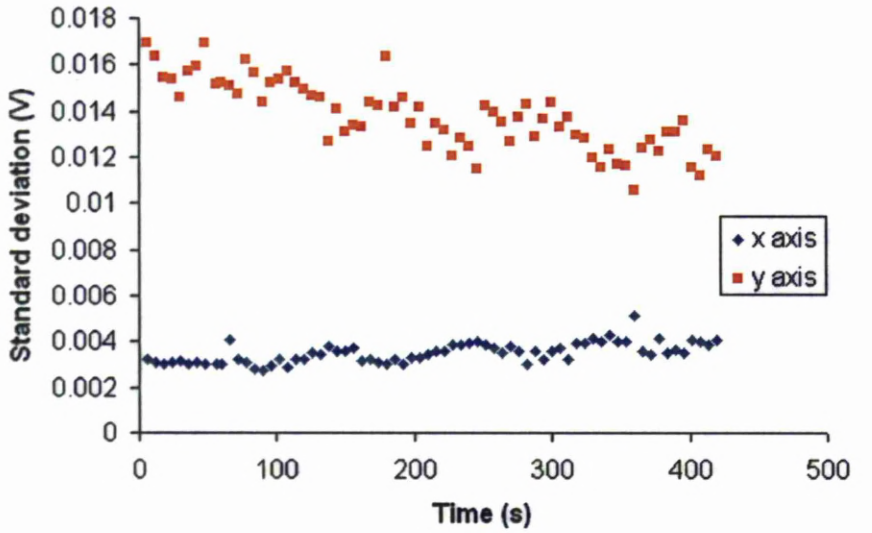

Figure 4.9: The standard deviation of the position of sphere held in a 70mW trap.

Neither of the graphs in **Figure 4.8** and **4.9** show any significant rise in the standard deviation in position. In fact, for the 70mW case (**Figure 4.9**), there is an overall decrease in the standard deviation of the sphere over time.

It is also noted, in both cases that the x axis appears to have a much smaller standard deviation than that in the y axis. If this is accurate it would imply greater trap stiffness in the x dimension than the y. This apparent smaller standard deviation in x compared with y could possibly be for one of two reasons.

Firstly, the standard deviation values shown are in Volts not metres. They are the direct outputs from the QD before a calibration converting Volts to metres was undertaken. It is possible that the conversion values were different for each of the x and y values. The most recent calibration procedure produced similar conversion factors in both x and y. However, it is possible that, in this particular setup, the conversion factors could have changed. So, 1 Volt on the x axis could imply a different number of metres to 1 Volt on the y axis. However, this was deemed unlikely as the various conversion factors calculated during the project were never greater than 8% from the mean conversion factor. As the original purpose of the experiment was to establish any localised heating in the trap it was not deemed necessary to consider the effect of these conversions, since a rise in temperature could be viewed just as easily in Volts as in metres.

The second possibility is that the result was accurate, in that the optical trap had greater trap stiffness in x than in y. This could be for a number of reasons, such as the direction of linear polarisation of the beam, and is investigated further in section 4.6 this chapter.

4.4 Determining Trap Stiffness

Since optical trapping has developed as a measurement tool, trap stiffness has increasingly become the quantity of choice to measure. Trapping efficiency, Q, as mentioned in Chapter 2 is an alternative parameter through which to quantify the performance of an optical trap. However, increasingly it is trap stiffness, k, that has become the parameter of choice. This is largely due to trap stiffness providing the capability for calibrated force measurements (usually of the piconewton range) which is a highly desired capability in a number of research fields but especially in the biosciences arena. There are commonly three methods of measuring the trap stiffness:

4.4.1 Method 1 – Based on Stokes' Law

4.4.1.1 Experimental Method

A sample was constructed in the 'spacer' design (as shown in figure 3.27) containing a dilute solution of 2.44μm diameter silica microspheres and then loaded into the system. A sphere was then trapped at a specific power and, as with the escape force experiment, the stage was translated at a known velocity.

While the stage is translated, a force is exerted on the trapped sphere causing a displacement from the trap centre, which is characteristic of the trap stiffness. Hence, as the stage was translated, the data acquiring program 'nanostage2b' was run to monitor this displacement. This was

repeated for a range of stage translation velocities to ascertain a displacement characteristic, the gradient of which was representative of trap stiffness. This was repeated, translating the stage in both directions in both the x and y axis.

4.4.1.2 Results and Discussion

In the following figures (**Figures 4.10 – 4.15**), the position and velocity measured in the range 30-80mW are presented graphically. The x axis on each graph shows the velocity with which the stage was translated, while the trap position is held constant. Negative velocity represents the translation of the stage in a different direction. Note that the positions are not normalised, hence why at zero velocity the centre of the trap in not at the origin.

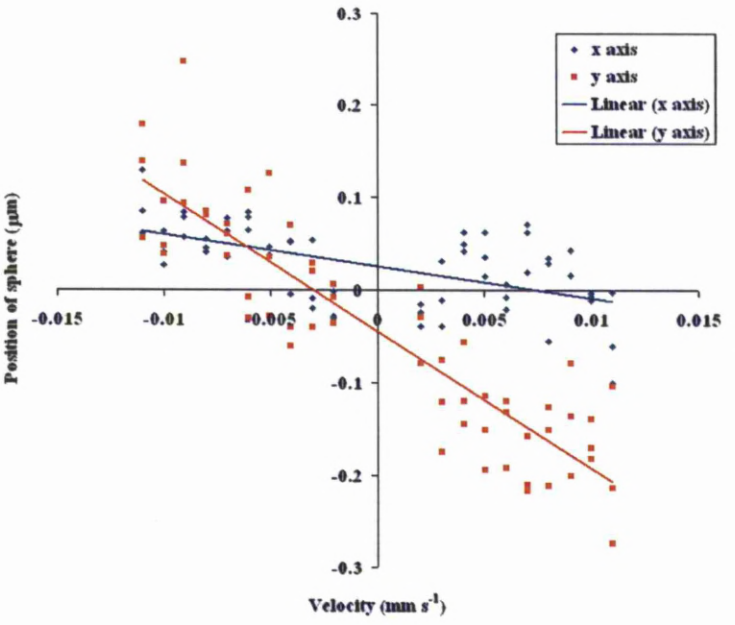

Figure 4.10: Position and velocity of sphere for a power of 30mW

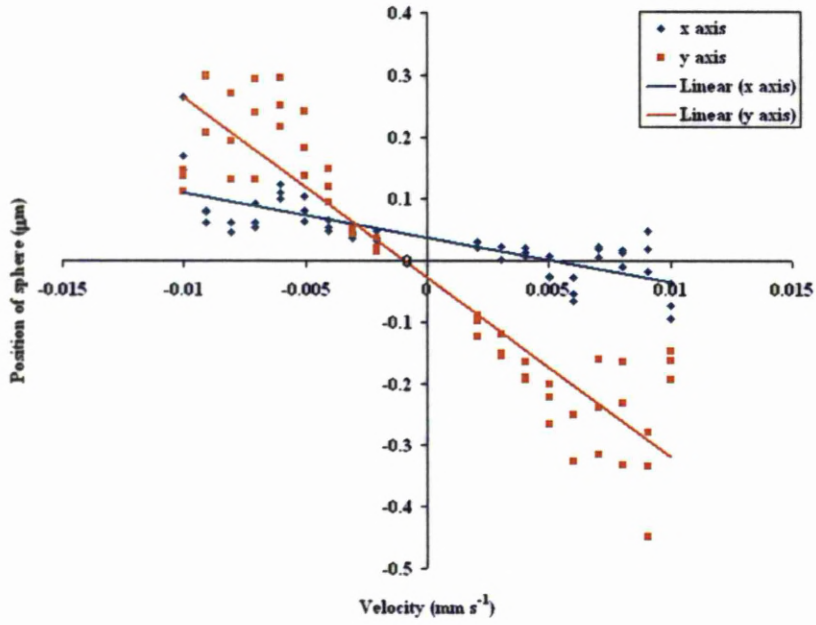

Figure 4.11: Position and velocity of sphere for a power of 40mW

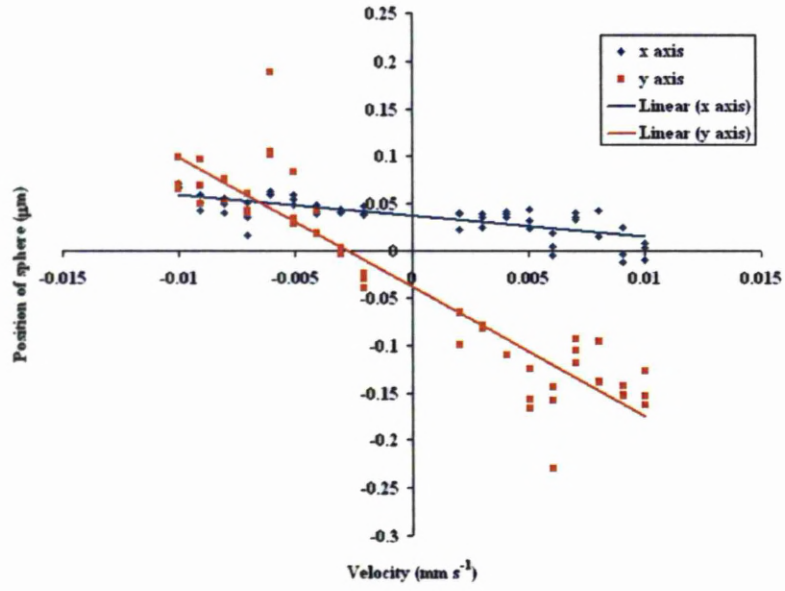

Figure 4.12: Position and velocity of sphere for a power of 50mW

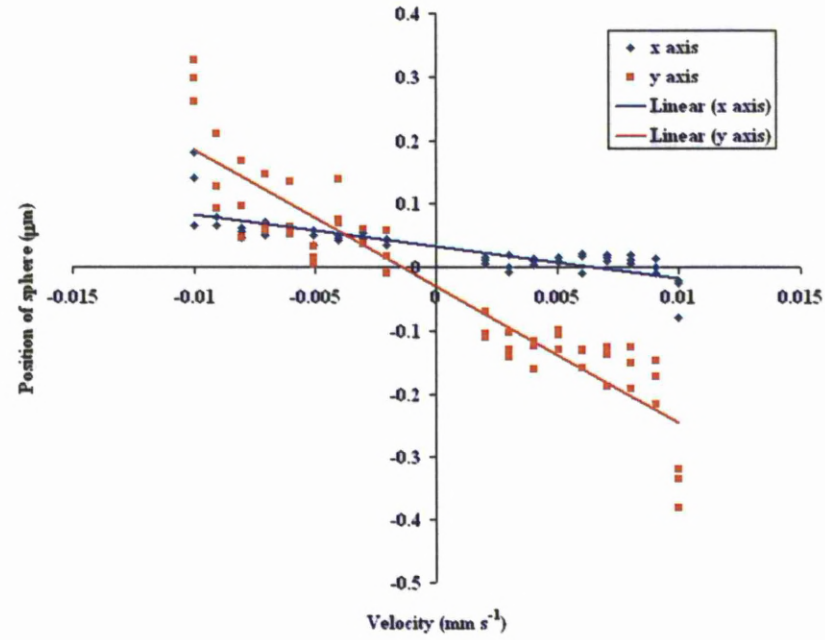

Figure 4.13: Position and velocity of sphere for a power of 60mW

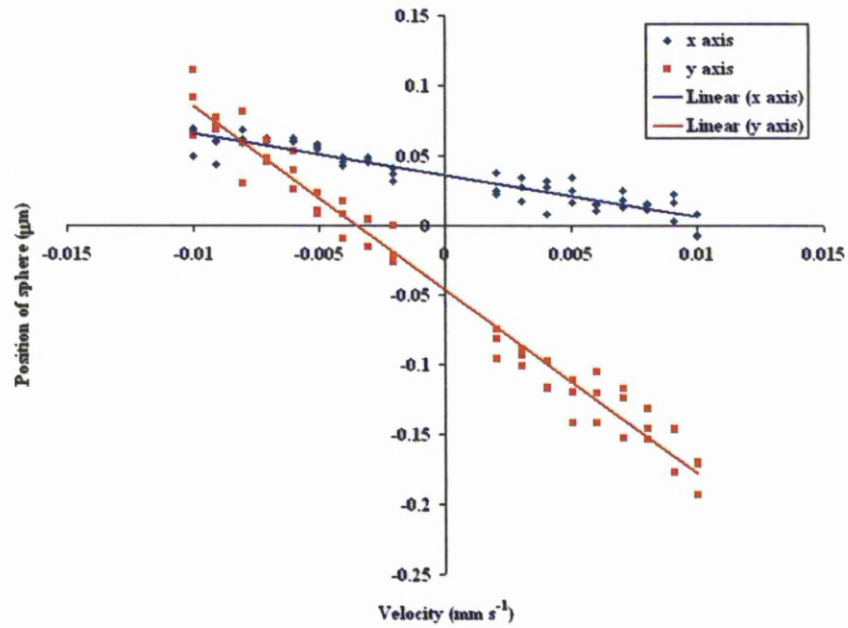

Figure 4.14: Position and velocity of sphere for a power of 70mW

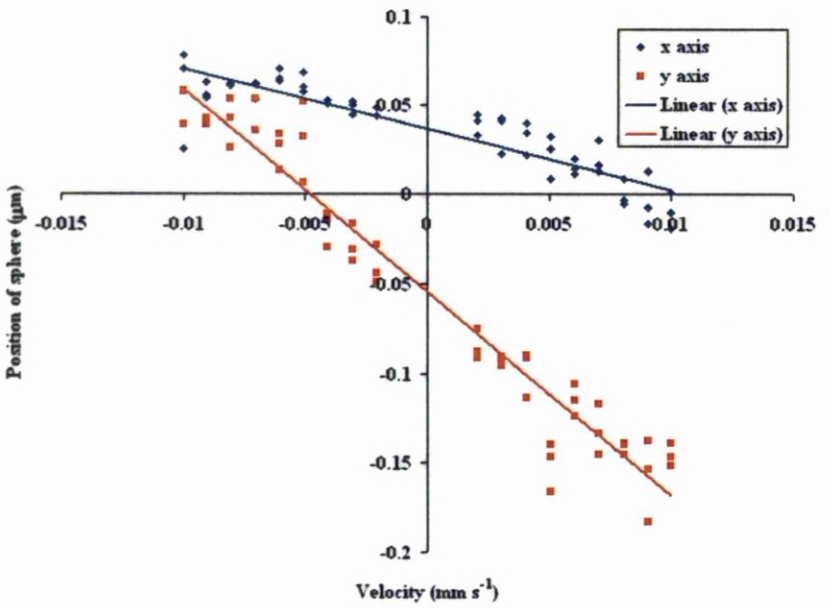

Figure 4.15: Position and velocity of sphere for a power of 80mW

The first thing to note is that the gradient for the x and y data are distinctly different to each other. As velocity can be converted to a drag force via Stokes' Law it is possible to quantify the trap stiffness. The gradient of each trendline in the preceding graphs was quantified and converted into trap stiffness in pN nm^{-1}. This data is shown in **Figure 4.16**.

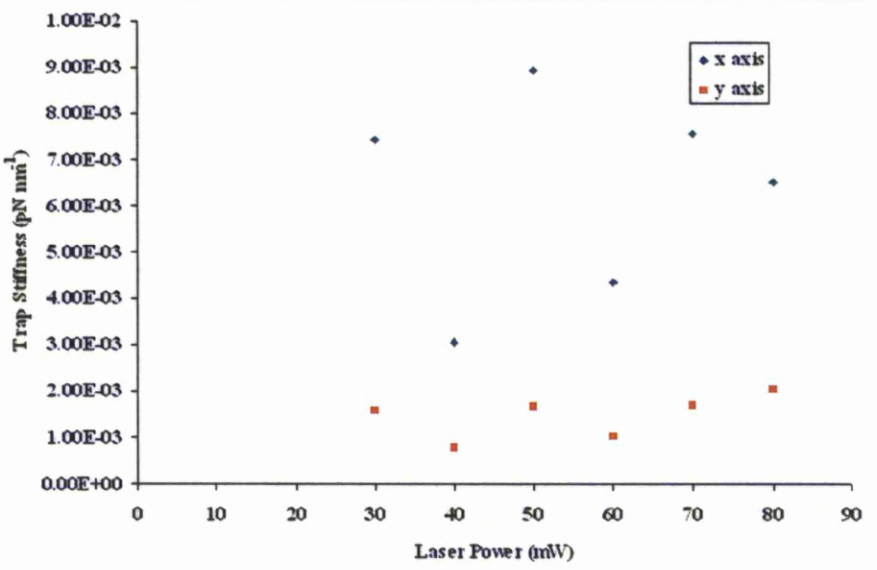

Figure 4.16: Trap stiffness at a series of laser powers in each of the x and y axes.

In spite of the linear relationships apparent in **Figure 4.10-4.15**, it appears their relative gradients were only loosely dependent upon the laser power, as seen in **Figure 4.16**. It appears that the laser produced a 'tighter' or 'stiffer' trap in the x dimension than the y. At this point in the research, it was suggested that this discrepancy could be caused by the direction of linear polarisation of the beam, and this is therefore discussed in more detail later in this chapter.

4.4.2 Method 2 – Based on Equipartition Theory

4.4.2.1 Experimental Method

Three samples containing different size microspheres were made up, using the 'spacer' method of sample preparation as set out in Chapter 3.

One of these samples was loaded into the system and a sphere optically trapped at a set laser power. This time the stages were held stationary throughout. The LabView program 'nanostage2b', which is discussed in Chapter 3, was then employed to track the trapped spheres' positions in time at a frequency of data acquisition of 100 kHz. Each data set contained 65536 data points for each of:

- Position of sphere in x, in Volts from the QD
- Position of the sphere in y, in Volts for the QD
- The sum value from the QD
- The time at which each of the above occurred.

Each data set was collected in approximately 0.6 seconds. So, multiple data sets could be taken in a short space of time. Once multiple sets had been taken at a set power, the power was then increased and the process repeated. Once multiple data sets had been taken at a series of powers, a new sample was loaded containing different sized microspheres and the process was repeated.

The position data was then converted from Volts to microns using the method set out earlier in this chapter. Then the principle of equipartition

was used to find values for the trap stiffness. The principle of equipartition is a classical statistical mechanics theorem that defines the relationship between the temperature of a system and the average energy of all the particles within it. It quantifies the thermal energy for each degree of freedom (x, y and z), thus the particles in each degree of freedom will possess an average energy related to the temperature according to **Eq.4.7** (105).

$$\frac{1}{2}k\left\langle \delta^2 \right\rangle = \frac{1}{2}k_b T \qquad \textbf{(Eq.4.7)}$$

Where, k is the trap stiffness, kb is the Boltzmann constant, T is the temperature (K) and δ is the standard deviation in the position data of the trapped sphere(106).

4.4.2.2 Results and Discussion

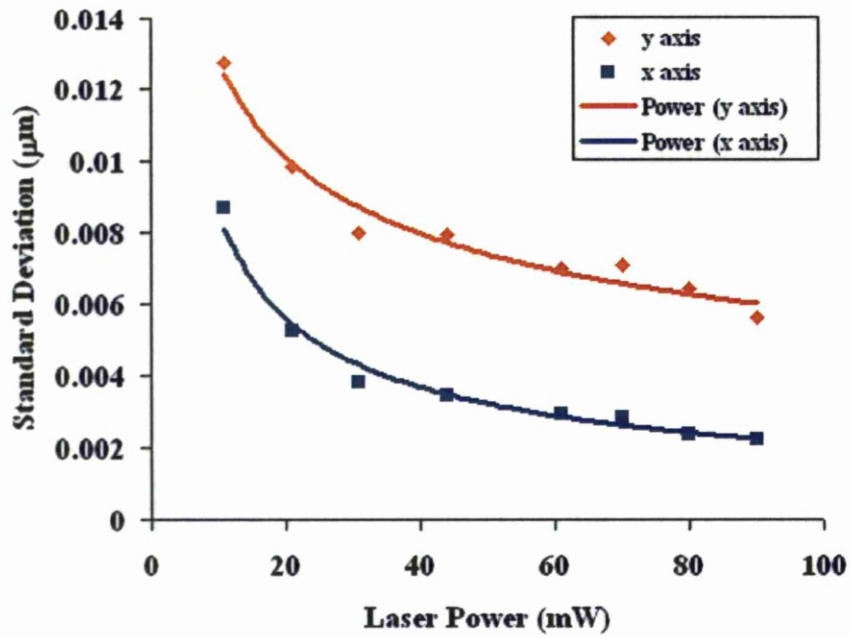

Figure 4.17: Position data from QD of a 1.54 µm silica sphere

Through use of the equipartition method, the standard deviation in the position of the sphere could be converted to trap stiffness and is plotted against laser power in **Figure 4.18.**

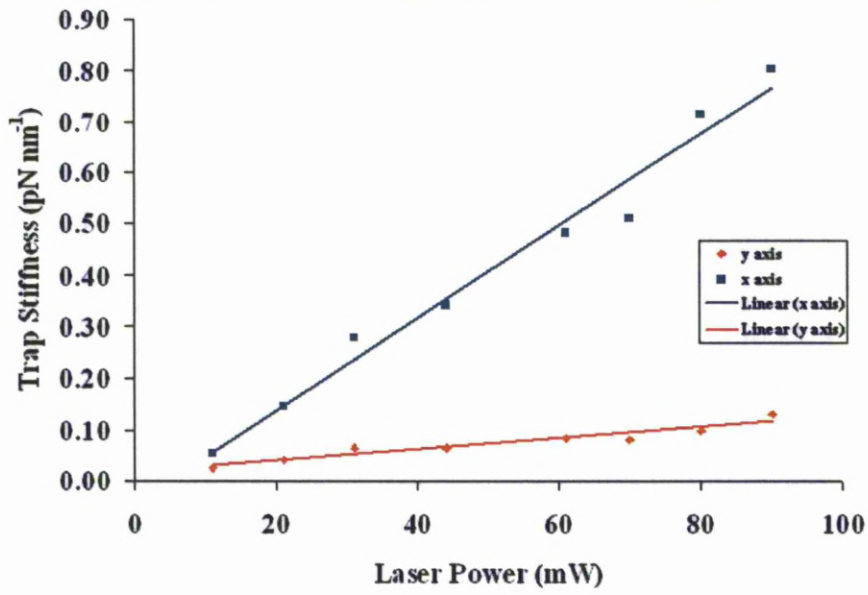

Figure 4.18: Trap stiffness calculated through the equipartition method for a series of laser powers

As with the Stokes' law method of determining the trap stiffness, the trap stiffness appears to be significantly larger in the x dimension than in the y. Unlike the Stokes' law case however, the equipartition produces a result showing a clear proportionality between the laser power and the trap stiffness which corresponds with similar work reported in the literature (32). The results in **Figure 4.17** and **4.18** led to an investigation into the effects of linear polarisation of the trap stiffness, undertaken in section 4.6 of this chapter. As mentioned in the previous section, these results implied the possibility that the direction of linear polarisation was influencing the trap stiffness.

4.4.3 Power Spectrum Method

4.4.3.1 Introduction

The power spectrum method uses knowledge of thermal motion physics to ascertain values for the trap stiffness. Numerous groups have investigated this method including various mathematical analyses (107-110). The idea behind it is that the frequency information of the microsphere is related to the trap stiffness. As the trap stiffness is increased the high frequency components of the movement become dominant. Conversely, as the trap stiffness is decreased lower frequency movements are more significant.

A one- sided power spectrum of the position data of a trapped sphere produces a graph with a characteristic 'corner frequency' which can be used to calculate the trap stiffness from the expression(27):

$$f_c = \frac{k}{2\pi\gamma} \qquad \textbf{(Eq.4.8)}$$

Where, f_c is the characteristic corner frequency, k is the trap stiffness and γ is the drag coefficient:

$$\gamma = 6\pi\eta r \qquad \textbf{(Eq.4.9)}$$

Where, η is the viscosity of the medium and r is the radius of the sphere.

4.4.3.2 Experimental Method

A sample was made using the spacer method of 2.44 μm diameter silica spheres (see figure 3.27). A sphere was trapped at a set laser power and held in a stationary position. The QD was used to acquire position data for the trapped sphere's damped Brownian motion as it was held in the optical trap. This data was then subjected to a 'Fast Fourier transform' to produce a one-sided power spectrum. A Lorentzian fit was then performed on the power spectrum to find a value for the corner frequency. A Matlab routine employing the Levenberg-Marquardt algorithm (111) was used to fit a Lorentzian curve to the data. The algorithm provided a quick method of finding the best parameters for the fit, where the 'best parameters' were found using a 'sum of least squares' method. The algorithm requires an initial 'guess' from the user for these parameters in order to initiate the iterative process. The power spectrum data is displayed with both the x and y axes logged in order to visualize the corner frequency, f_c. The corner frequency is defined in the Matlab routine as the frequency at which the power in the power spectrum has reached half its initial value.

At each laser power, multiple data sets were taken, then a power spectrum was taken of all data sets for a set laser power and an average value determined. The averaged one sided power spectrum was then fitted with the Lorentzian curve and the Matlab routine concluded by producing a corner frequency value.

Results and Discussion 4.4.3.3

Many results were taken and corner frequencies established but as can be seen from Table 4.1, there were problems with the data.

Laser Power (mW)	Test numbers	Corner frequency, f_c
20	2902-2911	59.7
30	2923-2932	170.8
40	2943-2952	57
50	2965-2974	94
60	2985-2995	78.8
70	3007-3016	63
80	3027-3036	91.6
90	3048-3057	67.7

Table.4.1: The corner frequency found from the average of 10 power spectrums of data acquired from the position of a trapped 5.44 μm sphere.

Table 4.1 is typical of corner frequency data acquired during this research. As can been seen from the Table 4.1 there appears to be no pattern linking the corner frequency and the laser power. The fact that the same method of data acquisition had been used with the equipartition method, shown is previous section to produce reasonable quality results, in terms of correlation between laser power and trap stiffness, suggests the issue is not with the data acquisition method, but could possibly be the fitting program used to establish the corner frequency. The log scales on both axes of these graphs mean that a very small movement in the position of the corner frequency on the y axis could lead to a vastly different frequency reading on the x axis.

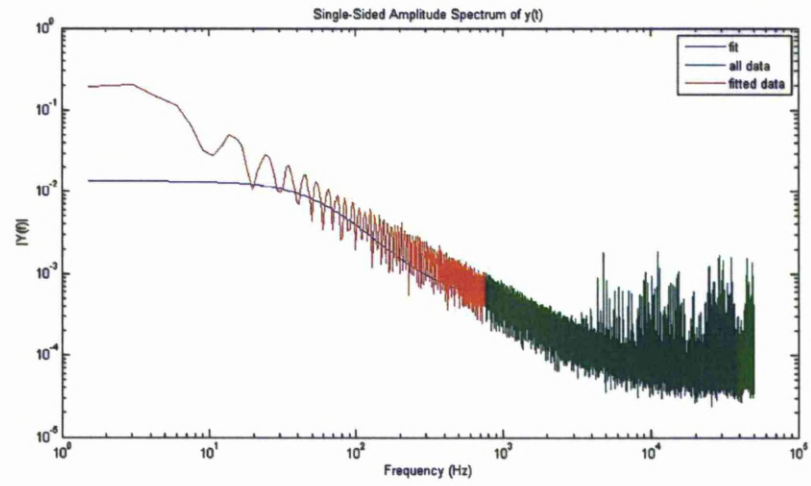

Figure 4.19: One-sided power spectrum of the position data from a 5.44 mm silica sphere held in a 20mW laser trap.

The red line represents the fitted data. The logarithmic nature of the data meant that, if the fit was calculated using all the data, it would be dominated by the high quantity of data produced in the high frequency region.

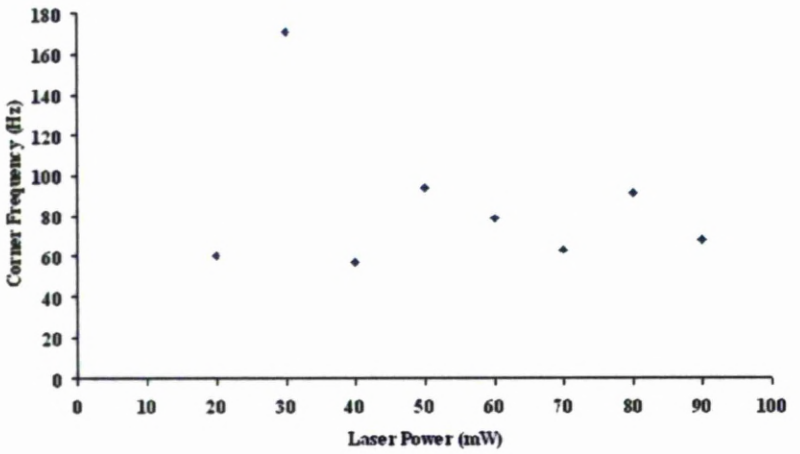

Figure 4.20: Effect of laser power on corner frequency. This graph represents the data shown in Table 4.1.

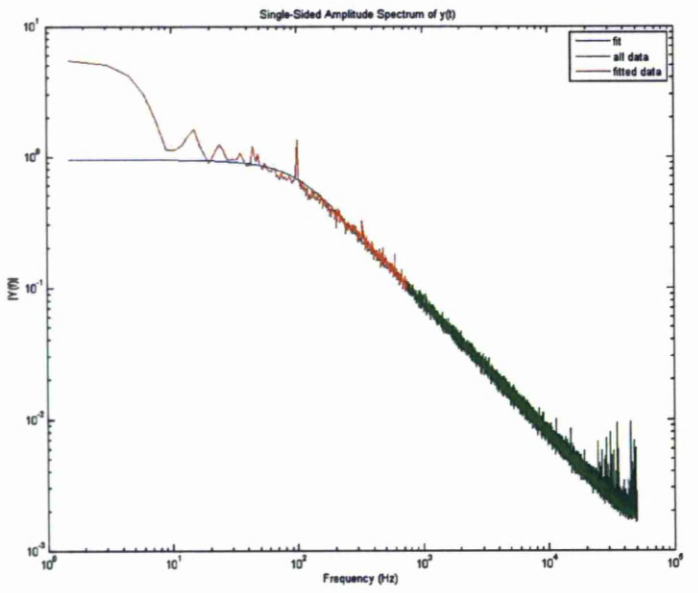

Figure 4.21: A single-sided averaged power spectrum of the position data of data from 70 independent data test with a 1.54μm sphere trapped in a trap of 70mW.

It is noted that increasing the number of independent data sets recorded then taking an average of these, increases the quality of the fit. However, the taking of 70 independent tests is a time-consuming process in comparison with the Stokes' law or equipartition methods of determining the trap stiffness. As can be seen from Figure 4.20, this research found that the corner frequency, when calculated from a relatively low number of samples, such as 10 as in Table 4.1, did not follow any clear trend as the laser power was increased. It is reasoned that the mathematical issue of defining the corner frequency. As can be seen from Figure 4.19, which represents one set of data, for lower quantities of data the corner is far less 'pronounced'. Whereas, Figure 4.21 which is an average of 70 power spectrums, a far clearer position of the corner can be seen. However, even when larger numbers of power spectrums were averaged, there was not a significant increase in the quality of the results. As part of a calibration process 100 independent power spectrums have been used (27) but not as a method of force measurement. The practicalities of doing 100 tests is justifiable for a not too regular calibration process, but taking 100 tests per measurement is less so. The longer the experimental process, the more likely external factors, such as a temperature change within the lab, will have an effect.

4.5 Effect of laser power (0-100mW) and microsphere diameter on the optical trap escape force

4.5.1 Introduction

The laser power is perhaps the most fundamental parameter to vary while monitoring the state of the optical trap. As discussed previously there are various ways of doing this.

Firstly, in this section, it is not the trap stiffness that is investigated but the escape force. As explained in chapter two, the optical trap can be thought of as a potential well – with the escape force defined by the well depth and the trap stiffness closely related to the gradient and width of the well as seen in Figure 4.22.

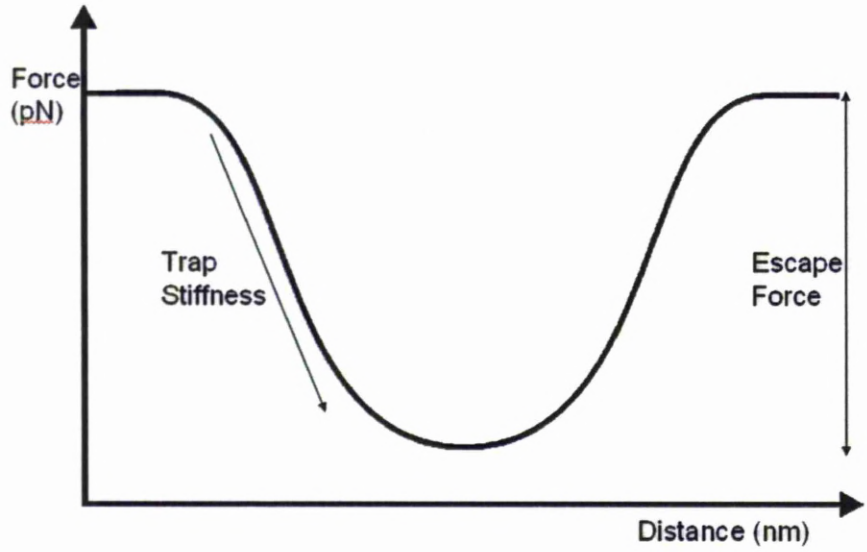

Figure 4.22: A graph to represent the forces of an optical trap. The escape force is the 'depth' in pN of the trap. The trap stiffness is closely related to the gradient of the well but also depends upon the width of the well.

It has been previously demonstrated (32) that the laser power is proportional to the escape force. Here this is tested alongside the effect of the size of the microsphere on the escape force.

This experiment was undertaken with the system in its secondary stage of development, as discussed in Chapter 3. This was before the integration of the QD. Consequently, this crude experiment was conceived as a method of evaluating the quality of the optical trap at a variety of powers.

4.5.1.1 Experimental Method

Samples of low concentrations of 0.5, 1.54, 2.44 and 5.44 μm diameter silica microspheres were constructed using the 'cavity microscope slide' method, as set out in Chapter 3. The first sample was then loaded into the system and a sphere was optically trapped. The micro stage was translated along the x axis at a series of known velocities while the trap position remained constant. Translating the whole medium is essentially the same as translating the trapped sphere through the medium. The velocity of this translation produced a drag force according to Stokes' law. Starting at a very low value, the velocity slowly increased until the drag force was too great for the optical trap to overcome and thus removed the microsphere from the trap. This velocity was then associated with the laser power used to achieve it. The power was then changed and the experiment repeated. Once velocity values for a full set of laser powers had been obtained, a new sample containing different size microspheres was loaded and the process was repeated.

4.5.1.2 Results and Discussion

The force calculated from the measured escape velocities, using Stokes' Law, and found at each power for each diameter of sphere is presented in **Figure 4.23**.

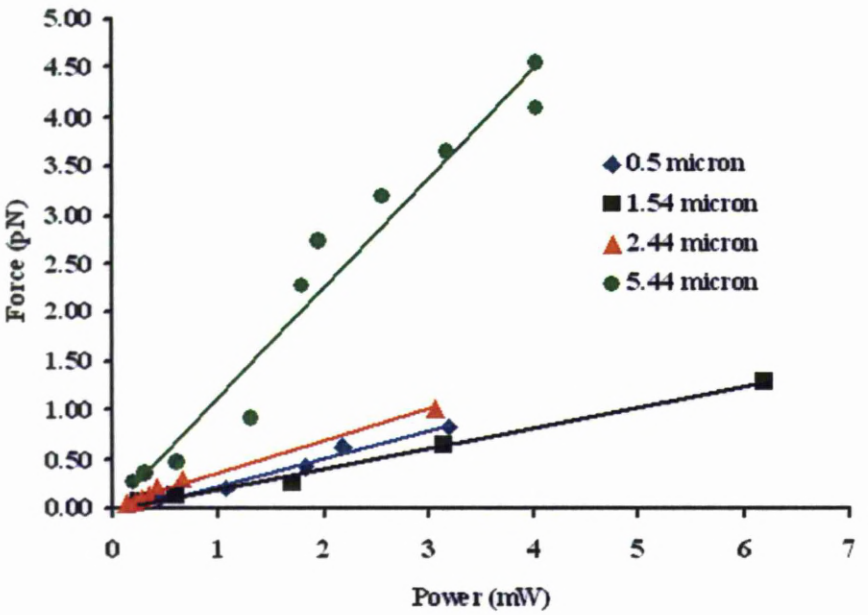

Figure 4.23: The escape force measured against laser power for 0.5, 1.54, 2.44 and 5.44 diameter silica spheres

Interestingly, **Figures 4.23** suggests that the larger the sphere, the greater the drag force required to remove it from the optical trap. This is perhaps counter-intuitive in that the larger spheres have considerably more mass, as shown in **Table 4.2**.

Diameter (μm)	Radius (μm)	Volume (μm^3)
5.44	2.72	84.29
2.44	1.22	7.60
1.54	0.77	1.91
0.5	0.25	0.07

Table 4.2: Showing how a relatively small change in the diameter leads to a vast change the relative volume.

As shown in table 4.2, a 5.44μm diameter sphere has approximately 42 times more mass than a 1.54μm diameter sphere of the same material. Yet the heavier sphere achieved greater escape velocities at each laser power. Hence, it is clear that the mass of the sphere is not the most significant factor in the laser's ability to manipulate a sphere. A second point of note is that it appears from **Figure 4.23** that the 5.44 μm diameter spheres are being trapped through a different mechanism to the 0.5, 1.54 and 2.44 μm diameter spheres. From an understanding of the different trapping regimes (the ray optics regime and the electric dipole regime), this is an unexpected development. The 1.54, 2.44 and 5.44 μm diameter spheres are all larger that the laser wavelength and so their trapping would be expected to adhere to the ray optics regime, whereas the 0.5 μm diameter sphere is very close to the wavelength of the laser and would therefore be expected to operate in a combination of the two regimes. However, consider that the larger sphere has a much greater surface area and thus receives a greater number of photons leading to a greater transfer of momentum. With regard to the

laser's ability to impart a force onto a sphere, for these sizes of sphere, the effect of receiving a greater number of photons appears to outweigh the sphere's mass as the most significant factor. **Figure 4.24** is drawn from the same raw data as **Figure 4.23**, but in this case it is the escape force per 'interaction area' (N m^{-2}) that is displayed, where interaction area is the surface area of one half of the sphere.

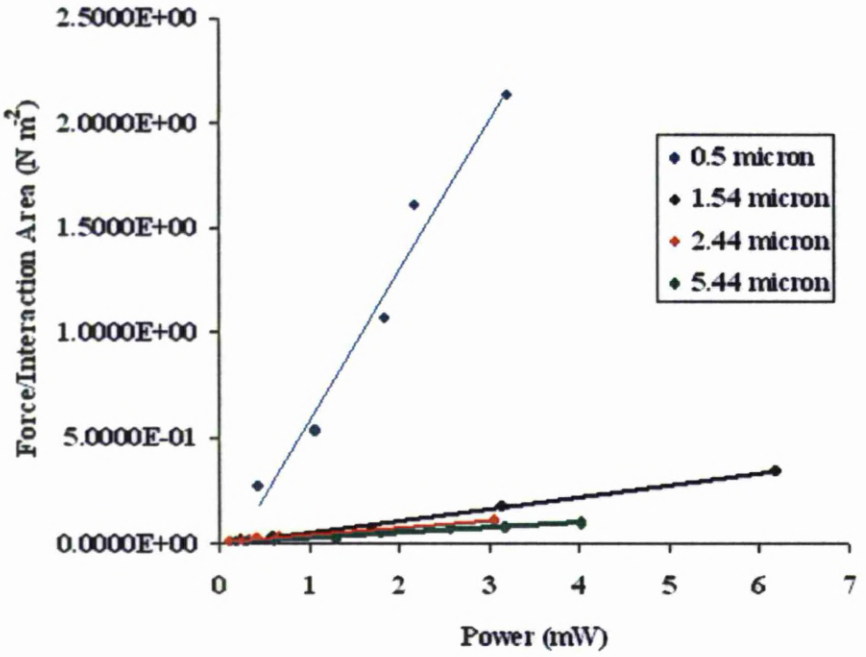

Figure 4.24: The drag force per unit of 'interaction area' (required to remove a sphere from the trap) against laser power for 0.5, 1.54, 2.44 and 5.44μm diameter spheres

The change is considerable from **Figure 4.23** and **4.24**. It is now clear that the 0.5 μm sphere is operating under a separate regime to the other three

sizes of sphere. In fact, this data suggests very little difference in the laser's ability to impart force into the larger spheres when viewed within the context of their relative surface areas. However, the graph does show a minor difference in the force per interaction area for the three larger diameter spheres. It appears that the 1.54 μm sphere achieves the greater force per interaction area per unit of power followed by the 2.44 and 5.44 μm diameter spheres respectively. This minor difference is most probably caused by the mass difference shown in table 4.2.

4.6 Effect of the direction on linear polarization on trap stiffness

4.6.1 Introduction

In the system described in Chapter 3, the 532nm laser passes through the attenuator setup in a state of linear polarisation. The direction of linear polarisation produced by the laser is vertical, but the direction can then be varied using the half wave plate alongside the glan laser polariser in the attenuator set up, as shown in **Figure 4.25.** Using this arrangement, it was then possible to measure how the trap stiffness in x and y is affected by a 90° change in the direction of linear polarisation.

4.6.2 Experimental Method

The direction of the beam linear polarisation was set to vertical by a second half wave plate installed immediately after the mechanical shutter on the 532nm laser line, as seen in figure 4.25.

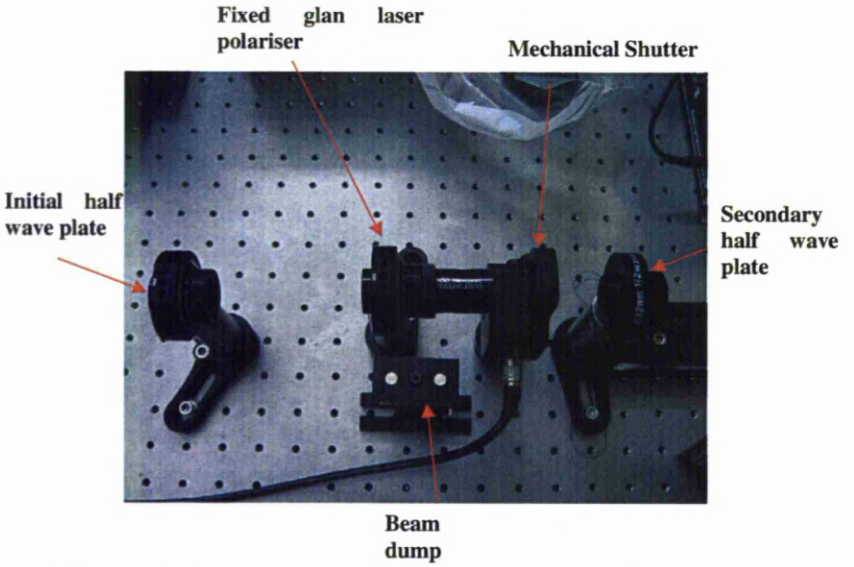

Figure 4.25: Attenuator setup with secondary half wave plate.

This setup allowed the linear polarisation of the light to be rotated by up to 90°.

A silica sphere was trapped and its position monitored with the QD for a series of powers with the beam, in a state of vertical polarisation. Then the polarisation was altered to horizontal and the process was repeated. The position data of the sphere could then be converted to a trap stiffness value using either the equipartition or the power spectrum method. Both are presented in the following results section.

4.5.3 Results and Discussion

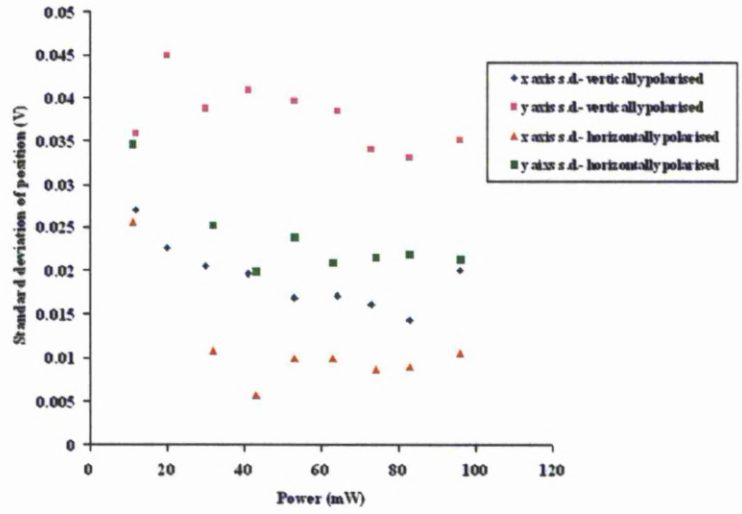

Figure 4.26: Mean standard deviation of sphere position from 5 tests at a set laser power and beam polarisation.

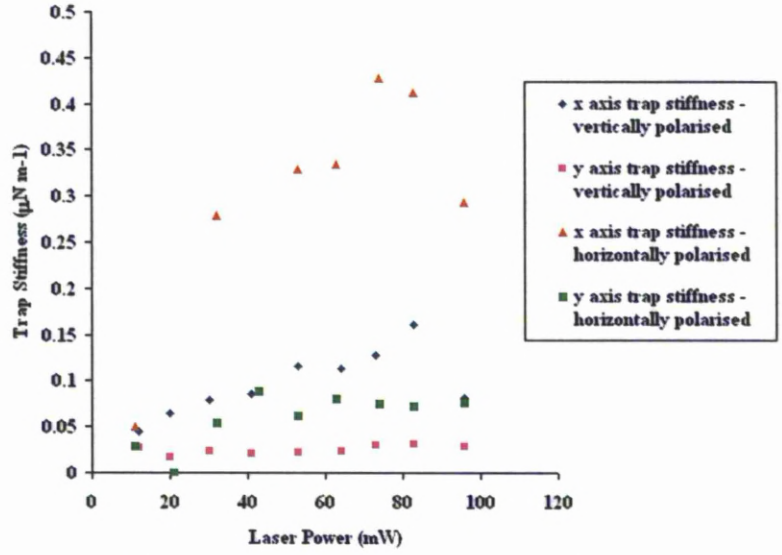

Figure 4.27: Converted from standard deviation data in **Figure 4.26**, through use of the equipartition theory. Trap stiffness data for a series of laser powers at set states of linear polarisation.

Had the direction of linear polarisation been the parameter responsible for the trap being stronger in one dimension (the x axis) than the other (the y axis), it is reasonable to deduce that a change in linear polarisation from vertical to horizontal would thus switch the axes' performance, i.e. make the trap stiffness stronger in y than in x. However, as can be seen from **Figure 4.26** and **4.27,** this is not the case. The offset between the two axes' 'performances' remains. The direction of linear polarisation can thus be ruled out as the cause of the offset in the x and y axes' trapping ability.

It is also possible that the ellipticity of the beam is responsible for the discrepancy in trap stiffness between the x and y axes. Consider **Figure 4.22**, representing the potential well of the trap in two dimensions. If the beam was slightly elongated in one axis then the three-dimensional potential well would be wider in one dimension than the other. Clearly an elongation in the beam will elongate the spot diameter. The dimension of the beam containing the elongation would most probably be the axis with the lower trap stiffness. This is because the equilibrium position, or centre of the trap, is elongated in this dimension, and thus the area in which the sphere can reside near equilibrium is larger, leading to a greater variance in the spheres position in that dimension. The cause of the ellipticity is the SLM. As the beam is expanded up onto the SLM, some of the beam is 'lost'. The SLM surface is slightly rectangular, so it reflects more photons in one axis than the other, when the beam is expanded to the point of overfilling it. This overfilling, and thus slightly rectangular beam leaving the SLM, is probably the cause of the discrepancy between the trap stiffnesses in the x and y axes, not the beam polarisation as previously hypothesised.

4.7 Use of St.Andrews Tracker (StAT) program to find trap stiffness values

4.7.1 Introduction

The St.Andrews Tracker is a piece of object tracking software written in LabView. The program has the capability of tracking numerous objects of different varieties simultaneously from pre-recorded video footage. The program offers an alternative method for tracking the position of a microsphere as opposed to a QD. As discussed previously, both methods have advantages and disadvantages. The tracking software is limited by the frame rate of the camera, which is generally much less than is achievable with a QD. Whereas a QD has the disadvantage of being limited to tracking one object at a time and requires a complex calibration procedure. Furthermore, any calibration on the QD is only accurate for the just acquired data. Thus, regular recalibration is required.

4.7.2 Experimental Method

Samples were constructed for each of the three sizes of sphere available, (i.e. 1.54, 2.44 and 5.44μm diameters) and each immersed in distilled water and 2 drops of the surfactant. The samples were constructed using the 'microscope slide with cavity' method (see figure 3.28). This method of sample construction was preferable to the 'spacer' method as it provided a much larger volume of sample to allow trapping of the spheres far from any surfaces, which could otherwise have distorting effects on the results. The sample containing the 1.54μm diameter spheres was trapped with the 532nm laser line. The power of the laser was measured with a power meter (positioned immediately after the mechanical shutter). A video was then

captured of the trapped sphere at a frame rate of 30 frames per second. Videos were then captured of the trapped sphere for a series of laser powers and then the process was repeated for each of the 2.44 and 5.44 μm diameter sphere samples.

The videos were then processed using the tracking program StAT. This program outputs the x and y position of the trapped sphere in pixels for each frame of the video. The pixel positions were converted in microns. The equipartition method of trap stiffness calculation was employed to convert the variance of the sphere's position into a value for the trap stiffness. A trap temperature of 298K was assumed for this experiment.

4.7.3 Results and Discussion

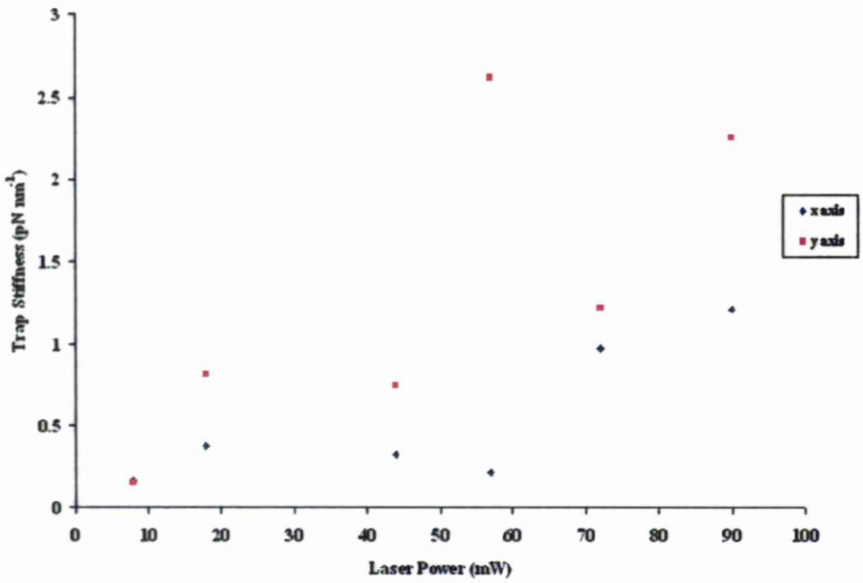

Figure 4.28: The Trap Stiffness as a function of laser power for a 1.54 μm sphere trapped in the 532nm laser line.

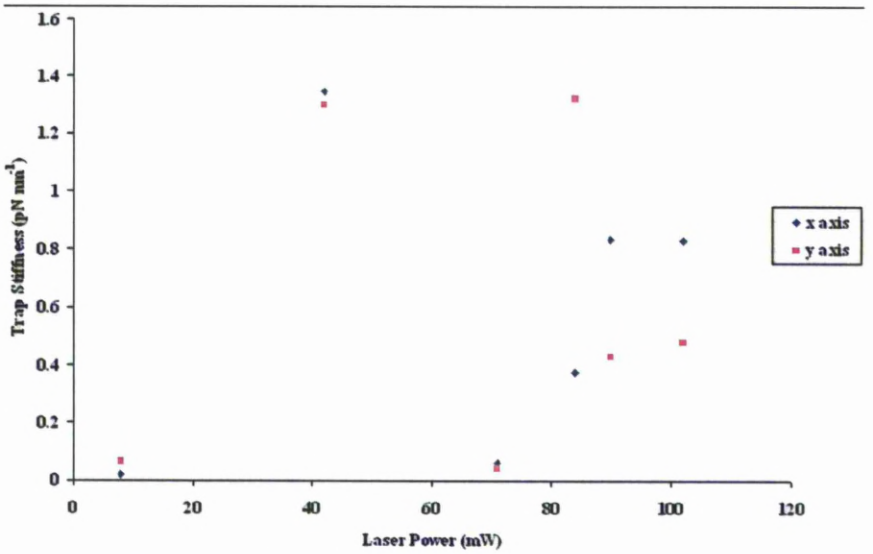

Figure 4.29: The Trap Stiffness as a function of laser power for a 2.44 μm sphere trapped in the 532nm laser line.

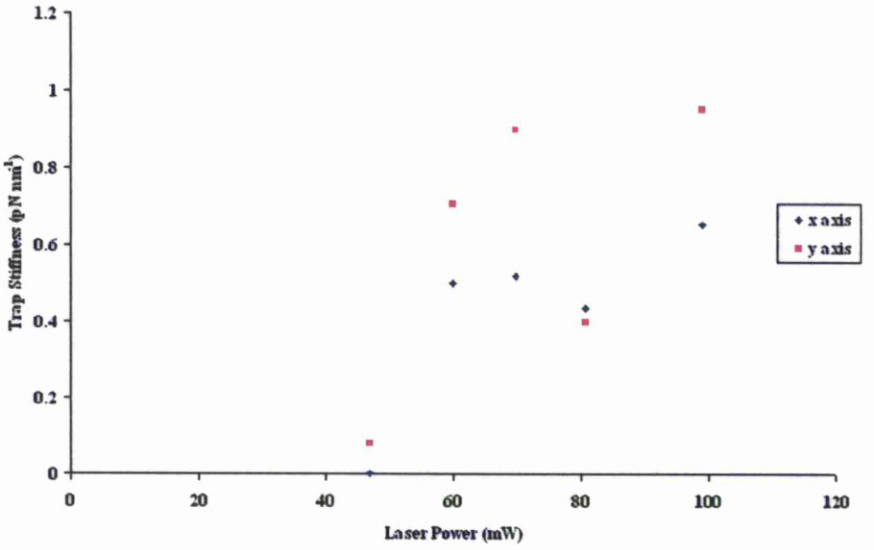

Figure 4.30: The Trap Stiffness as a function of laser power for a 5.44 μm sphere trapped in the 532nm laser line.

Each of the graphs in **Figure 4.28 to 4.30** displays an (expected) increase in trap stiffness with laser power. Furthermore the trap stiffness values produced, of the order of 1pN nm^{-1}, compare well with trap stiffness values found in other studies (31,32,112,113). However, these results also highlight the difficulties in both the use of a low frame rate camera for monitoring the trap position, and in the use of the equipartition method as a method of trap stiffness calculation. None of the graphs produced the expected linear relationship between laser power and trap stiffness. This does not compare favourably with the highly linear relationship found in the escape force experiment results

.

The equipartition method, see **Eq.4.7**, is dependent on both temperature and accurate knowledge of the sphere's variance in position. Accurate knowledge of localised temperature is very hard to achieve as discussed earlier in this chapter.

4.8 Discussion on the different methods of data acquisition, force calibration and force measurement

This chapter, together with the work in the force measurement section of chapter two, shows that there are currently a number of different methods of quantifying the quality, effectiveness or precise forces exerted, in an optical trap. Although some methods have become more popular than others it is clear there remains no consensus or universal method.

Each method has its advantages and disadvantages and the method of choice may well be determined by what hardware is available in a system. The power spectrum method is limited by the need for many independent

spectra to produce an accurate corner frequency and thus trap stiffness. It is also dependent upon the fitting routine, but it has the advantage that it is not temperature dependent; or rather, no temperature is assumed in the process of calculating the trap stiffness. Whereas, for the equipartition method, a temperature value is required in the calculation. The Stokes' law method is the most fundamental and provides a good knowledge of the trap stiffness at larger displacements from the trap centre. Both the power spectrum method and Stokes' law method require knowledge of the sphere's radius. Commercially available spheres of the micron scale quote confidences in the quoted diameters in the region of +/- 10% which is not inconsiderable. The equipartition method however, benefits from being independent of the trapped sphere's size. A downside to the equipartition method is its dependence upon variance which is inherently distorting. Variances are found from the squares of all the differences from the mean. Consequently, all values are positive and thus cumulative. Therefore, any noise or drift in the system will only serve to increase the variance and thus imply smaller trap stiffness than reality. Consequently, this method can often provide an overestimate of variance and hence an underestimate of the trap stiffness.

4.9 Measuring viscosity of the medium using a calibrated trap stiffness

One of the engineering, or indeed medical, applications proposed which could benefit from accurate knowledge of the forces involved in an optical trap, is an ability accurately to measure the viscosity of a medium. In the medical area it could potentially be possible to use such a system to measure the viscosity of a blood sample. The idea is that a blood sample could contain a small quantity of microspheres of known size and the sample could be loaded into a trapping system which has been previously

characterized and calibrated for knowledge of trap stiffness at a variety of powers. Then, one of the inserted microspheres could be trapped with a set power, and thus known trap stiffness. Then the stage could be translated at various velocities, with the displacement of the sphere being recorded by the QD at each velocity. Then, with the sphere displacement (x) and the trap stiffness (k) known from Hooke's law, the drag force on the object from the medium (F) could be deduced using:

$$F = -kx \qquad \textbf{(Eq.4.10)}$$

This force could then be used in Stokes' law to deduce the viscosity of the medium.

$$F = 6\pi\eta r v \qquad \textbf{(Eq.4.11)}$$

In the above equation, F = the drag force on the sphere (N), η = viscosity of the fluid (kg m^{-1} s^{-1}), r = radius of the sphere (m), v = velocity of the sphere in the medium (m s^{-1}).

4.10 Discussion

The various methods of force calibration and measurement have been demonstrated and discussed. The conclusions of this work are largely that the QD is a difficult device to harness to good and accurate effect. The need continually to re-calibrate the system due to inherent changes in the laser beam path to the QD from one experiment to the next makes the use of such a device time- consuming. QDs do nevertheless hold two distinct advantages over alternative methods, such as high frame rate cameras; these are the bandwidth and accuracy with which data can be ascertained.

In comparison the use of high speed cameras for the acquisition of position data has advantages of its own. Although not yet able to match QDs for bandwidth, they are far easier to calibrate and have the ability to track multiple particles simultaneously.

Currently, these two competing data acquisition methods are perhaps considered equal in terms of their advantages and disadvantages. However, with the constant development in high frame rate camera technology together with the ever improving tracking programs (such as StAT), it seems clear that that eventually the high speed camera and tracking software method of data acquisition will become the method of choice throughout the optical trapping world.

The escape force experiment undertaken in this chapter produced data that compared well with optical trapping theory to a high degree. It showed the linear relationship between the laser power and the potential well depth. It also showed the 'switch' in optical trapping regime as the 1.54, 2.44 and 5.44 μm diameter spheres' trendlines had vastly different gradients to the 0.5 μm diameter sphere's trendline. Access to a greater range of sphere diameters in the region around the wavelength could provide the ability to further investigate the cross-over between the tradition ray optics regime and the Rayleigh regime.

The investigation into the effect of the direction of linear polarisation suggested the trap stiffness is independent of the polarisation. Ellipticity in the beam appears to be the cause of discrepancies in the x and y axes' trap stiffness.

Accurate knowledge of the forces exerted in optical traps has been the driving force behind much of the biosciences-based optical trapping research. Engineering new and more accurate methods to achieve force

measurement results continues to be a large part of the optical trapping research field.

The work in this chapter enabled a greater understanding of the fundamental optical trapping forces and this knowledge became useful in the work carried out in the subsequent chapters.

Chapter 5

Fixing Silica Spheres to a Thermosetting Polymer using the Optical Trap

5.1 Introduction

The purpose of this experimental series was to establish to what extent microspheres can be fixed to a given surface and how well affiliated the microspheres would become to the surface.

Initially, it had been considered that the silica (SiO_2) microspheres could be directly fused to the glass cover slip. However, after some brief tests and basic mathematical analysis of the magnitude of powers required to fuse glass to glass, it quickly became apparent that this would not be possible. For example, the melting point of fused silica is approximately 1988 K and its specific heat capacity is approximately 700 J K^{-1} kg^{-1}. Hence, the amount of energy required to cause a single 5μm diameter fused silica microsphere to melt would be approximately 0.2μJ (based on silica density of 2.65 g cm^{-3}). Although this value does not appear high, the difficulty

arises in that silica is highly transmissive, so the vast majority of the photons would give the undesired effect of passing through the microsphere without being absorbed by the material. Furthermore, the microsphere's very high surface area to volume ratio means that any heat generated would dissipate at a fast rate, meaning that all the required energy would need to be deposited in a short time interval of melting to occur. Moreover, even if it were possible to achieve these levels of energy absorption by the silica sphere, this was not necessarily preferable. Given that the aim was to fuse or fix the sphere to a surface, it was worth considering that achieving a melt in the silica might well destroy their current sphericality and thus undermine the potential application of near field processing through the fixed microsphere. Consequently, it was clear that for this process to work it must be the surface material that is changed to accommodate a positioned sphere rather than the other way around. This reasoning led towards the use of a polymer layer in to which the microspheres could be embedded. Thus, having decided upon the use of a polymer, it was necessary to establish what properties would be essential for the polymer for this process to be possible. This ability to fuse microspheres to one another is discussed further in section 6.4.of this thesis.

The experimental work in this chapter is broken down into three sections:

1. Surface Roughness of spin coated of polymer
2. Curing localised area of polymer in the optical trapping system
3. Curing of localised polymer area while optically trapping a silica microsphere.

5.2 Principle of Experiment

The basic principle of this experiment was to coat a glass cover slip in a thin resin coating and then use this cover slip as one side of a sample container, which contained a sample of microspheres in water solution. A microsphere was then trapped, using either the 532nm or 1064nm laser line, and then brought down to the polymer surface. Next, with the sphere optically trapped and held as close to the resin surface as possible, the laser power was increased, in order to cure the resin and 'set' the resin around the microsphere. If successful, when the trapping laser shutter was closed, the sphere would remain in place. If it had not been fixed in place, then once the trapping laser shutter was closed the sphere would resume its Brownian motion and slowly move away from the trapping site. Once a sphere had been fixed, the sample could be removed from the system and then subjected to a chemical solvent which dissolved any uncured resin, leaving only the cured areas with embedded microspheres.

5.3 Selection of Material in which to Embed the Spheres

First it was necessary to establish what properties the material must possess as incorrect selection would make the task of embedding the microspheres significantly more difficult or impossible.

Polymers can be split into two main categories; thermosetting or thermoplastic. Thermoplastic polymers turn to melt if heated above the given threshold (generally anywhere between 65°C and 200°C depending on the specific polymer) and will set as they cool. However, reheating the

polymer will cause the weak (commonly Van der Waals or hydrogen) bonds to break as it turns back into a plastic state. On the other hand, thermosetting polymers cannot be caused to return to their molten state once cured. This is due to the strong cross-links formed during the primary curing. As a result, they lend themselves to applications which operate at high temperatures as the polymer will remain strong once cured.

With regard to this specific application, a thermosetting polymer is clearly preferable. A thermosetting polymer will only require localised initiation of the cross-linking process. Additionally, any successfully embedded spheres are likely to remain in the chosen location even if the cured polymer is again subjected to high temperatures.

The chosen polymer must also have the necessary significant optical and transmissive properties:

- The polymer needs to have a surface roughness not significantly higher than that of glass so as not to diminish the image quality or modify the wavefront of the laser.

- It must also possess a refractive index not too dissimilar from the glass. This is because the microscope objective is designed for a for an oil-glass-water setup. Adding the polymer layer will affect this. However, if the difference between the polymer and glass refractive indexes can be minimised, any effect will be reduced, and the high NA of the objective should be maintained.

- The transmission coefficient of a potential polymer choice must sit within a desired range. The polymer must transmit a sufficiently large proportion of the beam to ensure that enough photons pass through so that the trapping phenomenon still occurs. However, it

must also absorb enough of the beam so that sufficient heating (or an alternative mechanism) occurs for the curing to occur in localised area of the polymer.

After consideration of the above stated criteria, a thermosetting epoxy resin, made available by GEM Ltd, was chosen and it is the resin/polymer referred to throughout this chapter. This resin is the epoxy resin used in GEM's D58 ink. Its chemical composition is protected IP and is not the focus of this investigation. Although, advised that this polymer had good optical properties, these were not defined, so preliminary experiments were required to confirm it possessed the necessary optical properties.

5.4 Preliminary Experiments

5.4.1 Surface Roughness of Spin Coated Polymer

5.4.1.1 Experimental Setup and Procedure

The highly viscous nature of the polymer meant that it could not be placed on the surface of the cover slip through the conventional use of a pipette. The tip of the pipette was used to transfer a globule of resin on to the centre of a 0.17 μm thick glass cover slip. The cover slip was then placed in a spin coater (Laurell, Model No. Ws-650S-6NPP/LITE/UD).

The sample was then spun at specific parameters for RPM, acceleration and time. The sample was then removed from the system and placed on a white light interferometer (WYKO) which was used to evaluate the quality of the polymer layer, in terms or surface roughness and thickness,

produced by the spin coating. This was then repeated for a new set of parameters.

The RPM values ranged from 50 to 700 and the length of each spin coat lasted from 10 to 60 seconds. For each set of parameters, 3 samples were generated and then 3 values of surface roughness were generated for each sample. So for any giving combination of RPM and time, 9 surface roughness values were acquired. The surface roughness measure used, R_a, is the arithmetic mean of absolute values.

The layer thickness was established using both the white light interferometer and digital callipers.

5.4.1.2 Results and Discussion

The initial values for R_a, achieved before spin coater parameter optimisation, were of the order of 200-300nm. Initially, the RPM of the spin coater was varied with the results shown in Figure 5.1.

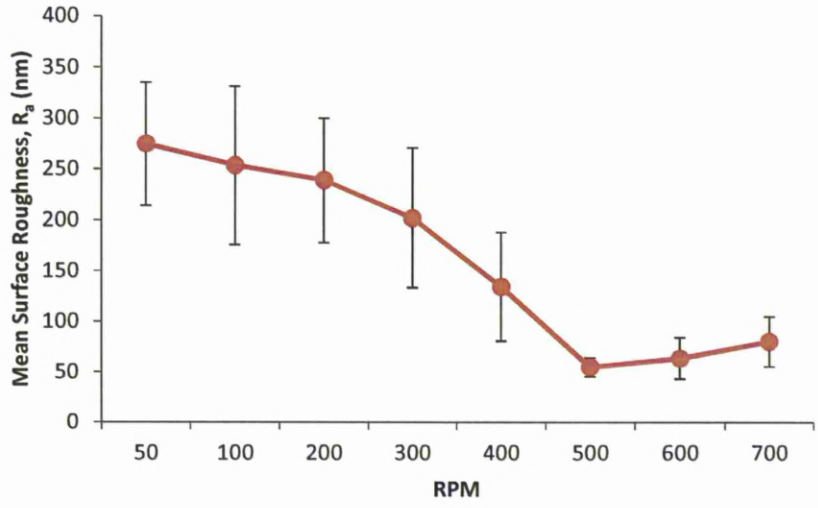

Figure 5.1: The mean surface Roughness, R_a, calculated from 9 areas from 3 separate samples at varying spin coating RPM over a 60 second period. The errors bars represent 1 standard deviation for each set of 9 values.

Having found a preferred RPM between 400 and 600 RPM, the time of each spin coating was varied as shown in Figure 5.2.

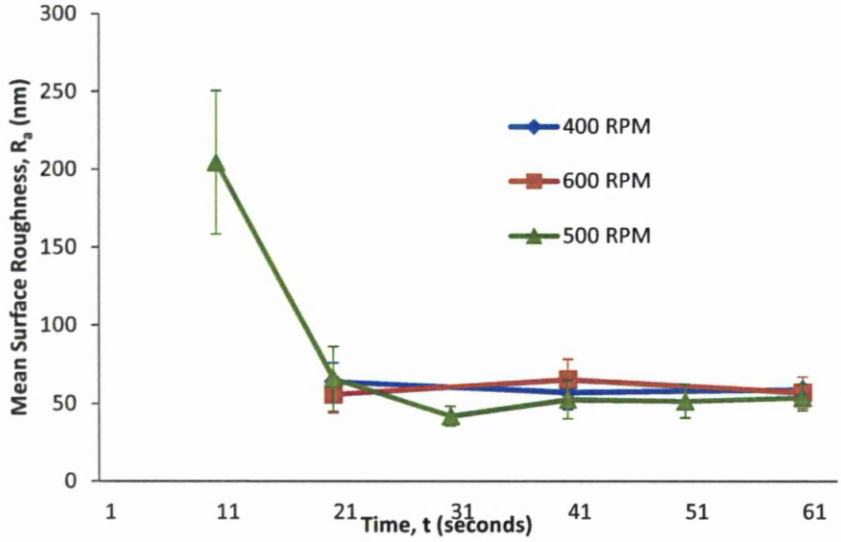

Figure 5.2: The mean surface Roughness R_a calculated from 9 areas from 3 separate samples at 400, 500 and 600 RPM over varying spin periods. The errors bars represent 1 standard deviation for each set of 9 values.

The best repeatable surface roughness value, R_a, was approximately 40-50nm, compared to a high quality plain glass cover slip having a surface roughness, R_a = 4nm. Although this seems a large discrepancy between the two, it could be observed by manually looking through the resin coated cover slip, this coating was near optical quality. Not being able to use a pipette meant that replicating the quantity of resin deposited on to the cover slip was difficult. Repetition was limited due to the imprecise process of placing the initial globule of resin onto the cover slip. Accordingly, the quantity of resin placed on the cover slip before spin coating, varied significantly each time. This limited the ability to achieve precise repeatable surface roughnesses.

The best results for surface roughness were achieved with the spin coater settings as follows:

Speed = 500 RPM, time = 30 seconds.

However, the 500 RPM results were only marginally better that the 400 and 600 RMP equivalent results. The time was more critical. With spins of less than 20 seconds not being long enough for the viscous polymer to spread out and form a smooth layer. Moreover, the quality of the surface appeared to deteriorate slightly for spins longer than 30 seconds. However, this decrease in quality with time is not statistically significant, but it is clear than there is certainly no improvement in surface roughness beyond the initial 30 seconds spin.

Under such settings the resin would spread to form a surface coating on the cover slip with a thickness of approximately 30-60μm, as measured with the WYKO white light interferometer and digital calipers. This thickness is of the order of 6-25 times larger than the sphere (depending on 2.44 μm or 5.44μm and 30-60 μm thickness).

Minimising this thickness was an important part of the task. Given that ultimately, the aspiration was to have a microsphere embedded on the surface of this material and then have the surrounding material washed away, it was integral the resin thickness was not too great, otherwise washing away the surrounding area would leave an unstable high aspect ratio resin 'pillar' as seen in **Figure 5.3**.

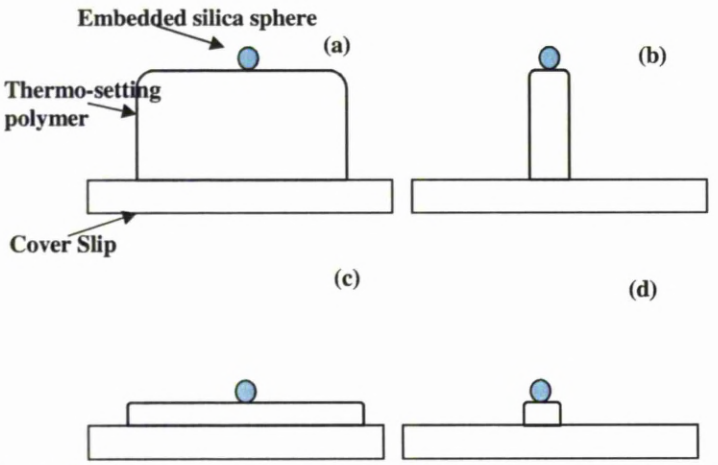

Figure 5.3: Representations of embedded silica spheres on resin surface. Diagram (a) shows a silica sphere embedded at the top of a thick layer of resin. Diagram (b) shows the high aspect ratio pillar produced once the surrounding area has been washed away using solvents. This 'pillar' would be far from stable and its optical quality in terms of light passing through the resin would be severely compromised. Therefore, it is necessary to reduce the resin layer thickness as much as possible, as seen in above in (c) so that once the surrounding uncured area has been washed away the remaining cured resin has a small aspect ratio and thus stable dimensions as shown in (d).

Furthermore, if the thickness of the layer is too great, the focus of the trapping laser will occur within the resin. If the laser does not focus beyond the resin and within the water-microsphere solution, optical trapping of the microspheres will not be possible.

5.4.2 Curing Localised areas of polymer in the optical trapping system

5.4.2.1 Experimental Setup and Procedure

Using the spin coater settings established in the previous section, a spin coated polymer layer on a 0.17mm cover slip was produced. The cover slip was then used to make up the bottom side (nearest the microscope objective) of the sample in the sample preparation method 2 (see figure 3.28) which uses a glass slide with a shallow bowl shaped cavity, with the microspheres and water sample contained within the cavity.

The final optical trap setup as explained in Chapter 3 (see Figures 3.32 and 3.33) and the sample setup is as shown in **Figure 5.4** are used throughout this chapter.

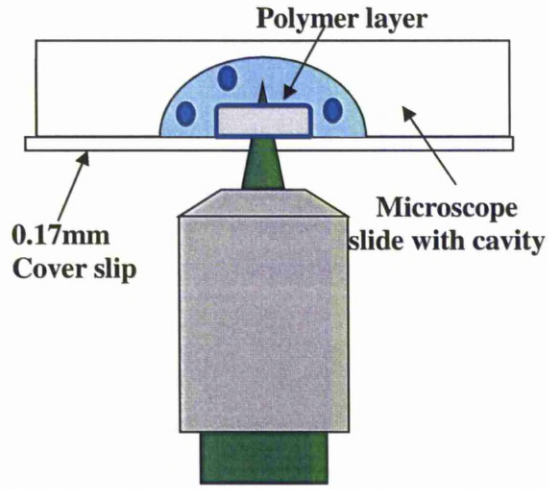

Figure 5.4: The sample configuration, showing the polymer coating on the glass cover slip nearest the microscope objective. Although not shown, there is also the 1064 laser line focussing beyond that of the green.

Once in the system, the polymer was subjected to both the green and infra-red laser line in an attempt to cure localised 'pillars' of polymer. After a

period of irradiation, the sample was then removed from the system and placed in a beaker of solvent which washed away any uncured areas, leaving only cured areas. These were then viewed under a microscope.

5.4.2.1 Results and Discussion

During a preliminary experiment the resin was cured in an oven. Temperatures of 80-100°C for 20 minutes were required for a 'full cure'. With a 'full cure' the resin became very hard and had a strong affiliation with the glass substrate. Ideally, this level of cure is what is required without the use of the oven which is attempted throughout this section.

Initially difficulties arose in attaining curing of any kind on the trapping system. This was seen when, following the attempted curing process and placing the cover glass in the beaker of solvent, no areas of polymer were found.

There were a number of possible reasons for this. Firstly, that the lasers are not providing sufficient area to an area to initiate the curing process. This was ruled out as samples were subject to high powers from both laser lines. For example, 250mW of the 532nm and 300mW of the 1064nm. The resin coated cover slip subject to these conditions again showed no cured areas when removed from the beaker of solvent. However, some loose particles were seen within the solvent suggesting that curing may be occurring but that the cured layer is not fully affiliating to the glass cover slip. It was reasoned that this was due to the intrinsic nature of a high numerical aperture microscope objective having a very small depth of focus. The thickness of the resin was approximately 50μm. In order for the cured

areas to have a strong affiliation to the glass (as with the oven curing) it is important to ensure that the resin is cured through the full thickness especially at the glass end of the resin (as opposed to the top surface with the water interface). A program was written in LabView to ensure the full thickness of the polymer at a particular point is cured. The program achieves this by oscillating the stage in the z axis (i.e. along the axis of the laser beam). **Figure 5.5,** shows a series of localised areas which have been cured using both lasers alongside the oscillating stage but without a sphere embedded. In these preliminary experiments, with abundant laser energy, both in terms of power and irradiation time, much larger cured areas may have been produced than is required. However, this was necessary to establish the capability of curing the resin while it is loaded in the trapping system.

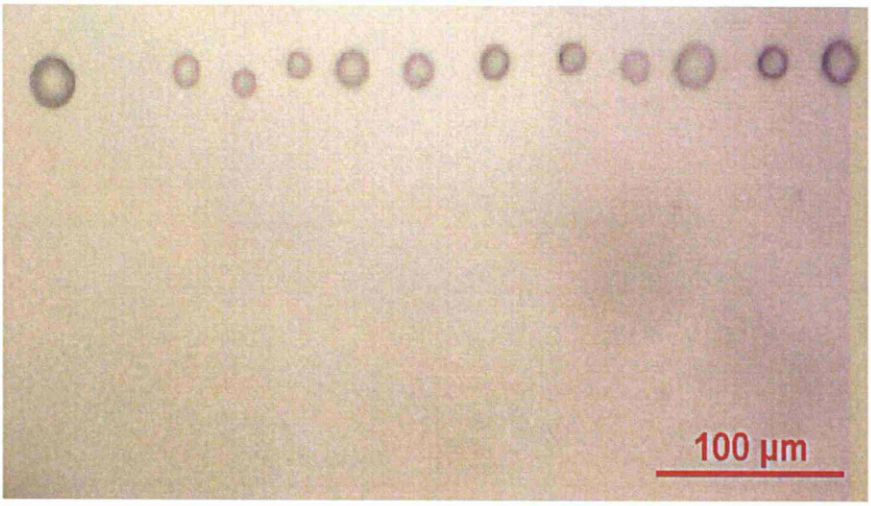

Figure 5.5: A line of cured areas of the polymer on the glass substrate after the uncured areas have been dissolved.

It is worth noting that the cured area only remained on the glass cover slip, once uncured areas had been dissolved, if:

- It was a full cure in the volume in contact with the glass cover slip, thus forming a strong bond between the two materials, just as the cured resin and glass did in the oven cured sample.

- The produced resin 'pillar' was sufficiently stable, strong and securely affiliated to the glass surface that it could withstand the relatively large forces of the uncured material and solvent washing passed it.

The cured areas in Figure 5.5 were achieved with the 532 laser at 100mW and the 1064nm laser pulsed at 10kHz and 300mW. Each area was subject to 16 oscillations of amplitude 60μm with the stage moving at a speed of 2μm s^{-1}.

5.5 Curing of localised polymer areas while optically trapping a silica microsphere

5.5.1 Experimental Setup and Procedure

The sample preparation is as above but with attention now on the microspheres. The microspheres (5.44 μm diameter silica spheres – Banglabs, confidence values ≈ 10-15%) were held in the 532nm laser trap at high power (200-300mW).

The 532nm laser was used as the trapping laser and the 1064 laser was used as the curing laser.

The 1064nm laser naturally reaches focus beyond that of the 532nm beam. However, the adjustable nature of the system allows for tuning of the green

line's focus position. This allowed the two laser line focuses to be brought close together. As both lasers are capable of trapping, it was easy to check their relative focus positions by switching one off and seeing the position at which the other traps. This allowed for the slow adjusting of the system, bringing the two focuses closes together.

Next, the position of the surface of the resin was found within the sample. The easiest way to achieve this was to trap a silica sphere and then move the microsphere down (or in practice, the entire stage up while the laser focus remains constant) to the resin surface. Once the focus of the laser was no longer within the solution but within the resin, the trap failed and the sphere was lost. Repeating this procedure several times, each time noting down the z position of the stage at which the sphere was lost from the trap, provided a quick technique for establishing the approximate position of the resin surface. For each new sample this process had to be repeated due to the varying thickness of the resin and general drift in the system.

Once an approximate position for the resin surface had been established, the process of fixing the sphere to the resin could begin. Using the green, 532nm laser line, a silica sphere was trapped and brought down slowly to the approximate resin surface position. At times, the sphere would be lost if the resin is slightly thicker at that point than the previously found approximate thickness – in which case the process was repeated. Once a sphere had been successfully trapped and brought down to the approximate resin surface position; the 1064nm laser was introduced in to the process.

The 1064nm laser was operated at a pulse rate of 1-25 kHz, and a power of 20- 200mW.

Once the localised area around the trapped microsphere had been subjected to both lasers for a specific time (t), both shutters were closed and the video image was viewed to establish if the microsphere had become fixed to the resin surface. If successful, the sphere would remain fixed, if unsuccessful, the sphere would be seen to continue its thermal motion.

If successful, the 1064nm laser shutter was opened and the z translation function part of the 'Joystick Control' program, discussed in Chapter 3, and in the previous section was harnessed to ensure curing right through the resin thickness at the point below the sphere. The distance of translation was set at just over the approximate resin thickness, 50μm. Then the stage was translated at a slow velocity, 2-5 μm s^{-1} down through the resin and then back up at the same velocity.

Once a series of the translations in z had been performed the sample was removed from the system, the polymer covered slide was separated from the rest if the sample and placed in a beaker of solvent for 10 minutes. The slide then viewed under an optical microscope separate from the trapping system.

5.5.2 Results and Discussion

The solvent dissolved uncured areas leaving only small areas of cured polymer (as seen in **Figure 5.5**). When a sphere had been successfully deposited then it could be seen through conventional microscopy techniques.

Experiments were aimed at attaining an embedded sphere, rather than achieving it efficiently, so the area was filled with laser power in both the green and the infrared wavelengths to ensure that there was sufficient power to achieve a full cure while holding the sphere against, or close to, the resin surface.

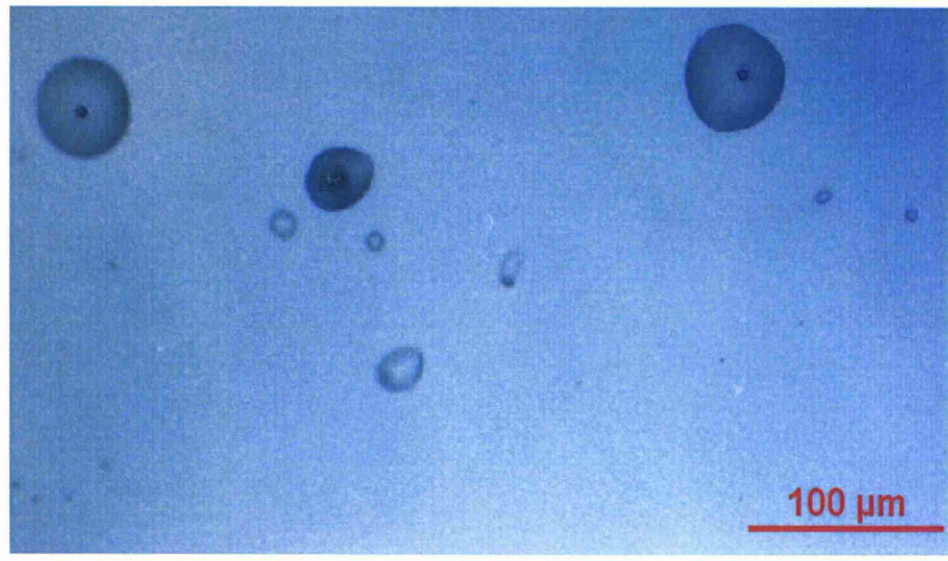

Figure 5.6: Microscope camera image of three areas of polymer. Each of these three areas has a central dot within it which is the affiliated silica microsphere.

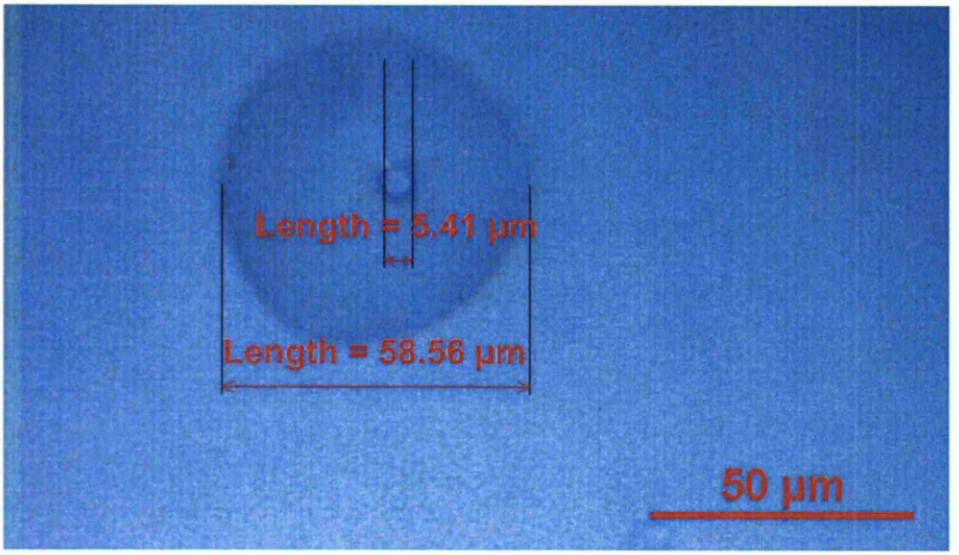

Figure 5.7: A higher magnification of such an area shows clearly a 5.44µm silica sphere affiliated to a small area of polymer.

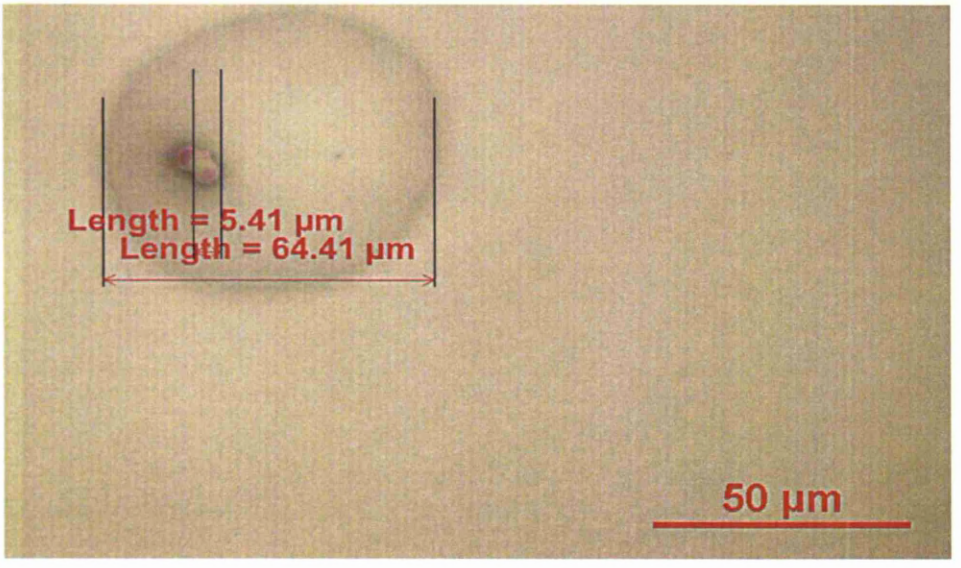

Figure 5.8: Microscope camera image of two 5.44µm silica spheres both affiliated to a small area of polymer.

5.5.3 Disappearing Spheres Phenomena

During the attempted placement of a 2.44μm diameter sphere an interesting phenomenon occurs. While holding the sphere in place close to the surface, the image of the sphere begins to lose clarity until eventually, after 60-90 seconds the sphere has completed 'disappeared.'

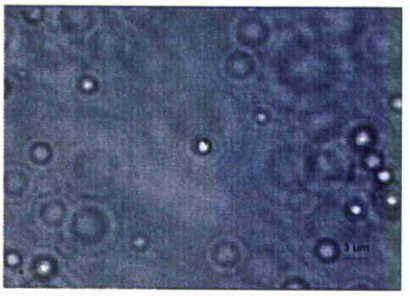

Figure 5.9: Trapped sphere after 0 seconds.

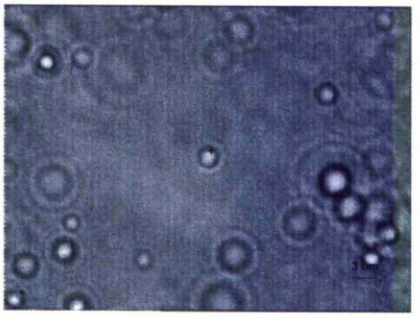

Figure 5.10: Trapped sphere after 40 seconds.

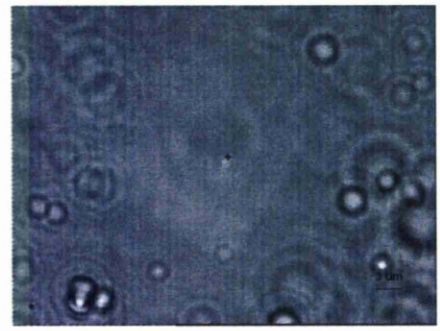

Figure 5.11: Trapped sphere after 80 seconds.

Figures 5.9, 5.10 and **5.11** show the 'disappearing' process. Figure 5.9 was taken at 0 seconds with the sphere at the centre of the image trapped tightly and having been just brought down to the resin surface. Figure 5.10 was taken after 40 seconds and Figure 5.11 was taken after 80 seconds. In Figure 5.11 the sphere is no longer visible. It appears that the sphere has migrated into the resin. This phenomenon occurred repeatedly with the 2.44μm silica microspheres.

Perhaps the similarity of the resin's and the sphere's refractive index are responsible for this loss of image. This phenomenon has repeatedly occurred in attempts to fix spheres to the resin. It is also worth noting that on the occasions where the disappearing sphere phenomenon occurred, if the subsequent stages of the experiment were conducted as if the sphere had become fixed, and then the sample was removed from the system, subjected to solvent and then viewed by a standard optical microscope, no affiliated spheres were found. The various parameters used and the outcomes reached at each one are set out in Table 5.1 and Table 5.2.

20kHz	z translation 2 reps	Outcome		
532nm Laser Power	1064nm Laser Power	Experiment No.		
(mW)	(mW)	1	2	3
100	100	a	a	a
100	150	a	a	a
100	200	a	a	a
100	250	a	a	a
100	300	a	a	a
150	100	a	a	a
150	150	a	a	a
150	200	a	a	a
150	250	a	a	a
150	300	a	a	a
200	100	a	a	a
200	150	a	b	a
200	200	a	a	a
200	250	a	a	b
200	300	a	a	b
250	100	a	a	a
250	150	b	a	a
250	200	a	a	a
250	250	b	a	c
250	300	a	b	c

Table 5.1: Initial investigation to find parameters at which a 2.44μm sphere will fix to a resin surface. Outcomes: (a) Indicated no response, i.e. the sphere's Brownian motion recommenced once the laser shutters were closed. (b) The 'disappearing sphere effect' was witnessed. (c) The sphere's Brownian motion did not recommence once the lasers were shut off, indicating a level of affiliation between the microsphere and the resin surface. (d) A sphere was found on a cured pillar after being subjected to the solvent and inspected on a separated optical microscope.

As can be seen from Tables 5.1, under these parameters, although some spheres appeared to affiliate to the resin surface while on the trapping system, no spheres were found once the samples had been subjected to the

solvent and inspected with a separate optical microscope. Table 5.1 also shows that the spheres only remain fixed when the lasers are operated at the higher powers. It is also worth noting that at all powers sometimes no response occurs. At lower powers, when this happens more frequently, this is because the curing process is not initiating. At higher powers, the sphere drifting away on some occasions, after the attempted fixing process, is due to the varying thickness in the resin surface. So there may be enough laser power to cure the resin, but if the sphere is being trapped at a position with a gap to the resin's surface, then it obviously will not affiliate.

Attention was now turned to ensuring the curing of the resin right through the layer, to ensure a stable enough pillar, to withstand the forces caused by being placing in the beaker of solvent. As such the high laser powers used at the bottom of Table 5.1, 532nm – 250mW and 1064nm = 300mW, were now used alongside greater numbers of z translation reps and at slower z translation speeds for a 2.44 μm silica sphere.

532nm Power= 250mW	**1064nm Power = 300mW**		
z translation speed (mm s^{-1})	**No. of z translation reps**	**Pillar Observed**	**Sphere affiliated**
0.002	2	N	n/a
0.004	2	N	n/a
0.006	2	N	n/a
0.008	2	Y	Y
0.01	2	N	n/a
0.002	8	Y	N
0.004	8	N	n/a
0.006	8	N	n/a
0.008	8	N	n/a
0.01	8	N	n/a
0.002	16	Y	N
0.004	16	Y	Y
0.006	16	Y	Y
0.008	16	Y	Y
0.01	16	N	n/a

0.002	32	Y	N
0.004	32	Y	N
0.006	32	Y	N
0.008	32	Y	N
0.01	32	Y	N

Table 5.2: Secondary investigation to establish the parameters required to cure a stable resin 'pillar'.

Tables 5.1 and 5.2 show the process is more complex than simply immersing the desired area in maximum power. Table 5.2 shows that the successfully generated resin pillars were generally at higher z translations, i.e. 16 or 32, although some pillars were achieved at lower numbers of z translations. The parameters at which the spheres were observed to have affiliated to the resin were not very consistent. Perhaps surprisingly, it appears that although using a higher number of translations does result in stable resin pillars it does not result in the successful conversion to affiliated microspheres.

The procedure of fixing spheres to a resin surface has been demonstrated but is still a developing process. Further repeats of the above experiment are required to establish a greater understanding of the factors involved in generating the pillars and more crucially, affiliating the microspheres.

5.6 Discussion

The ability to fix microspheres in a close to optical quality resin has been demonstrated. Unlike other work, this study achieved such microsphere placement without any chemical coating of the microspheres. Clearly a

chemical coating has been used on the cover slip surface instead on the sphere but this is a significant difference to coating the spheres. As the eventual aim for such an aim could be to produce a device which harnesses these micron-scale silica spheres as micro lenses (see Figure 5.12 below) it is critical their optical properties are not diminished. Coating the spheres in a chemical coating could decrease their highly transmissive nature and/or cause them to lose their sphericality.

The efficiency of the process needs to be improved significantly. If a minimum amount of energy is put into the system in the sphere fixing process then the width of the polymer 'pillars' may be greatly reduced allowing for spheres to be placed closer together. This could possibly be achieved through a resin/laser wavelength combination that produced more efficient cross linking of the polymer. However, such a reduction in the pillar diameter increases the aspect ratio of the pillars and reduces their stability. Therefore, before efforts to reduce the pillar diameter can be attempted, efforts to achieve a thinner layer of polymer must be achieved. The resin used in this work, was selected due to its s strong optical properties and availability which has allowed the proof of this in principle. However, if this work were to be further developed, a more thorough investigation of other available thermosetting polymers which still possess excellent optical properties but are less viscous and can thus be used with a pipette and can be spin coated into thinner layers would be essential in improving the process.

Once these spheres can be fixed in a more controlled manner, then perhaps a reusable device with the spheres fixed in a specific array (such as a 5x5 grid) could be manufactured for near field processing. The phenomenon of the 'disappearing sphere' also needs further investigation. This could possibly be achieved through the use of alternative techniques such as

SEM which may allow for the confirmation that the sphere has migrated into the resin. However, the lack of a reasonable alternative explanations, suggest this is likely to be the explanation.

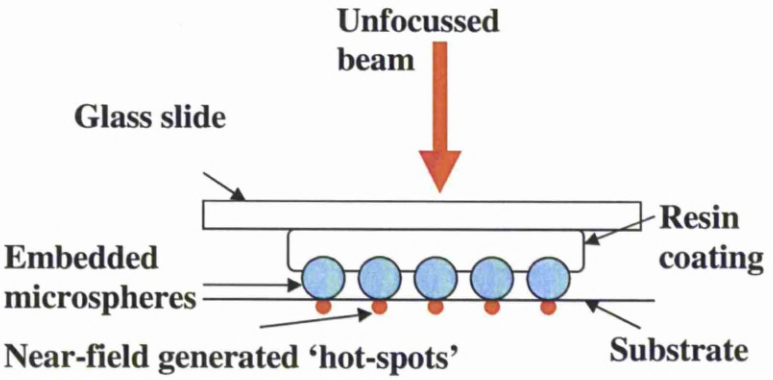

Figure 5.12: An example of what a reusable device for near field processing would consist of

This ability to place spheres is crucial. Until now near-field processing of large areas has been restricted to random arrays of spheres (55,56) or self-assembling arrays of spheres (57,58). This development could lead to the manufacturing of a reusable device for near-field processing, as an example of the layout of such a device is shown in **Figure 5.12**. Subsequent studies would look to evaluate the reusability of such a device. The complexity in developing such as device means that without reusability this is never going to be a viable tool. So efforts to focus on developing the reusability of the device are critical. The reusability is going to be dependent upon:

- Minimising the thickness of the resin layer to increase the stability of the pillars.

- Maximising the bond between the resin pillars and the glass cover slip.

Methods of evaluating the proportion of microsphere embedded, possibly through use of AFM or SEM, would be beneficial. Especially, if given such methods, the relation between the trap stiffness/force down into the resin and the proportion of microspheres embedded in the resin could be investigated and quantified.

Chapter 6

Other Engineering Applications of the Optical Trap

6.1 Introduction

The purpose of the research presented in this thesis was to find and develop new engineering based applications for optical traps. Over the course of this research many different potentially useful applications were attempted, the most successful being presented in chapters four and five. In this chapter, a number of other investigations and experiments are presented, that although of great interest have either shown promising outcomes that cannot yet be fully exploited or less clear outcomes that may have potential. Also presented are applications where the problems encountered tend to indicate that the process is unviable for the system used here.

6.2 Ability to Trap Coloured Spheres (Black, Blue, Red, Pink, Yellow)

6.2.1 Introduction

As the previous chapter shows, the embedding of microspheres in a surface is possible, but not without its difficulties. The similarities in refractive index between the colourless silica spheres and the *glass-like* resin made it easy to 'lose' a microsphere into the resin. Therefore, the use of coloured spheres was attempted to determine if the beads were entering the resin or being lost by another mechanism.

However, one complications with this experiment was that the silica spheres were not available in any form other that colourless and therefore a different type of bead had to be used instead and these were polystyrene. To test if the change from silica to polystyrene beads had any affect the behaviour of the colourless beads of both types were compared and they were found to behave in a similar manner.

6.2.2 Experimental Method

The system setup used was the final system detailed in Chapter 3. The sample setup involved each colour (black, blue, red, pink and yellow) sphere solution (polystyrene, 1μm diameter in distilled water) being further diluted with distilled water (only one colour of sphere in any one sample). One drop of Kodak photo solution was added as a surfactant to minimise clumping of spheres. Without the surfactant, the spheres tend to affiliate

strongly to each other and the glass surfaces. The sample was placed in the cavity microscope slide-cover slip setup, see **Figure 6.1**.

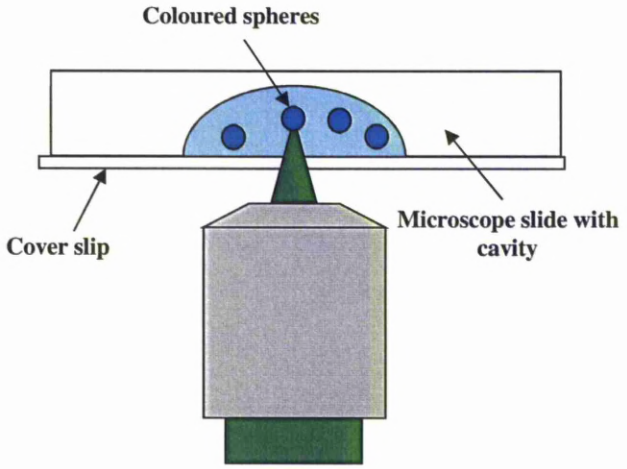

Figure 6.1: Sample setup employing the Cavity Microscope Slide-Cover Slip Setup

The sample was then addressed by the 532nm laser at low power. The dye within the polystyrene spheres makes them much less transmissive than clear polystyrene and thus leads to some momentum transfer by the photons.

The laser was almost fully attenuated, thus allowing a power of less than 1mW through to the sample. The laser was then used to attempt to trap a coloured sphere. If, as was frequent for close to zero powers, there was no response by the microsphere, for example the sphere was neither trapped nor pushed away from the trapping plane, the laser power was increased slightly. At this point, the sphere would either trap or be 'fired' from the trap. If the sphere was removed then the power was noted. If the sphere was not ejected from the trap, the laser power was slowly increased until the sphere was forced out of the trap and the laser power recorded.

6.2.3 Results and Discussion

Sphere Colour	Power at which spheres are fired from trap (mW)
Black	<1
Red	<1
Blue	<1
Pink	10-20
Yellow	20-30

Table 6.1 – Sphere Colour and Laser Power

As can be seen in **Table 6.1**, the darker coloured spheres (black, red and blue) were barely 'trappable' at all. At even the lowest of powers, the forces produced by photon absorption and reflection outweighed the scattering forces produced by the small proportion of photons being transmitted through the microsphere.

The lighter colours (pink and yellow) appeared to transmit sufficient energy at low powers that the scattering forces generated by refracted photons prevail over the pushing forces produced by the reflected and absorbed photons. To put this into context, the clear spheres, both silica and polystyrene have no upper limit for power at which they can be trapped. As seen the chapter 4, for clear spheres, the greater the laser power the greater the trapping force.

Interestingly, it would be expected that the percentage of photons reflected, transmitted and absorbed would stay the same as the power is increased as

a material's transmission coefficient is not dependent upon power (34). A transmission coefficient is simply a ratio. Therefore, if the forces at low powers are sufficiently balanced that the object can be trapped, why does doubling the power, for example, mean that the trap is no longer sustainable? It seems reasonable to expect a doubling of the laser power would double each of the forces, as has been shown to be the case for colourless spheres (32). As can be seen from the table, at low powers even the lighter coloured spheres are no longer trappable as the pushing forces become too great for the scattering forces to overcome.

A possible cause of this problem is a change in the energy distribution of the beam through the attenuation process. A power meter measures the power incident upon its detector, so as attenuation is reduced, the power meter detects more power, however, it does not measure any change in the distribution of the energy. A Gaussian beam will exist regardless of the level of attenuation; however, the distribution of power in the Gaussian may vary. For example, for a highly attenuated beam, the 'wings' or 'edges' of the beam may make up a greater proportion of the beam than a non-attenuated beam, in the centre of which resides the vast majority of the beam power. Consequently, though the percentage of the total power incident upon a sphere transmitted and absorbed should not change, as the power varies, the dimensions of the Gaussian may vary. The highly attenuated beam will possess greater relative power in its 'edges' and thus generate greater relative scattering forces. In contrast, the non-attenuated beam will have much less power in its edges, as a proportion, and thus, the gradient forces will dominate and the pushing forces caused by photons reflecting or being absorbed will outweigh the small scattering forces.

Another suggested possible cause is differential heating across the sphere, with the side nearest the laser being heated relative to the sphere side

furthest from the laser, causing a resultant force. However, this is ruled out as a cause of the sphere's expulsion from the trap due to the instantaneous and high energy nature of the sphere's ejection once the laser reaches a critical power. If differential heating were the cause, it is reasonable to assume there would three regimes:

1. A critical power below which heat is dissipated as quickly as it was accumulated by the microsphere.

2. A range of powers at which there was a slow temperature rise on one side of the sphere generating a force.

3. A critical power at which the sphere's temperature was increased quickly enough to cause an 'instantaneous' ejection from the trap.

The second phase, as set out above, was not observed during any of the experiments. The laser power was either low enough to loosely trap the microsphere (or not affect it at all) or large enough to instantly 'fire' the sphere from the trap and out of the focal plane of the camera.

In summary, it has been shown that the transparency of a sphere is critical for optical trapping to occur. Without transmission of the vast majority of photons, no scattering force is generated, causing the sphere to be trapped in x and y but then 'fired' in the direction of the beam. This is in line with previously reported work which, although used transparent spheres, did not have a high enough NA objective to generate the scattering forces (1,7,8,20,114). Going beyond the literature, it has been reasoned that the relative power distribution of the beam is the likely cause of the witnessed effect of coloured spheres being ejected from the optical trap above a critical laser power. This knowledge can be used to reason further, that for the transparent microspheres, it is not simply laser power that affects the

trap stiffness (although this is still a major factor) but the distribution of the photon flux across the sphere. For example, a less sharply pointed Gaussian beam, with a greater proportion of energy at the extremities of the laser spot would generate greater scattering forces but would produce smaller the gradient forces. This may manifest itself as an apparent lower trap stiffness, but in reality the stiffness of the trap would have been reduced in x and y but increased along the z axis (the direction of the laser).

6.3 Manipulating Metallic Particles Using Annular Shaped Beams From Spatial Light Modulator (SLM)

6.3.1 Introduction

Optical trapping naturally lends itself to objects made of a highly transmissive material such as silica or uncoloured polystyrene. However, in an attempt to develop engineering applications it is necessary to explore the possible use of other materials such as metals. The major difference between metallics and dielectrics, in the context of optical trapping, is the transmission/absorption coefficients. As conventional optical trapping is entirely dependent on the scattering of photons, as discussed in chapter 2, it is clear the trapping of metallics will require a different phenomenon.

Here, annular beams are produced using an SLM, as a method of manoeuvring copper particles. It is worth noting that unlike the silica spheres used in other studies, the copper particles are not uniform. They vary in shape and have diameters ranging from approximately 1-10 μm.

6.3.2 Experimental Method

A low concentration sample was made up using micro-scale copper particles in distilled water, with a drop of the Kodak solution. The sample was sealed in the microscope cavity-cover slip setup shown in **Figure 6.1**. The sample was then loaded into the system which is described in detail in Chapter 3.

Using the *Holoeye* software, computer generated holograms (CGH) were pre-generated and then used on the SLM, which is the 532nm laser line, to produce an image of choice. This method does not have the real time modification ability available with the *Blue Tweezers* software, but does allow for the production of simple holograms of any given two dimensional shape. The software is set up to take bitmap (.bmp) files and produce the associated Computer Generated Hologram or CGH.

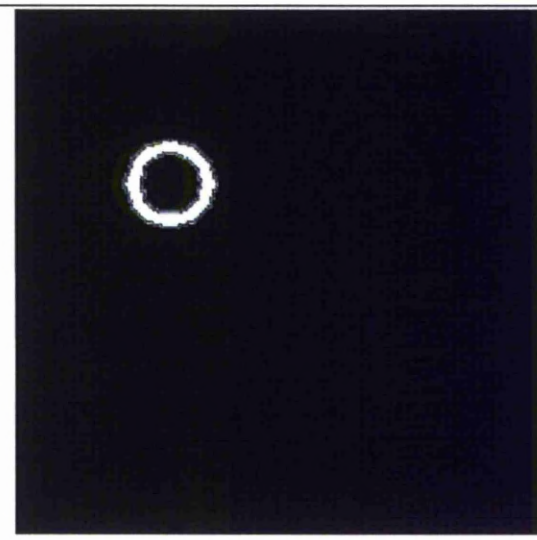

Figure 6.2: The bitmap, made simply in *Microsoft Paint,* is then inputted into the *Holoeye* software to produce the hologram shown in the subsequent figure.

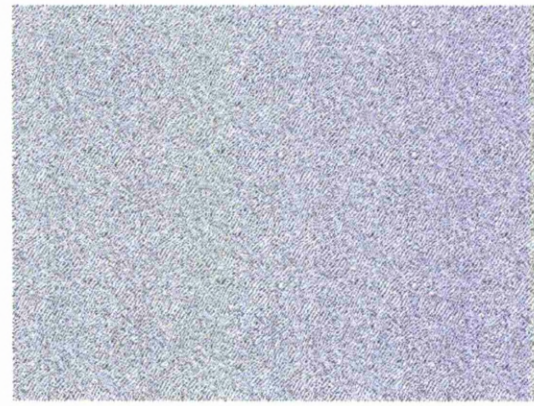

Figure 6.3: The CGH produced by the *Holoeye* software from the bitmap image shown in the previous figure.

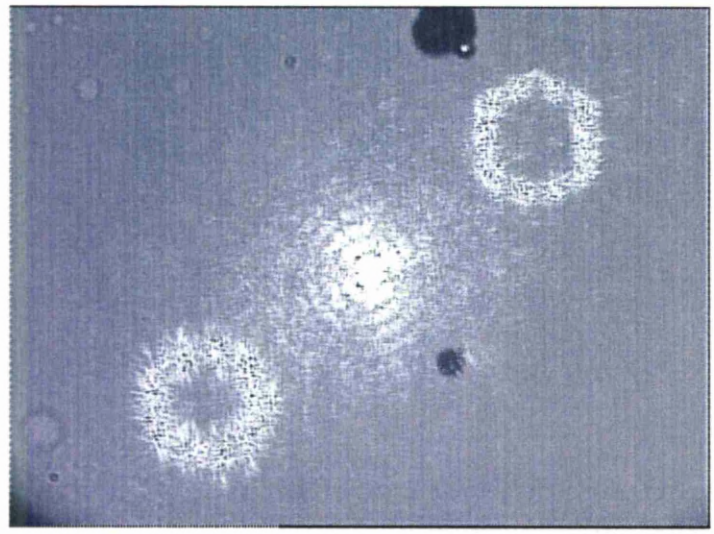

Figure 6.4: Image of the produced annular ring. The top right annular ring is the real image. The bottom left ring is the 'ghost' image with considerably less power. In the centre is the zero order which still contains over half of the total power. The dark objects are micro scale copper particles.

6.3.3 Results and Discussion

It was found that at high power, as the edge of the annular beam comes into contact with a copper particle, the particle is 'pushed' out of the focal plane by the photon momentum forces due to photon absorption/reflection at the copper surface, in the direction of laser beam propagation.

At low power, the beam is unable to impart sufficient momentum in the copper particle to cause any change in the object position.

However, it was found that if the power is 'tuned' precisely, it was possible to select a laser power which will gain a response from the copper particle

large enough to move it, but small enough that the copper particle does not leave the focal plane.

This precise power is difficult to quantify for a variety of reasons. Firstly, as described in Chapter 3, all powers are measured after the mechanical shutter in the standard setup. Secondly, when the SLM is in use, a large proportion, approximately 50-60%, of the power remains in the zero order. The rest will be in higher orders, such as the generated annular beam. Furthermore, the power distribution around the annular beam is not necessarily uniform. Finally, as the copper particles are non-uniform, they vary in size and thus mass. Consequently different sized objects require different powers. That said, it was found that, for most particles, powers of 10-20mW were capable of moving the objects without causing too large a momentum transfer.

The correct power selection is only part of the issue. The other critical factor is the beam shape, specifically (as shown in Figure 6.5) the diameter across the 'no beam' area of the annular beam, β, and the width of the ring, α.

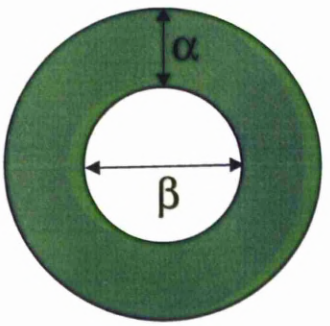

Figure 6.5: The dimensions of annular beam

It was found that minimising α is desirable. As it is just the inside of the ring that makes contact with the copper object before the particle moves, the rest of the ring is not assisting in the process but merely using energy that could be better employed elsewhere. With α minimised the process is markedly more efficient. With α minimised manipulation of the copper objects can be achieved with less than 1mw. Before α was minimised this required power was ≥30mW.

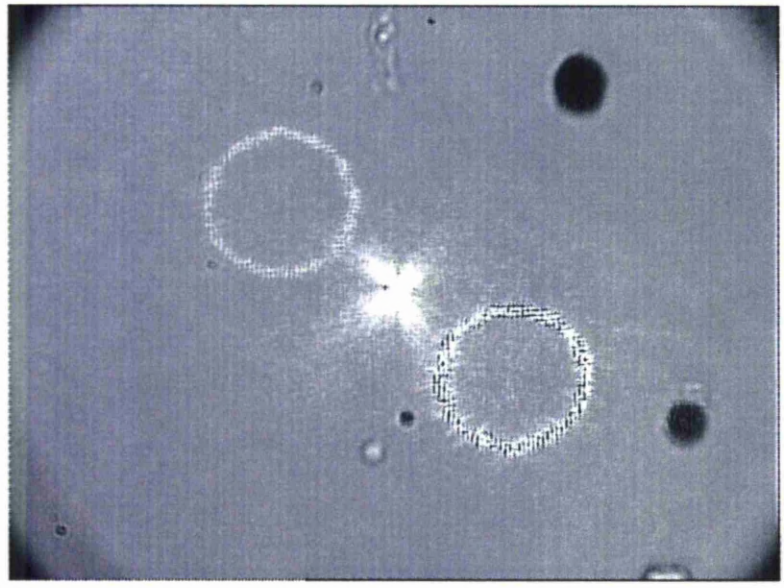

Figure 6.6: Annular beams generated using a smaller value of α than used in Figure 6.4. The upper left ring is the actual beam. The bright spot in the centre is the zero order.

The lower value of α produces the ring in **Figure 6.6** and allows a greater proportion of the laser power to be utilised by the ring in manipulating the copper particles as opposed to being wasted in the outer surface of the ring which will never come into contact with the copper objectives.

Secondly, the dimension β, must also be carefully selected. If β is too small, then both sides of the laser ring may simultaneously make contact with the copper object causing it to be pushed out of the focal plane.

If β is too large, as in **Figure 6.6**, then the process of using the beam to manipulate particles becomes slower. This is because the process is essentially a micro 'poker' or 'prodder', so if β is too large then more time will pass between each 'poke' or 'prod'. Whereas, if the diameter, β, is only marginally larger than the copper particle then the 'pokes' will occur more regularly, thus achieving a much greater speed of manipulation.

An alternative method of optical 'poking' is to use the raw beam as a point source of momentum, rather than an SLM generated annular beam. During the work in section 6.4, a need to bring two particles together occurred. Using a ring, it is impossible to bring two particles into contact. As one particle is brought towards the other, the outer part of the annular beam repeatedly pushes the non-trapped object further away. In such circumstances, using the raw beam, at low power (less than 5mW), incident upon the opposite side of the particle to the desired direction of movement, it is possible to manipulate the particle, slowly, to a desired location.

To summarise, it has been shown that the 'tuning' of the laser power and the dimensions α and β provide for the manipulation of the metallic objects in this annular beam method. This process is not equivalent to the other optical trapping of metallics shown in the literature. Svoboda *et al* trapped Gold particles but of a much smaller size regime, 36nm diameter, using a laser with wavelength of 1047nm (115). As discussed in chapter 2, for objects much smaller than the wavelength of the laser, the Rayleigh regime governs the optical trapping phenomena. This is as opposed to the ray

optics or scattering regime, which is dominant for in the work in this chapter for objects larger than the wavelength of the laser. Zhan *et al* have modelled the trapping of metallic objects in the Rayleigh regime using radial polarisation (116). Probably the work in in the literature most similar to that demonstrated in this section was achieved by Sato *et al* who used a 1064nm beam at low power (less than 10 mW) to trap micron scale (2-15 μm) gold, silver and bronze particles (117). Sato used the pushing forces, generated by reflections and absorptions of photons at the metal surface, like the work in this chapter, to form a 'cage' around the particle. Sato's work was only able to trap in 2-dimensions. By not using a surfactant and allowing the metallic particle to remain affiliated the glass cover slip and keeping laser power low to stop the laser from pushing the metallic object off of the glass surface.

It is speculated that although acousto optic deflectors (AODs) (118)operate quite differently to SLMs (an AOD rapidly scans the beam to multiple locations whereas an SLM splits the beam into multiple spots or a new shape), AODs may nevertheless be able to manipulate metallic objects in the same way as has demonstrated by SLMs in this section.

In summary, this section has shown a new method for simple manipulation of metallic or highly reflective objects, for systems containing an SLM. This method is not true optical trapping in the tradition sense, as defined by Ashkin, but does represent, a simple method for manoeuvring metallic objects into a desired formation. As can be seen in the subsequent section, the ability to place metallic objects in a specific location enables further work and opens new possibilities to optical trapping engineering tool.

6.4 Fusing microspheres to each other

6.4.1 Introduction

As the purpose of this thesis was to find and develop engineering applications for optical traps it was natural that nano (or indeed micro) fabrication would be an avenue of interest. It was hypothesised that optical traps could be used as a construction tool for nano or micro scale devices. The ability of optical traps to manipulate and position objects in precise formations or arrays could be harnessed, as already shown by attaching them to a substrate in chapter 5, but another possibility would be to bond them to each other to form a more complex structure. The most fundamental technique required to achieve this aim of taking unit pieces of material and turn them into a useful tool is a method of joining the pieces of material together. In macro scale devices joining methods can be split into roughly three methods:

1. Using a small 'joining device' the equivalent of a nail or screw.

2. Using a chemical bonder of some sort, i.e. either an adhesive or some form of solvent based welding.

3. Using a physical process which involves no extra part or chemical reaction except for that caused by the heat from the laser beam like welding.

As the silica microspheres are already of such a small size (1.54, 2.44 or 5.44 μm) it seems natural to dismiss attempting to recreate the above method 1. However, either of the subsequent two methods are possible options for methods of joining the microspheres. Method 2 would require

the microspheres to have a chemical coating of some sort and has been previously achieved as discussed in chapter 2(43,44). Method 3 would represent new work though it is perhaps the most difficult method to control as it is simply attempting to raise the temperature of the microspheres sufficiently high that they are able to fuse while holding them firmly against one another. Nevertheless, method 3 represented a new engineering based application for optical trapping and was consequently pursued.

There were various difficulties with this task. The most fundamental issue was associated with the transmissivity of the fusing material. If the coefficient of transmission is too large, the photons will simply pass through the material without imparting any heat into the microsphere. Equally, if the coefficient of transmission is too small, too many photons will be absorbed, (indeed leading to heating) or reflected, leading to the passing of the collective momentum of the photons to the microsphere causing the 'firing' of the microsphere away from the trap focus.

The final problematic issue was the surface area to volume ratio. The microspheres have exceptionally large surface areas relative to their volumes and are consequently extremely effective at losing heat to their surroundings. This means that the microspheres dissipate heat rapidly, thus making it harder to achieve the necessary high temperatures. Moreover, attempting to heat an object surrounded by a natural coolant, such as water, is difficult. Consequently, it was decided that, assuming the initial tests were unsuccessful, secondary tests would be undertaken on 'dried out' samples to see if greater temperatures could be achieved without the water coolant.

6.4.2 Experimental Method

The samples were set up without the use of a nail polish seal around the edge of the sample as the drying out of samples was desired for secondary tests to see if without the water coolant, higher temperatures in the microspheres could be reached. Both the attempts to fuse the silica and the metallic particles (copper, gold and zinc) employed the spacer method of sample setup (as opposed to the microscope slide cavity method) as shown in **Figure 6.7**:

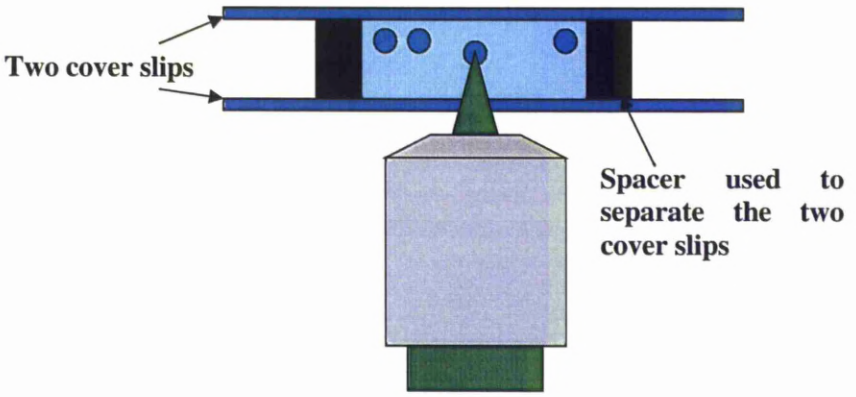

Figure 6.7: The spacer method of sample preparation. The spacer is a thin polymer square sticker with a circular hole within which the microsphere filled water sits. It is encased by two (0.17mm thick) cover slips.

The green 532nm trapping laser was operated at 125-175mW in order to maximise the trap stiffness to increase the stability of the trapped sphere. Also, any additional heating caused by the laser would only assist the process.

The 1064nm laser (SPI) was used as the heating laser and was operated in pulsed mode with a repetition rate of 125 kHz at an average power of 200mW.

The first experiment used silica microsphere (1.54, 2.44 and 5.44 μm) and the second experiment used metallic particles on the micron scale. The metallic particles used were copper, gold and zinc, these particles are far less uniform than the silica spheres but are observed to be on the region of 2-10μm in diameter. The set up above was the same for both the silica and metallic experiments. However, the method employed for the fusing of silica and then the fusing of metallics was different and has consequently been set out below in separate sections.

6.4.2.1 Experimental Method for Fusing of Silica

Initially, the SLM was harnessed to produce two trapping sites and to then bring the two spheres together (through use of Glasgow's *Blue Tweezers* program). However, one trapping site would usually overpower the other trapping site leading to both microspheres falling into the same trap. This is an inherent difficulty with using an SLM to bring two small objects together, where small is defined as smaller than the spot size generated by the SLM (which is approximately 5μm). This is less problematic for larger objects, where the diameters of the objects are much greater than the width of the optical trap potential well. In these instances, both objects can be trapped with their surfaces in contact with each other, without them being drawn into the same trapping well.

The solution for bringing two silica spheres together was to find a silica sphere adhered to the cover slip surface (even with a drop of surfactant within the sample there are still a proportion of sphere that affiliate strongly to the cover slip surface). The SLM was then used to produce one trapping site to trap and move a free moving sphere over to the 'fixed' sphere. Once the spheres were pressed firmly against one another, with the contact point positioned at the point of focus of the higher power 1064nm beam (which was focused to the same plain as the 532nm beam), the pulsed beam shutter was opened allowing the higher power infrared beam to strike the point of contact in an attempt to cause fusion.

For the dried out sample (with all the spheres are now adhered to the surface) the sample was scanned to find two spheres in contact. At which point the 1064nm laser was aimed at the point of contact and the shutter opened. This did not require the use of the optical trap and was a simple experiment to establish if enough heat could be absorbed by the silica to melt its surface and cause two spheres to fuse.

6.4.2.2 Experimental Method for Fusing of Metallics

The metallic particles were generally larger than the silica microspheres usually used in the trap. They were also not spherical. Their random shapes made the repetition of experiments difficult. As seen in section 6.3, metallic particles cannot be conventionally trapped like silica sphere can due to their low transmission and high reflection coefficients. Consequently, the metallic particles were brought together using the 532nm trapping laser at low power as an optical 'poker' as discussed in section 6.3. Once two particles were in contact, the focus of the 1064nm pulsed high power laser (SPI) was positioned carefully at the point of

contact between the two particles using the stage positioning software. Once in position the laser was fired at the point of contact. The particles were then ejected from the focal plane as the photons impacted and were absorbed at the surface of the particles and thus transferring their momentum to the particles.

The metallic samples were then allowed to 'dry out' in order to allow all the metallic objects to become affiliated to the cover slip surface. The dried out samples (with all the metallic particles now adhering to the surface) were then scanned in an attempt to find two metallic particles in contact. Then, the 1064nm laser focus was targeted at the point of contact and the shutter opened.

6.4.2.3 Results and Discussion

As these tests are largely binary in outcome, that is, they fuse or do not fuse, it is difficult to show visually the results. Nevertheless, **Table 6.2** shows the outcome of attempts to fuse two spheres of the same material. The wet sample column shows the results for when the spheres were in water. The dry sample column shows the results for attempts made on spheres once the water had dried out.

Material	Size (μm)	Wet sample	Dry sample
Silica	1.54, 2.44, 5.44	No evidence of any absorption or fusion by the silica beads.	Once the samples dry, the silica spheres were fixed firmly to the cover slip surface. After which no discernible effect could be

			achieved with no evidence of the spheres fusing together.
Copper	$2\leq$ x $\leq \leq 10$	While in the water, they are highly absorbent and thus are 'fired' away from the focal plane whenever they are hit by any large powers, see **Figure 6.9**.	Some evidence of fusion of two copper particles documented, see **Figure 6.9**. Ablation of the glass cover slip was achieved in areas below a copper particle as the copper particle assisted in the coupling in of the 1064nm laser into the surface, see **Figure 6.11** and **6.12**.
Gold	$2\leq$ x $\leq \leq 10$	'Fired' away by photon momentum.	No effect observed.
Zinc	$2\leq$ x $\leq \leq 10$	'Fired' away by photon momentum.	Some coupling in of energy, as with copper, observed, but to a far smaller degree than with the copper particles.

Table 6.2 – Laser fusing of microspheres within an optical trap

As can be seen from the table, the ability to fuse metallics in water is extremely difficult due to the transmission properties of the materials. Equally, the high transmissivity of silica meant that only a small proportion of the available energy was absorbed, resulting in little heating of the particles.

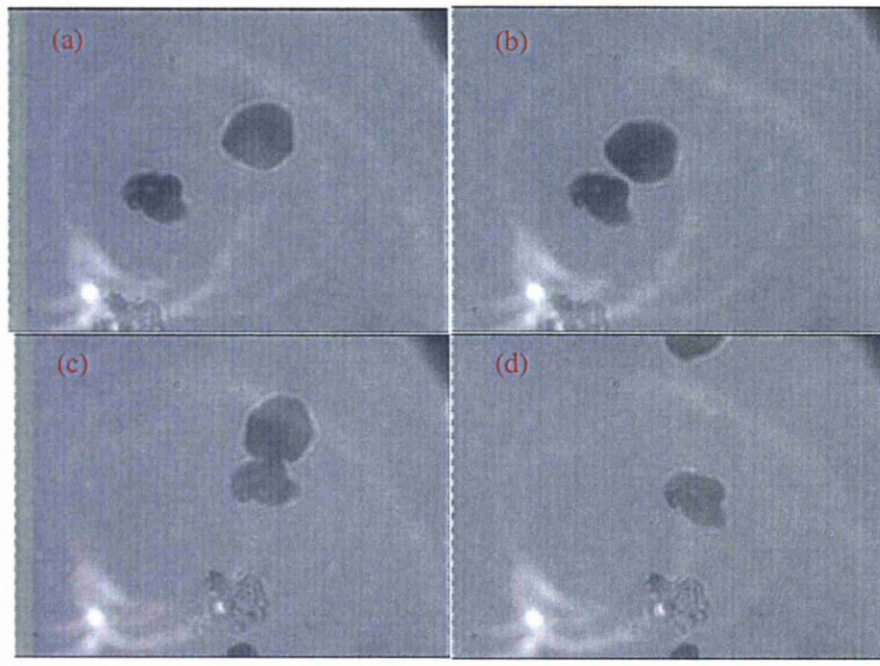

Figure 6.8: Four stages of an attempt to fuse two copper particles

Figure 6.8 shows the 'optical poking' method, described in section 6.3, employed to bring two copper particles together in (a) and (b). Once the two particles were in contact the 1064nm laser was targeted at the point of contact in (c) and the shutter was opened. Instantly, the upper particle was 'fired' away, (d), upon the impact of the photons on one edge of the object.

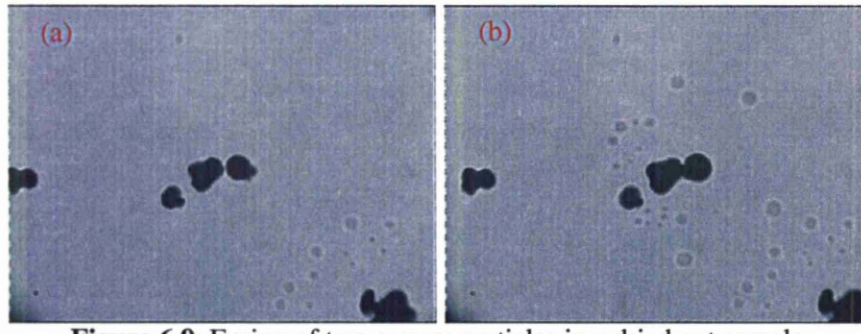

Figure 6.9: Fusing of two copper particles in a dried out sample.

Figure 6.9 shows the fusing of two copper objects using the 1064nm laser in a dried out sample. With no water in the sample, the objects rest on the cover slip and the photon momentum forces are outweighed by the Van der Waals forces. Here, the sample was scanned to find two separate particles, (a) which set very close together. With their position fixed at the surface by the Van der Waals forces, the photons cannot 'push' the particles away through photon absorption or reflection. Consequently, the photons couple in to the particles at the regions nearest each other and, after approximately 1-10 seconds, they appear to have fused.

One of the interesting outcomes of the work, while trying to fuse the copper, was the initiation of ablation of the near glass cover slip but only in areas with copper above it. It was noticed that rather than causing any response from the copper, the glass cover slip quickly began to ablate. However, when the laser was directed at the glass, in areas without copper, the laser would either not ablate or take much longer to generate an initial ablation. The setup is shown in **Figure 6.10**.

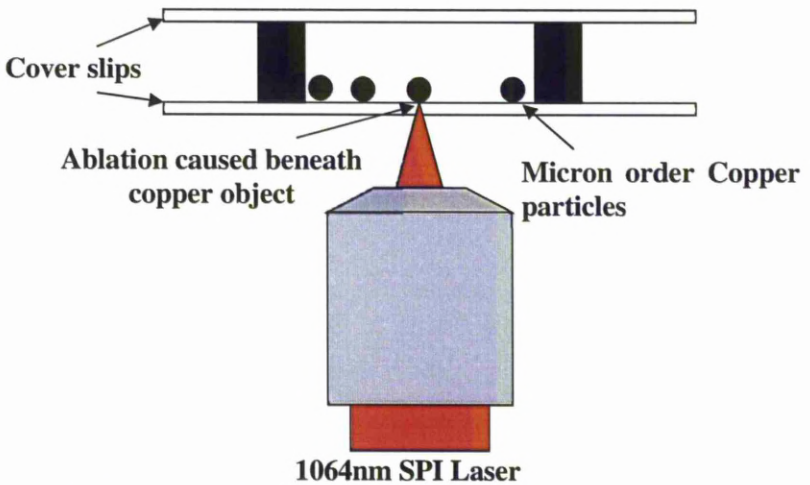

Figure 6.10: Setup with which the ablation of the cover slip was achieved.

Once ablation was initiated in an area underneath a copper particle, the stage was then translated and the ablation would continue along the glass, even in areas of no copper as shown in **Figure 6.11**.

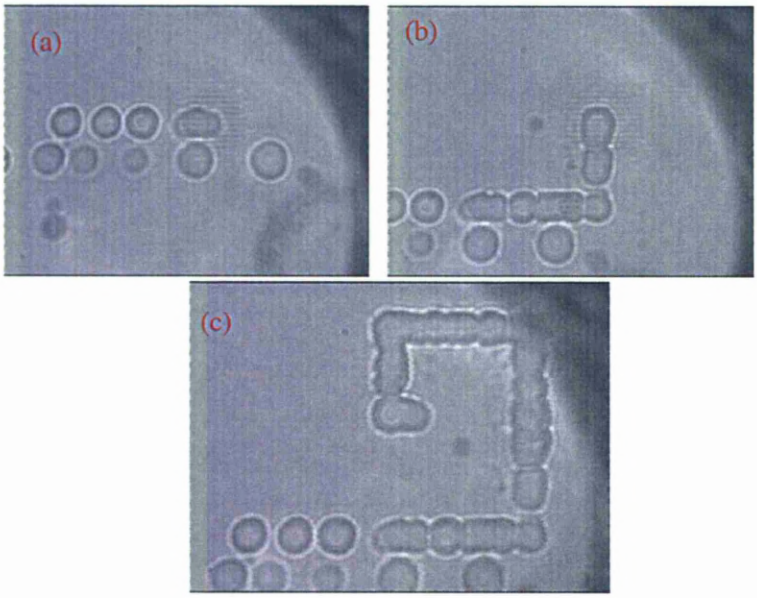

Figure 6.11: (a) Initial ablations of glass. (b) Further ablation of the glass cover slip. (c) Continuous line ablated

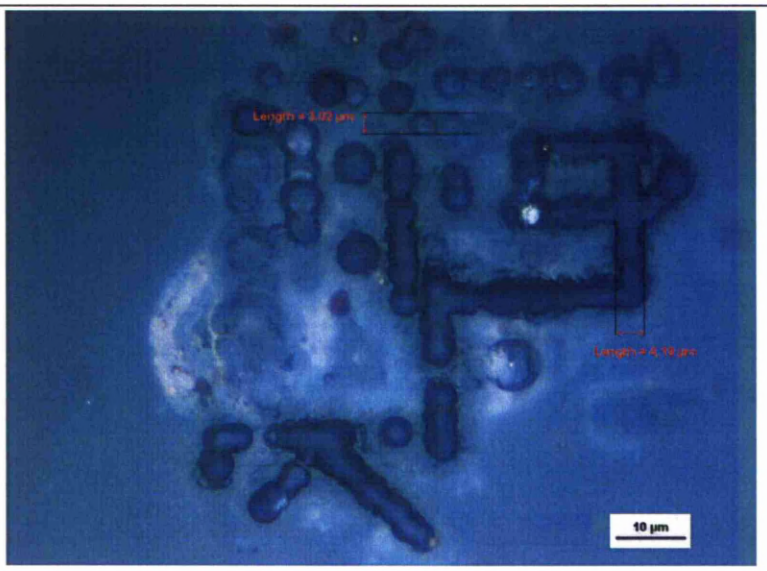

Figure 6.12: The ablations in the glass cover slip produced by the 1064nm laser with the assistance of the surface copper in a dried out sample.

Figure 6.11 consists of screen shots taken of the ablations while still on the trapping system, whereas **Figure 6.12** is taken later on an optical microscope. The optical microscope image shows that this method achieves spot widths of approximately 4.2µm. Although this value is still an order of magnitude larger than the diffraction limit, it is nevertheless a small and repeatable feature size. Furthermore, the phenomenon of copper on the glass surface assisting in ablation of the glass is an interesting outcome of the work. Although not previously seen in an optical trapping setting, it is not a new concept to use a coating to assist a laser in coupling in to a substrate (119,120). However, the new aspect to this result is that the 'coating', the copper particles, is beyond the glass substrate (i.e. not on the side of the glass that the laser is incident), and surface ablated is the far side of the glass substrate relative to the laser, as shown in figure 6.10. As

the copper particles are beyond the glass substrate it seems a reasonable assumption that the copper particles are either reflecting photons back directly, or heating up and then dissipating their heat to the surrounding area including the glass substrate. This could have implications for traditional laser materials processing.

6.5 General Discussion and Conclusions

This chapter shows that there are still many avenues to explore with regards to engineering applications for optical traps.

The attempted, and for certain parameters, successful, manipulation of coloured spheres was revealing in that it reinforced trapping theory. The trapping of the darker coloured spheres appears to be beyond conventional trapping techniques. As it is, the z trapping force is insufficient to accommodate the greater absorption of photon momentum caused by darker coloured spheres. A microscope objective of higher numerical aperture (NA) would provide a greater trapping force in z. The NA of the current objective is already 1.2, so there are not major increases available. Currently, microscope objectives are available in the region of 1.4 NA. Even if higher NA objectives were available, they would only be useful in situations where a significant proportion of photons were refracted through the sphere, which currently does not appear to be the case. It is possible that though these spheres are highly absorbent to visual wavelengths, they may be more transmissive at other wavelengths. Accordingly, attempts to trap coloured spheres using other wavelength lasers should be investigated.

As for the lighter coloured spheres, pink and yellow, as discussed previously, it may be the relative shape of the Gaussian beam that is the significant factor. Therefore, it may be possible to manipulate the Gaussian's relative shape using the SLM, in order to place more energy into the 'wings' of the beam. With further investigation this may provide for the ability to trap the lighter coloured spheres at greater laser power and thus greater trap stiffness. Alternatively, although in a different context, work has been reported in the optical trapping field which used radial polarisation to increase the scattering forces relative to the gradient forces and thus reduced the resultant pushing effect (116,121). Radial polarisation would require non-typical optics to be added to the system (122).

Fusing of particles directly, without chemical assistance, seems unlikely due to the inherent problem with achieving the correct level of absorption/transmission. Additionally, the natural cooling effect of the surrounding water further compounds the problem. However, with use of a chemical coating, the process of joining particles is significantly more manageable (44,123)

The process of ablating the glass, discovered during the copper experiment, produced very fine features in a controlled manner. The feature sizes are not as small as those produced using near field processing, but the process could be an alternative to the near field processing work being undertaken by other research groups (57,124).

Manipulation of metallics, as opposed to dielectrics such as silica, with optical traps, is clearly a quite different phenomenon and needs to be treated as such. For basic manoeuvring applications, the optical 'poking' method suggested in this Chapter is sufficient. However, for genuine optical trapping of metallics, Rayleigh regime sized particles have been trapped (17,116) and by using unconventional optics to generate Bessel

beams, optical trapping of micron scale metallics (125) has been previously demonstrated. However, for optical trapping systems already employing an SLM, the 'ring' method suggested in this chapter offers a simple method for quick metallic particle placement and manipulation within an optical trapping system.

Chapter 7

Conclusions and Future work

7.1 Conclusions

The work in this thesis has focussed upon two main areas:

1. Developing a complex and versatile optical trapping system for use as an engineering tool.

2. Investigating new and novel engineering applications for the optical trap.

The main outcomes of this research study are:

- The design, building and development of a multifaceted optical trapping system which includes a dual laser line setup with the

ability to shift their relative focuses, giving the system unique capabilities.

- The investigation and relative merit of various methods of determining the trap stiffness.
- The investigation into the effect of the direction of linear polarisation of the trap stiffness which suggests the direction of polarisation does not have a major effect on trap stiffness.
- The successful embedding of 5.44μm silica spheres into a thermosetting polymer in a controlled manner.
- The harnessing of SLMs to generate annular beam profiles for the indirect manipulation of metallic particles. This process has been refined for greater efficiency.
- The observation of repeatable ablations (4μm) in width, on glass cover slips with copper particles on the surface, used to assist in the coupling in of photon energy into the glass substrate.

Optical Trapping is still a developing technology. It is imperative for its continued development that its users look to increase its capabilities. It is natural for users, for example in the biosciences field, to continue to pursue experiments and investigations already achievable with current optical trapping setups. As successful as many of these investigations may be, it is important that such successes do not lead the technology to fail to progress. Consequently, it is essential for optical engineers to maintain strong relations with the biosciences field, so that as new studies are devised,

which require greater capabilities from an optical trapping system, engineers can be readily available to address such issues.

Despite the continued assistance in the biosciences field, it is important not to categorise optical trapping as an entirely biosciences tool. Indeed, doing so might well lead to its fulfilment as such, but could deprive science of many other potential applications for optical traps.

The work in this thesis outlines the current 'state of the art' of optical trapping, particularly with regard to its engineering applications, and it pursues a variety of engineering applications; suggesting progress and research possibilities and documenting various applications which showed less research promise.

The embedding of spheres in a controlled manner has the potential to be a new and novel tool within micro manufacturing, so developing the optical trapping research landscape.

7.2 Future Work

The outcomes in Chapter 5 of this document suggest the need for further work. The manufacture of a device, containing embedded microspheres in a specific accurate array, capable of controlled near field processing would be the next step in the development of such work and could open up a whole new technology for industrial laser processing, allowing marking of materials well below the diffraction limit in large and repeatable arrays.

The work in Chapter 4 attempted to quantify and evaluate the forces in optical trapping, investigating the asymmetry of the trapping forces and

how such forces change with various parameters. Such a study shows the current difficulties associated with the use of QDs and why many research groups are now considering high frame rate cameras as the superior, or perhaps more accurately, simpler option.

The developing technology of SLMs is increasingly providing for greater control and beam manipulation. The latest generation of SLMs now provide the capability for precise selection of the polarisation state of the beam. A thorough study investigating the effect on trap stiffness of novel polarization states would certainly be of interest from a fundamental perspective. From a modelling perspective, there now exist two types of model; one for each of the two trapping regimes. Attempts to bridge the gap have been limited so it seems natural that the next direction for such work would be to create a model to describe optical trapping for objects in the size region between the two regimes. The escape force experiment in Chapter 4 showed the existence of two distinct trapping force regimes. With access to additional sizes of microsphere this could be investigated experimentally.

References

(1) Ashkin A. Acceleration and Trapping of Particles by Radiation Pressure. Phys Rev Lett 1970;24(4):156-159.

(2) Maxwell JC. A Treatise on Electricity and Magnetism. Oxford Clarendon Press 1873;2.

(3) Nichols EF, Hull GF. A preliminary communication on the pressure of heat and light radiation. Physical Review (Series I) 1901;13(5):307-320.

(4) Lebedev PN. Experimental examination of light pressure. Ann Phys 1901(6):433.

(5) Nichols EF, Hull GF. The pressure due to radiation. (Second Paper.). Physical Review (Series I) 1903;17(1):26-50.

(6) Nichols EF, Hull GF. The pressure due to radiation. (second paper.). Physical Review (Series I) 1903;17(2):91-104.

(7) Ashkin A, Dziedzic JM. Optical levitation by radiation pressure. Appl Phys Lett 1971;19(8):283-285.

(8) Ashkin A, Dziedzic JM. Stability of optical levitation by radiation pressure. Appl Phys Lett 1974;24(12):586-588.

(9) Ashkin A, Dziedzic JM. Optical levitation of liquid drops by radiation pressure. Science 1975;187(4181):1073-1075.

(10) Ashkin A, Dziedzic JM, Bjorkholm JE, Chu S. Observation of a single-beam gradient force optical trap for dielectric particles. Opt Lett 1986;11(5):288-290.

(11) Moffitt JR, Chemla YR, Smith SB, Bustamante C. Recent advances in optical tweezers. Annual Review of Biochemistry 2008;77:205-228.

(12) Neuman KC, Block SM. Optical trapping. Rev Sci Instrum 2004;75(9):2787-2809.

(13) Ashkin A, Dziedzic JM. Optical trapping and manipulation of viruses and bacteria. Science 1987;235(4795):1517-1520.

(14) Ashkin A. Forces of a single-beam gradient laser trap on a dielectric sphere in the ray optics regime. Biophys J 1992;61(2 I):569-582.

(15) Wright WH, Sonek GJ, Berns MW. Parametric study of the forces on microspheres held by optical tweezers. Appl Opt 1994;33(9):1735-1748.

(16) Malagnino N, Pesce G, Sasso A, Arimondo E. Measurements of trapping efficiency and stiffness in optical tweezers. Opt Commun 2003;214(1-6):15-24.

(17) Wright WH, Sonek GJ, Berns MW. Radiation trapping forces on microspheres with optical tweezers Appl Phys Lett 1993;63(6):715.

(18) Ashkin A, Dziedzic JM. Observation of radiation-pressure trapping of particles by alternating light beams. Phys Rev Lett 1985;54(12):1245-1248.

(19) Ashkin A. Optical trapping and manipulation of neutral particles using lasers. Proc Natl Acad Sci U S A 1997;94(10):4853-4860.

(20) Svoboda K, Block SM. Biological applications of optical forces. Annu Rev Biophys Biomol Struct 1994;23:247-285.

(21) Ashkin A, Dziedzic JM. Internal cell manipulation using infrared laser traps Proc Natl Acad Sci U S A 1989 Oct;86(20):7914-7918.

(22) Dholakia K, Reece P, Gu M. Optical micromanipulation Chem Soc Rev 2008;37(1):42.

(23) Batchelor GK. An introduction to fluid dynamics Cambridge: Cambridge University Press; 2000.

(24) Peterman EJG, Gittes F, Schmidt CF. Laser-Induced Heating in Optical Traps Biophys J 2003;84(2):1308 <last_page> 1316.

(25) Tolić-Nørrelykke SF, Schäffer E, Howard J, Pavone FS, Jülicher F, Flyvbjerg H. Calibration of optical tweezers with positional detection in the back focal plane. Rev Sci Instrum 2006;77(10).

(26) Visscher K, Gross SP, Block SM. Construction of multiple-beam optical traps with nanometer-resolution position sensing. IEEE Journal on Selected Topics in Quantum Electronics 1996;2(4):1066-1076.

(27) Gittes F, Schmidt CF. Thermal noise limitations on micromechanical experiments. European Biophysics Journal 1998;27(1):75-81.

(28) Berg-Sørensen K, Flyvbjerg H. Power spectrum analysis for optical tweezers. Rev Sci Instrum 2004;75(3):594-612.

(29) Ermilov S, Anvari B. Dynamic measurements of transverse optical trapping force in biological applications. Ann Biomed Eng 2004;32(7):1016-1026.

(30) Simmons RM, Finer JT, Chu S, Spudich JA. Quantitative measurements of force and displacement using an optical trap. Biophys J 1996;70(4):1813-1822.

(31) Keen S, Leach J, Gibson G, Padgett MJ. Comparison of a high-speed camera and a quadrant detector for measuring displacements in optical tweezers. Journal of Optics A: Pure and Applied Optics 2007;9(8):S264-S266.

(32) Halliday D, Resnick R, Walker J. Fundamentals of physics Hoboken, NJ: Wiley; 2005.

(33) Malagnino N, Pesce G, Sasso A, Arimondo E. Measurements of trapping efficiency and stiffness in optical tweezers. Opt Commun 2003;214(1-6):15-24.

(34) Ashkin A. Forces of a single-beam gradient laser trap on a dielectric sphere in the ray optics regime. Biophys J 1992;61(2 I):569-582.

(35) Theoretical calculation of trapping forces in oil-immersed microscope objectives. Proceedings of SPIE - The International Society for Optical Engineering; 2005.

(36) Mao F-, Xing QR, Wang K, Lang L-, Chai L, Wang Q-. Calculation of axial optical forces exerted on medium-sized particles by optical trap. Opt Laser Technol 2007;39(1):34-39.

(37) Calculation of optical forces on a dielectric bead in a geometrically aberrated trap. Proceedings of SPIE - The International Society for Optical Engineering; 2009.

(38) Rohrbach A, Stelzer EHK. Trapping forces, force constants, and potential depths for dielectric spheres in the presence of spherical aberrations. Appl Opt 2002;41(13):2494-2507.

(39) Rohrbach A, Stelzer EHK. Optical trapping of dielectric particles in arbitrary fields. Journal of the Optical Society of America A: Optics and Image Science, and Vision 2001;18(4):839-853.

(40) Lock JA. Calculation of the radiation trapping force for laser tweezers by use of generalized Lorenz-Mie theory. I. Localized model description of an on-axis tightly focused laser beam with spherical aberration. Appl Opt 2004;43(12):2532-2544.

(41) Nieminen TA, Rubinsztein-Dunlop H, Heckenberg NR, Bishop AI. Numerical modelling of optical trapping. Comput Phys Commun 2001;142(1-3):468-471.

(42) Microfabrication by optical tweezers. Proceedings of SPIE - The International Society for Optical Engineering; 2011.

(43) Production of functional microtool using size-classified gel-microbeads. 2008 International Symposium on Micro-NanoMechatronics and Human Science, MHS 2008; 2008.

(44) Whyte G, Gibson G, Leach J, Padgett M, Robert D, Miles M. An optical trapped microhand for manipulating micron-sized objects. Optics Express 2006;14(25):12497-12502.

(45) Ikin L, Carberry DM, Gibson GM, Padgett MJ, Miles MJ. Assembly and force measurement with SPM-like probes in holographic optical tweezers. New Journal of Physics 2009;11.

(46) Ito S, Yoshikawa H, Masuhara H. Laser manipulation and fixation of single gold nanoparticles in solution at room temperature. Appl Phys Lett 2002;80(3):482-484.

(47) Kawata S, Sun H-, Tanaka T, Takada K. Finer features for functional microdevices. Nature 2001;412(6848):697-698.

(48) Lachish-Zalait A, Zbaida D, Klein E, Elbaum M. Direct surface patterning from solutions: Localized microchemistry using a focused laser. Advanced Functional Materials 2001;11(3):218-223.

(49) Real three dimensional micro fabrication using stereo lithography and metal molding. IEEE Micro Electro Mechanical Systems; 1993.

(50) Strickler JH, Webb WW. 3-D optical data storage by two-photon excitation. Adv Mater 1993;5(6):479-481.

(51) Maruo S, Nakamura O, Kawata S. Three-dimensional microfabrication with two-photon-absorbed photopolymerization. Opt Lett 1997;22(2):132-134.

(52) Galajda P, Ormos P. Complex micromachines produced and driven by light. Appl Phys Lett 2001;78(2):249-251.

(53) Optical resonance and near-field effects: Applications for nanopatterning. Proceedings of SPIE - The International Society for Optical Engineering; 2004.

(54) Lu YF, Zhang L, Song WD, Zheng YW, Luk'yanchuk BS. Laser writing of a subwavelength structure on silicon (100) surfaces with particle-enhanced optical irradiation. JETP Letters 2000;72(9):457-459.

(55) McLeod E, Arnold CB. Subwavelength direct-write nanopatterning using optically trapped microspheres. Nature Nanotechnology 2008;3(7):413-417.

(56) Wang XC, Zheng HY, Tan CW, Wang F, Yu HY, Pey KL. Fabrication of silicon nanobump arrays by near-field enhanced laser irradiation. Appl Phys Lett 2010;96(8).

(57) Mehta AD, Rief M, Spudich JA, Smith DA, Simmons RM. Single-molecule biomechanics with optical methods. Science 1999;283(5408):1689-1695.

(58) Ashkin A, Dziedzic JM, Yamane T. Optical trapping and manipulation of single cells using infrared laser beams. Nature 1987;330(6150):769-771.

(59) Ashkin A, Schutze K, Dziedzic JM, Euteneuer U, Schliwa M. Force generation of organelle transport measured in vivo by an infrared laser trap. Nature 1990;348(6299):346-348.

(60) MacDonald MP, Neale S, Paterson L, Richies A, Dholakia K, Spalding GC. Cell cytometry with a light touch: Sorting microscopic matter with an optical lattice. J Biol Regul Homeost Agents 2004;18(2):200-205.

(61) Sorting via injection of particle streams into an optical lattice. Proceedings of SPIE - The International Society for Optical Engineering; 2005.

(62) Jordan P, Leach J, Padgett M, Blackburn P, Isaacs N, Goksör M, et al. Creating permanent 3D arrangements of isolated cells using holographic optical tweezers. Lab on a Chip - Miniaturisation for Chemistry and Biology 2005;5(11):1224-1228.

(63) Guck J, Ananthakrishnan R, Mahmood H, Moon TJ, Cunningham CC, Käs J. The optical stretcher: A novel laser tool to micromanipulate cells. Biophys J 2001;81(2):767-784.

(64) Svoboda K, Schmidt CF, Branton D, Block SM. Conformation and elasticity of the isolated red blood cell membrane skeleton. Biophys J 1992;63(3):784-793.

(65) Colon JM, Sarosi P, McGovern PG, Askin A, Dziedzic JM, Skurnick J, et al. Controlled micromanipulation of human sperm in three dimensions with an infrared laser optical trap: effect on sperm velocity Fertil Steril 1992 Mar;57(3):695-698.

(66) Nascimento JM, Botvinick EL, Shi LZ, Durrant B, Berns MW. Analysis of sperm motility using optical tweezers J Biomed Opt 2006 Jul-Aug;11(4):044001.

(67) Tadir Y, Wright WH, Vafa O, Ord T, Asch RH, Berns MW. Micromanipulation of sperm by a laser generated optical trap Fertil Steril 1989 Nov;52(5):870-873.

(68) Sheetz MP. Laser tweezers in cell biology. Introduction. Methods Cell Biol 1998;55:xi-xii.

(69) Moffitt JR, Chemla YR, Smith SB, Bustamante C. Recent advances in optical tweezers. Annual Review of Biochemistry 2008;77:205-228.

(70) Optical trapping for engineering manufacture. 26th International Congress on Applications of Lasers and Electro-Optics, ICALEO 2007 - Congress Proceedings; 2007.

(71) Escandon GJ, Liu Y, Sonek GJ, Berns MW. Beam magnification and the efficiency of optical trapping with 790-nm AlGaAs laser diodes. IEEE Photonics Technology Letters 1994;6(5):597-600.

(72) Liesener J, Reicherter M, Haist T, Tiziani HJ. Multi-functional optical tweezers using computer-generated holograms. Opt Commun 2000;185(1-3):77-82.

(73) Holographic optical tweezers with real-time hologram calculation using a phase-only modulating LCOS-based SLM at 1064 nm. Proceedings of SPIE - The International Society for Optical Engineering; 2008.

(74) Song Q, Wen C, Zhang Y, Wang G, Ye A. Calibration of optical tweezers based on acousto-optic deflector and field programmable gate array. Chinese Optics Letters 2008;6(8):600-602.

(75) Vermeulen KC, Van Mameren J, Stienen GJM, Peterman EJG, Wuite GJL, Schmidt CF. Calibrating bead displacements in optical tweezers using acousto-optic deflectors. Rev Sci Instrum 2006;77(1):1-6.

(76) Hasman E, Biener G, Niv A, Kleiner V. Space-variant polarization manipulation. Progress in Optics 2005;47:215-289.

(77) Kuang Z, Liu D, Perrie W, Edwardson S, Sharp M, Fearon E, et al. Fast parallel diffractive multi-beam femtosecond laser surface micro-structuring. Appl Surf Sci 2009;255(13-14):6582-6588.

(78) Kuang Z, Perrie W, Liu D, Edwardson S, Cheng J, Dearden G, et al. Diffractive multi-beam surface micro-processing using 10 ps laser pulses. Appl Surf Sci 2009;255(22):9040-9044.

(79) Spatial light modulators for optical computing and information processing. Proceedings of the Hawaii International Conference on System Science; 1989.

(80) Programmable focal spot shaping of amplified femtosecond laser pulses and their application to micromachining. Proceedings of SPIE - The International Society for Optical Engineering; 2006.

(81) Sanner N, Huot N, Audouard E, Larat C, Huignard J-. Direct ultrafast laser micro-structuring of materials using programmable beam shaping. Optics and Lasers in Engineering 2007;45(6):737-741.

(82) Samek O, Hommes V, Hergenröder R, Kukhlevsky SV. Femtosecond pulse shaping using a liquid-crystal display: Applications to depth profiling analysis. Rev Sci Instrum 2005;76(8):1-3.

(83) Sinclair G, Jordan P, Leach J, Padgett MJ, Cooper J. Defining the trapping limits of holographical optical tweezers. Journal of Modern Optics 2004;51(3):409-414.

(84) Kozawa Y, Sato S. Optical trapping of micrometer-sized dielectric particles by cylindrical vector beams. Optics Express 2010;18(10):10828-10833.

(85) Leach J, Sinclair G, Jordan P, Courtial J, Padgett MJ, Cooper J, et al. 3D manipulation of particles into crystal structures using holographic optical tweezers. Optics Express 2004;12(1):220-226.

(86) Sinclair G, Leach J, Jordan P, Gibson G, Yao E, Laczik ZJ, et al. Interactive application in holographic optical tweezers of a multi-plane Gerchberg-Saxton algorithm for three-dimensional light shaping. Optics Express 2004;12(8):1665-1670.

(87) Sun B, Roichman Y, Grier DG. Theory of holographic optical trapping. Optics Express 2008;16(20):15765-15776.

(88) Grieve JA, Ulcinas A, Subramanian S, Gibson GM, Padgett MJ, Carberry DM, et al. Hands-on with optical tweezers: A multitouch interface for holographic optical trapping. Optics Express 2009;17(5):3595-3602.

(89) Leach J, Wulff K, Sinclair G, Jordan P, Courtial J, Thomson L, et al. Interactive approach to optical tweezers control. Appl Opt 2006;45(5):897-903.

(90) Gibson G, Carberry DM, Whyte G, Leach J, Courtial J, Jackson JC, et al. Holographic assembly workstation for optical manipulation. Journal of Optics A: Pure and Applied Optics 2008;10(4).

(91) Mogensen PC, Glückstad J. Dynamic array generation and pattern formation for optical tweezers. Opt Commun 2000;175(1):75-81.

(92) Jordan P, Cooper J, McNay G, Docherty FT, Smith WE, Sinclair G, et al. Three-dimensional optical trapping of partially silvered silica microparticles. Opt Lett 2004;29(21):2488-2490.

(93) G. F. Milne.
Optical Sorting and Manipulation of
Microscopic ParticlesUniversity of St.Andrews; 2007.

(94) Gerchberg RW, Saxton WO. PRACTICAL ALGORITHM FOR THE DETERMINATION OF PHASE FROM IMAGE AND DIFFRACTION PLANE PICTURES. Optik (Stuttgart) 1972;35(2):237-250.

(95) Comparison of backward-scattered detection and forward-scattered detection for measuring optical force in optical tweezers. Proceedings of SPIE - The International Society for Optical Engineering; 2010.

(96) Tolić-Nørrelykke SF, Schäffer E, Howard J, Pavone FS, Jülicher F, Flyvbjerg H. Calibration of optical tweezers with positional detection in the back focal plane. Rev Sci Instrum 2006;77(10).

(97) Trapping force calibration in biological applications of optical tweezers. Proceedings of SPIE - The International Society for Optical Engineering; 2003.

(98) Calibration of the characteristic frequency of an optical tweezer using a recursive least-squares approach. Proceedings of the American Control Conference; 2004.

(99) Van Der Horst A, Forde NR. Calibration of dynamic holographic optical tweezers for force measurements on biomaterials. Optics Express 2008;16(25):20987-21003.

(100) Osterman N. TweezPal - Optical tweezers analysis and calibration software. Comput Phys Commun 2010;181(11):1911-1916.

(101) Optical manipulation of plasmonic nanoparticles using laser tweezers. Proceedings of SPIE - The International Society for Optical Engineering; 2010.

(102) Ohlinger A, Nedev S, Lutich AA, Feldmann J. Optothermal escape of plasmonically coupled silver nanoparticles from a three-dimensional optical trap. Nano Letters 2011;11(4):1770-1774.

(103) Mori H. Transport, Collective Motion, and Brownian Motion Progress of Theoretical Physics 1965;33(3):423 <last_page> 455.

(104) D. tH. Chapter 2 - The Maxwell-Boltzmann Distribution. Elements of Statistical Mechanics (Third edition) Oxford: Butterworth-Heinemann; 1995. p. 36-58.

(105) BOLTZMANN L. On Certain Questions of the Theory of Gases Nature 1895;51(1322):413 <last_page> 415.

(106) Berg-Sørensen K, Flyvbjerg H. Power spectrum analysis for optical tweezers. Rev Sci Instrum 2004;75(3):594-612.

(107) Mahamdeh M, Campos CP, Schäffer E. Under-filling trapping objectives optimizes the use of the available laser power in optical tweezers. Optics Express 2011;19(12):11759-11768.

(108) Tolić-Nørrelykke SF, Schäffer E, Howard J, Pavone FS, Jülicher F, Flyvbjerg H. Calibration of optical tweezers with positional detection in the back focal plane. Rev Sci Instrum 2006;77(10).

(109) Nørrelykke SF, Flyvbjerg H. Power spectrum analysis with least-squares fitting: Amplitude bias and its elimination, with application to optical tweezers and atomic force microscope cantilevers. Rev Sci Instrum 2010;81(7).

(110) Marquardt D. J Soc Indust Appl Math 1963;11(2):431-441.

(111) Malagnino N, Pesce G, Sasso A, Arimondo E. Measurements of trapping efficiency and stiffness in optical tweezers. Opt Commun 2002 12/15;214(1-6):15-24.

(112) Inouye Y, Shoji S, Furukawa H, Nakamura O, Kawata S. Pico-Newton friction force measurements using a laser-trapped microsphere. Jpn J Appl Phys Part 2 Letter 1998;37(6 A):L684-L686.

(113) Ashkin A, Dziedzic JM. Optical levitation in high vacuum. Appl Phys Lett 1976;28(6):333-335.

(114) Svoboda K, Block SM. Optical trapping of metallic Rayleigh particles. Opt Lett 1994;19(13):930-932.

(115) Zhan Q. Trapping metallic Rayleigh particles with radial polarization. Optics Express 2004;12(15):3377-3382.

(116) Sato S, Harada Y, Waseda Y. Optical trapping of microscopic metal particles Opt Lett 1994; 1994;19(22):1807.

(117) Emiliani V, Sanvitto D, Zahid M, Gerbal F, Coppey-Moisan M. Multi force optical tweezers to generate gradients of forces Optics Express 2004;12(17):3906.

(118) Bouhafs D. Design and simulation of antireflection coating systems for optoelectronic devices: Application to silicon solar cells Solar Energy Mater Solar Cells 1998;52(1-2):79 <last_page> 93.

(119) Zhou W, Tao M, Chen L, Yang H. Microstructured surface design for omnidirectional antireflection coatings on solar cells J Appl Phys 2007;102(10):103105.

(120) Nieminen TA, Heckenberg NR, Rubinsztein-Dunlop H. Forces in optical tweezers with radially and azimuthally polarized trapping beams Opt Lett 2008; 2008;33(2):122.

(121) Oron R, Blit S, Davidson N, Friesem AA, Bomzon Z, Hasman E. The formation of laser beams with pure azimuthal or radial polarization Appl Phys Lett 2000;77(21):3322.

(122) Ikin L, Carberry DM, Gibson GM, Padgett MJ, Miles MJ. Assembly and force measurement with SPM-like probes in holographic optical tweezers. New Journal of Physics 2009;11.

(123) Huang SM, Wang ZA, Sun Z, Wang ZB, Luk'yanchuk B. Theoretical and experimental investigation of the near field under ordered silica spheres on substrate. Applied Physics A: Materials Science and Processing 2009;96(2):459-466.

(124) Svoboda K, Block SM. Optical trapping of metallic Rayleigh particles. Opt Lett 1994;19(13):930-932.

(125) Arlt J, Garces-Chavez V, Sibbett W, Dholakia K. Optical micromanipulation using a Bessel light beam. Opt Commun 2001;197(4-6):239-245.

(1) Ashkin A. Acceleration and Trapping of Particles by Radiation Pressure. Phys Rev Lett 1970;24(4):156-159.

(2) Maxwell JC. A Treatise on Electricity and Magnetism. Oxford Clarendon Press 1873;2.

(3) Nichols EF, Hull GF. A preliminary communication on the pressure of heat and light radiation. Physical Review (Series I) 1901;13(5):307-320.

(4) Lebedev PN. Experimental examination of light pressure. Ann Phys 1901(6):433.

(5) Nichols EF, Hull GF. The pressure due to radiation. (Second Paper.). Physical Review (Series I) 1903;17(1):26-50.

(6) Nichols EF, Hull GF. The pressure due to radiation. (second paper.). Physical Review (Series I) 1903;17(2):91-104.

(7) Ashkin A, Dziedzic JM. Optical levitation by radiation pressure. Appl Phys Lett 1971;19(8):283-285.

(8) Ashkin A, Dziedzic JM. Stability of optical levitation by radiation pressure. Appl Phys Lett 1974;24(12):586-588.

(9) Ashkin A, Dziedzic JM. Optical levitation of liquid drops by radiation pressure. Science 1975;187(4181):1073-1075.

(10) Ashkin A, Dziedzic JM, Bjorkholm JE, Chu S. Observation of a single-beam gradient force optical trap for dielectric particles. Opt Lett 1986;11(5):288-290.

(11) Moffitt JR, Chemla YR, Smith SB, Bustamante C. Recent advances in optical tweezers. Annual Review of Biochemistry 2008;77:205-228.

(12) Neuman KC, Block SM. Optical trapping. Rev Sci Instrum 2004;75(9):2787-2809.

(13) Ashkin A, Dziedzic JM. Optical trapping and manipulation of viruses and bacteria. Science 1987;235(4795):1517-1520.

(14) Ashkin A. Forces of a single-beam gradient laser trap on a dielectric sphere in the ray optics regime. Biophys J 1992;61(2 I):569-582.

(15) Wright WH, Sonek GJ, Berns MW. Parametric study of the forces on microspheres held by optical tweezers. Appl Opt 1994;33(9):1735-1748.

(16) Ashkin A. Forces of a single-beam gradient laser trap on a dielectric sphere in the ray optics regime. Biophys J 1992;61(2 I):569-582.

(17) Svoboda K, Block SM. Optical trapping of metallic Rayleigh particles. Opt Lett 1994;19(13):930-932.

(18) Malagnino N, Pesce G, Sasso A, Arimondo E. Measurements of trapping efficiency and stiffness in optical tweezers. Opt Commun 2003;214(1-6):15-24.

(19) Wright WH, Sonek GJ, Berns MW. Radiation trapping forces on microspheres with optical tweezers Appl Phys Lett 1993;63(6):715.

(20) Ashkin A, Dziedzic JM. Observation of radiation-pressure trapping of particles by alternating light beams. Phys Rev Lett 1985;54(12):1245-1248.

(21) Ashkin A. Optical trapping and manipulation of neutral particles using lasers. Proc Natl Acad Sci U S A 1997;94(10):4853-4860.

(22) Svoboda K, Block SM. Biological applications of optical forces. Annu Rev Biophys Biomol Struct 1994;23:247-285.

(23) Ashkin A, Dziedzic JM. Internal cell manipulation using infrared laser traps Proc Natl Acad Sci U S A 1989 Oct;86(20):7914-7918.

(24) Dholakia K, Reece P, Gu M. Optical micromanipulation Chem Soc Rev 2008;37(1):42.

(25) Batchelor GK. An introduction to fluid dynamics Cambridge: Cambridge University Press; 2000.

(26) Peterman EJG, Gittes F, Schmidt CF. Laser-Induced Heating in Optical Traps Biophys J 2003;84(2):1308 <last_page> 1316.

(27) Tolić-Nørrelykke SF, Schäffer E, Howard J, Pavone FS, Jülicher F, Flyvbjerg H. Calibration of optical tweezers with positional detection in the back focal plane. Rev Sci Instrum 2006;77(10).

(28) Visscher K, Gross SP, Block SM. Construction of multiple-beam optical traps with nanometer-resolution position sensing. IEEE Journal on Selected Topics in Quantum Electronics 1996;2(4):1066-1076.

(29) Gittes F, Schmidt CF. Thermal noise limitations on micromechanical experiments. European Biophysics Journal 1998;27(1):75-81.

(30) Berg-Sørensen K, Flyvbjerg H. Power spectrum analysis for optical tweezers. Rev Sci Instrum 2004;75(3):594-612.

(31) Ermilov S, Anvari B. Dynamic measurements of transverse optical trapping force in biological applications. Ann Biomed Eng 2004;32(7):1016-1026.

(32) Simmons RM, Finer JT, Chu S, Spudich JA. Quantitative measurements of force and displacement using an optical trap. Biophys J 1996;70(4):1813-1822.

(33) Keen S, Leach J, Gibson G, Padgett MJ. Comparison of a high-speed camera and a quadrant detector for measuring displacements in optical tweezers. Journal of Optics A: Pure and Applied Optics 2007;9(8):S264-S266.

(34) Halliday D, Resnick R, Walker J. Fundamentals of physics Hoboken, NJ: Wiley; 2005.

(35) Malagnino N, Pesce G, Sasso A, Arimondo E. Measurements of trapping efficiency and stiffness in optical tweezers. Opt Commun 2003;214(1-6):15-24.

(36) Theoretical calculation of trapping forces in oil-immersed microscope objectives. Proceedings of SPIE - The International Society for Optical Engineering; 2005.

(37) Mao F-, Xing QR, Wang K, Lang L-, Chai L, Wang Q-. Calculation of axial optical forces exerted on medium-sized particles by optical trap. Opt Laser Technol 2007;39(1):34-39.

(38) Calculation of optical forces on a dielectric bead in a geometrically aberrated trap. Proceedings of SPIE - The International Society for Optical Engineering; 2009.

(39) Rohrbach A, Stelzer EHK. Trapping forces, force constants, and potential depths for dielectric spheres in the presence of spherical aberrations. Appl Opt 2002;41(13):2494-2507.

(40) Rohrbach A, Stelzer EHK. Optical trapping of dielectric particles in arbitrary fields. Journal of the Optical Society of America A: Optics and Image Science, and Vision 2001;18(4):839-853.

(41) Lock JA. Calculation of the radiation trapping force for laser tweezers by use of generalized Lorenz-Mie theory. I. Localized model description of an on-axis tightly focused laser beam with spherical aberration. Appl Opt 2004;43(12):2532-2544.

(42) Nieminen TA, Rubinsztein-Dunlop H, Heckenberg NR, Bishop AI. Numerical modelling of optical trapping. Comput Phys Commun 2001;142(1-3):468-471.

(43) Microfabrication by optical tweezers. Proceedings of SPIE - The International Society for Optical Engineering; 2011.

(44) Production of functional microtool using size-classified gel-microbeads. 2008 International Symposium on Micro-NanoMechatronics and Human Science, MHS 2008; 2008.

(45) Whyte G, Gibson G, Leach J, Padgett M, Robert D, Miles M. An optical trapped microhand for manipulating micron-sized objects. Optics Express 2006;14(25):12497-12502.

(46) Ikin L, Carberry DM, Gibson GM, Padgett MJ, Miles MJ. Assembly and force measurement with SPM-like probes in holographic optical tweezers. New Journal of Physics 2009;11.

(47) Ito S, Yoshikawa H, Masuhara H. Laser manipulation and fixation of single gold nanoparticles in solution at room temperature. Appl Phys Lett 2002;80(3):482-484.

(48) Kawata S, Sun H-, Tanaka T, Takada K. Finer features for functional microdevices. Nature 2001;412(6848):697-698.

(49) Lachish-Zalait A, Zbaida D, Klein E, Elbaum M. Direct surface patterning from solutions: Localized microchemistry using a focused laser. Advanced Functional Materials 2001;11(3):218-223.

(50) Real three dimensional micro fabrication using stereo lithography and metal molding. IEEE Micro Electro Mechanical Systems; 1993.

(51) Strickler JH, Webb WW. 3-D optical data storage by two-photon excitation. Adv Mater 1993;5(6):479-481.

(52) Maruo S, Nakamura O, Kawata S. Three-dimensional microfabrication with two-photon-absorbed photopolymerization. Opt Lett 1997;22(2):132-134.

(53) Galajda P, Ormos P. Complex micromachines produced and driven by light. Appl Phys Lett 2001;78(2):249-251.

(54) Optical resonance and near-field effects: Applications for nanopatterning. Proceedings of SPIE - The International Society for Optical Engineering; 2004.

(55) Lu YF, Zhang L, Song WD, Zheng YW, Luk'yanchuk BS. Laser writing of a subwavelength structure on silicon (100) surfaces with particle-enhanced optical irradiation. JETP Letters 2000;72(9):457-459.

(56) McLeod E, Arnold CB. Subwavelength direct-write nanopatterning using optically trapped microspheres. Nature Nanotechnology 2008;3(7):413-417.

(57) Wang XC, Zheng HY, Tan CW, Wang F, Yu HY, Pey KL. Fabrication of silicon nanobump arrays by near-field enhanced laser irradiation. Appl Phys Lett 2010;96(8).

(58) Mehta AD, Rief M, Spudich JA, Smith DA, Simmons RM. Single-molecule biomechanics with optical methods. Science 1999;283(5408):1689-1695.

(59) Ashkin A, Dziedzic JM, Yamane T. Optical trapping and manipulation of single cells using infrared laser beams. Nature 1987;330(6150):769-771.

(60) Ashkin A, Schutze K, Dziedzic JM, Euteneuer U, Schliwa M. Force generation of organelle transport measured in vivo by an infrared laser trap. Nature 1990;348(6299):346-348.

(61) MacDonald MP, Neale S, Paterson L, Richies A, Dholakia K, Spalding GC. Cell cytometry with a light touch: Sorting microscopic matter with an optical lattice. J Biol Regul Homeost Agents 2004;18(2):200-205.

(62) Sorting via injection of particle streams into an optical lattice. Proceedings of SPIE - The International Society for Optical Engineering; 2005.

(63) Jordan P, Leach J, Padgett M, Blackburn P, Isaacs N, Goksör M, et al. Creating permanent 3D arrangements of isolated cells using holographic optical tweezers. Lab on a Chip - Miniaturisation for Chemistry and Biology 2005;5(11):1224-1228.

(64) Guck J, Ananthakrishnan R, Mahmood H, Moon TJ, Cunningham CC, Käs J. The optical stretcher: A novel laser tool to micromanipulate cells. Biophys J 2001;81(2):767-784.

(65) Svoboda K, Schmidt CF, Branton D, Block SM. Conformation and elasticity of the isolated red blood cell membrane skeleton. Biophys J 1992;63(3):784-793.

(66) Colon JM, Sarosi P, McGovern PG, Askin A, Dziedzic JM, Skurnick J, et al. Controlled micromanipulation of human sperm in three dimensions with an infrared laser optical trap: effect on sperm velocity Fertil Steril 1992 Mar;57(3):695-698.

(67) Nascimento JM, Botvinick EL, Shi LZ, Durrant B, Berns MW. Analysis of sperm motility using optical tweezers J Biomed Opt 2006 Jul-Aug;11(4):044001.

(68) Tadir Y, Wright WH, Vafa O, Ord T, Asch RH, Berns MW. Micromanipulation of sperm by a laser generated optical trap Fertil Steril 1989 Nov;52(5):870-873.

(69) Sheetz MP. Laser tweezers in cell biology. Introduction. Methods Cell Biol 1998;55:xi-xii.

(70) Moffitt JR, Chemla YR, Smith SB, Bustamante C. Recent advances in optical tweezers. Annual Review of Biochemistry 2008;77:205-228.

(71) Optical trapping for engineering manufacture. 26th International Congress on Applications of Lasers and Electro-Optics, ICALEO 2007 - Congress Proceedings; 2007.

(72) Escandon GJ, Liu Y, Sonek GJ, Berns MW. Beam magnification and the efficiency of optical trapping with 790-nm AlGaAs laser diodes. IEEE Photonics Technology Letters 1994;6(5):597-600.

(73) Liesener J, Reicherter M, Haist T, Tiziani HJ. Multi-functional optical tweezers using computer-generated holograms. Opt Commun 2000;185(1-3):77-82.

(74) Holographic optical tweezers with real-time hologram calculation using a phase-only modulating LCOS-based SLM at 1064 nm. Proceedings of SPIE - The International Society for Optical Engineering; 2008.

(75) Song Q, Wen C, Zhang Y, Wang G, Ye A. Calibration of optical tweezers based on acousto-optic deflector and field programmable gate array. Chinese Optics Letters 2008;6(8):600-602.

(76) Vermeulen KC, Van Mameren J, Stienen GJM, Peterman EJG, Wuite GJL, Schmidt CF. Calibrating bead displacements in optical tweezers using acousto-optic deflectors. Rev Sci Instrum 2006;77(1):1-6.

(77) Hasman E, Biener G, Niv A, Kleiner V. Space-variant polarization manipulation. Progress in Optics 2005;47:215-289.

(78) Kuang Z, Liu D, Perrie W, Edwardson S, Sharp M, Fearon E, et al. Fast parallel diffractive multi-beam femtosecond laser surface micro-structuring. Appl Surf Sci 2009;255(13-14):6582-6588.

(79) Kuang Z, Perrie W, Liu D, Edwardson S, Cheng J, Dearden G, et al. Diffractive multi-beam surface micro-processing using 10 ps laser pulses. Appl Surf Sci 2009;255(22):9040-9044.

(80) Spatial light modulators for optical computing and information processing. Proceedings of the Hawaii International Conference on System Science; 1989.

(81) Programmable focal spot shaping of amplified femtosecond laser pulses and their application to micromachining. Proceedings of SPIE - The International Society for Optical Engineering; 2006.

(82) Sanner N, Huot N, Audouard E, Larat C, Huignard J-. Direct ultrafast laser micro-structuring of materials using programmable beam shaping. Optics and Lasers in Engineering 2007;45(6):737-741.

(83) Samek O, Hommes V, Hergenröder R, Kukhlevsky SV. Femtosecond pulse shaping using a liquid-crystal display: Applications to depth profiling analysis. Rev Sci Instrum 2005;76(8):1-3.

(84) Sinclair G, Jordan P, Leach J, Padgett MJ, Cooper J. Defining the trapping limits of holographical optical tweezers. Journal of Modern Optics 2004;51(3):409-414.

(85) Kozawa Y, Sato S. Optical trapping of micrometer-sized dielectric particles by cylindrical vector beams. Optics Express 2010;18(10):10828-10833.

(86) Leach J, Sinclair G, Jordan P, Courtial J, Padgett MJ, Cooper J, et al. 3D manipulation of particles into crystal structures using holographic optical tweezers. Optics Express 2004;12(1):220-226.

(87) Sinclair G, Leach J, Jordan P, Gibson G, Yao E, Laczik ZJ, et al. Interactive application in holographic optical tweezers of a multi-plane Gerchberg-Saxton algorithm for three-dimensional light shaping. Optics Express 2004;12(8):1665-1670.

(88) Sun B, Roichman Y, Grier DG. Theory of holographic optical trapping. Optics Express 2008;16(20):15765-15776.

(89) Grieve JA, Ulcinas A, Subramanian S, Gibson GM, Padgett MJ, Carberry DM, et al. Hands-on with optical tweezers: A multitouch interface for holographic optical trapping. Optics Express 2009;17(5):3595-3602.

(90) Leach J, Wulff K, Sinclair G, Jordan P, Courtial J, Thomson L, et al. Interactive approach to optical tweezers control. Appl Opt 2006;45(5):897-903.

(91) Gibson G, Carberry DM, Whyte G, Leach J, Courtial J, Jackson JC, et al. Holographic assembly workstation for optical manipulation. Journal of Optics A: Pure and Applied Optics 2008;10(4).

(92) Mogensen PC, Glückstad J. Dynamic array generation and pattern formation for optical tweezers. Opt Commun 2000;175(1):75-81.

(93) Jordan P, Cooper J, McNay G, Docherty FT, Smith WE, Sinclair G, et al. Three-dimensional optical trapping of partially silvered silica microparticles. Opt Lett 2004;29(21):2488-2490.

(94) G. F. Milne.
Optical Sorting and Manipulation of
Microscopic ParticlesUniversity of St.Andrews; 2007.

(95) Gerchberg RW, Saxton WO. PRACTICAL ALGORITHM FOR THE DETERMINATION OF PHASE FROM IMAGE AND DIFFRACTION PLANE PICTURES. Optik (Stuttgart) 1972;35(2):237-250.

(96) Comparison of backward-scattered detection and forward-scattered detection for measuring optical force in optical tweezers. Proceedings of SPIE - The International Society for Optical Engineering; 2010.

(97) Tolić-Nørrelykke SF, Schäffer E, Howard J, Pavone FS, Jülicher F, Flyvbjerg H. Calibration of optical tweezers with positional detection in the back focal plane. Rev Sci Instrum 2006;77(10).

(98) Trapping force calibration in biological applications of optical tweezers. Proceedings of SPIE - The International Society for Optical Engineering; 2003.

(99) Calibration of the characteristic frequency of an optical tweezer using a recursive least-squares approach. Proceedings of the American Control Conference; 2004.

(100) Van Der Horst A, Forde NR. Calibration of dynamic holographic optical tweezers for force measurements on biomaterials. Optics Express 2008;16(25):20987-21003.

(101) Osterman N. TweezPal - Optical tweezers analysis and calibration software. Comput Phys Commun 2010;181(11):1911-1916.

(102) Optical manipulation of plasmonic nanoparticles using laser tweezers. Proceedings of SPIE - The International Society for Optical Engineering; 2010.

(103) Ohlinger A, Nedev S, Lutich AA, Feldmann J. Optothermal escape of plasmonically coupled silver nanoparticles from a three-dimensional optical trap. Nano Letters 2011;11(4):1770-1774.

(104) Mori H. Transport, Collective Motion, and Brownian Motion Progress of Theoretical Physics 1965;33(3):423 <last_page> 455.

(105) D. tH. Chapter 2 - The Maxwell-Boltzmann Distribution. Elements of Statistical Mechanics (Third edition) Oxford: Butterworth-Heinemann; 1995. p. 36-58.

(106) BOLTZMANN L. On Certain Questions of the Theory of Gases Nature 1895;51(1322):413 <last_page> 415.

(107) Berg-Sørensen K, Flyvbjerg H. Power spectrum analysis for optical tweezers. Rev Sci Instrum 2004;75(3):594-612.

(108) Mahamdeh M, Campos CP, Schäffer E. Under-filling trapping objectives optimizes the use of the available laser power in optical tweezers. Optics Express 2011;19(12):11759-11768.

(109) Tolić-Nørrelykke SF, Schäffer E, Howard J, Pavone FS, Jülicher F, Flyvbjerg H. Calibration of optical tweezers with positional detection in the back focal plane. Rev Sci Instrum 2006;77(10).

(110) Nørrelykke SF, Flyvbjerg H. Power spectrum analysis with least-squares fitting: Amplitude bias and its elimination, with application to optical tweezers and atomic force microscope cantilevers. Rev Sci Instrum 2010;81(7).

(111) Marquardt D. J Soc Indust Appl Math 1963;11(2):431-441.

(112) Malagnino N, Pesce G, Sasso A, Arimondo E. Measurements of trapping efficiency and stiffness in optical tweezers. Opt Commun 2002 12/15;214(1-6):15-24.

(113) Inouye Y, Shoji S, Furukawa H, Nakamura O, Kawata S. Pico-Newton friction force measurements using a laser-trapped microsphere. Jpn J Appl Phys Part 2 Letter 1998;37(6 A):L684-L686.

(114) Ashkin A, Dziedzic JM. Optical levitation in high vacuum. Appl Phys Lett 1976;28(6):333-335.

(115) Svoboda K, Block SM. Optical trapping of metallic Rayleigh particles. Opt Lett 1994;19(13):930-932.

(116) Zhan Q. Trapping metallic Rayleigh particles with radial polarization. Optics Express 2004;12(15):3377-3382.

(117) Sato S, Harada Y, Waseda Y. Optical trapping of microscopic metal particles Opt Lett 1994; 1994;19(22):1807.

(118) Emiliani V, Sanvitto D, Zahid M, Gerbal F, Coppey-Moisan M. Multi force optical tweezers to generate gradients of forces Optics Express 2004;12(17):3906.

(119) Bouhafs D. Design and simulation of antireflection coating systems for optoelectronic devices: Application to silicon solar cells Solar Energy Mater Solar Cells 1998;52(1-2):79 <last_page> 93.

(120) Zhou W, Tao M, Chen L, Yang H. Microstructured surface design for omnidirectional antireflection coatings on solar cells J Appl Phys 2007;102(10):103105.

(121) Nieminen TA, Heckenberg NR, Rubinsztein-Dunlop H. Forces in optical tweezers with radially and azimuthally polarized trapping beams Opt Lett 2008; 2008;33(2):122.

(122) Oron R, Blit S, Davidson N, Friesem AA, Bomzon Z, Hasman E. The formation of laser beams with pure azimuthal or radial polarization Appl Phys Lett 2000;77(21):3322.

(123) Ikin L, Carberry DM, Gibson GM, Padgett MJ, Miles MJ. Assembly and force measurement with SPM-like probes in holographic optical tweezers. New Journal of Physics 2009;11.

(124) Huang SM, Wang ZA, Sun Z, Wang ZB, Luk'yanchuk B. Theoretical and experimental investigation of the near field under ordered silica spheres on substrate. Applied Physics A: Materials Science and Processing 2009;96(2):459-466.

(125) Arlt J, Garces-Chavez V, Sibbett W, Dholakia K. Optical micromanipulation using a Bessel light beam. Opt Commun 2001;197(4-6):239-245.